Spin-torch experiment on reaction centers of Rhodobacter sphaeroides

Sai Sankar Gupta, K.B.

Spin-torch experiments on reaction centers of *Rhodobacter sphaeroides*

Karthick Babu Sai Sankar Gupta

Karthick Babu Sai Sankar Gupta
Spin-torch experiments on reaction centers of *Rhodobacter sphaeroides*
Ph.D. Thesis, Leiden University, 22nd December 2011

ISBN: 978-90-818475-0-6 (Print)

Cover figure designed by Dr. Amol Patil (amolvp@gmail.com)
Thesis Printed by Smart Printing Solutions, www.sps-print.eu

Spin-torch experiments on reaction centers of *Rhodobacter sphaeroides*

Proefschrift

ter verkrijging van de graad van Doctor
aan de Universiteit Leiden,
op gezag van de Rector Magnificus Prof. Mr. P. F. van der Heijden,
volgens besluit van het College voor Promoties
te verdedigen op donderdag 22 december 2011
klokke 11.15 uur

door

Karthick Babu Sai Sankar Gupta

geboren te Bangalore, India in 1979

Promotiecommissie

Promotor:	Prof. dr. Huub de Groot
Copromotor:	Dr. Jörg Matysik
Overige Leden:	Prof. dr. Jaap Brouwer
	Prof. dr. Matthias Ernst (ETH Zűrich)
	Dr. Peter Gast
	Prof. dr. Marcellus Ubbink
	Prof. dr. Silvia Völker (UL Leiden, VU Amsterdam)

To Nature

Table of Contents

List of abbreviations

1D	one-dimensional
2D	two-dimensional
A	absorptive
ADF	Amsterdam density functional
ADP	adenosine-di-phosphate
AFM	atomic force microscopy
ALA	δ-aminolevulinic acid
ATP	adenosine-tri-phosphate
B_A	accessory BChl on the "active" branch A
B_B	accessory BChl on the "inactive" branch B
BChl *a*	bacteriochlorophyll *a*
BPhe *a*, Φ	bacteriopheophytin *a*
BR-24	Burum and Rhim pulse sequence
C7	seven phase-shifted radiofrequency pulse cycle
Car	carotenoid
CI	continuous illumination
Corr	corrected
CP	cross-polarization
CS	chemical shift
CSA	chemical shift anisotropy
CW	continuous wave decoupling
CYCLOPS	cyclically ordered phase sequence
DARR	dipolar-assisted rotational resonance
DD	differential decay
Dec	decoupling
DFT	density functional theory
DRAMA	dipolar recovery at the magic angle
DUMBO	a numerically optimized sequence
E	emissive
EDTA	ethylene-diamine-tetra-acetic acid
ENDOR	electron nuclear double resonance
EPR	electron paramagnetic resonance
eq	equation
ET	electron transfer reactions
FSLG	frequency-switched Lee-Goldburg
FWHH	full width at half height
HH	Hartmann-Hahn condition
His	histidine
HOMO	highest occupied molecular orbital
LDAO	lauryldimethylamine-oxide (N,N-dimethyldodecylamine-N-oxide)
LG	Lee-Goldburg
LG-CP	Lee-Goldburg cross-polarization

LH	light harvesting antenna complexes
MAS	magic angle spinning
mix	mixing time
MREV-8	Mansfield-Rhim-Elleman-Vaughn sequence
NMR	nuclear magnetic resonance
NSD	normal coordinate structural decomposition
P	Special Pair in ground state (primary donor)
P*	Special Pair in excited state
PCET	proton coupled electron transfer
PDB	protein data bank
PDSD	proton driven spin diffusion
Photo-CIDNP	photochemically induced dynamic nuclear polarization
P_L	part of the Special Pair on the "active" branch A (L polypeptide)
P_M	part of the Special Pair on the "inactive" branch B (M polypeptide)
PMLG	phase-modulated Lee-Goldburg
ppm	parts per million
PSU	photosynthetic unit
Q_A	ubiquinones-10 on the "active" branch A
Q_B	ubiquinones-10 on the "inactive" branch B
R. sphaeroides	*Rhodobacter sphaeroides*
R3	rotary resonance recoupling
RC	reaction center
REDOR	rotational echo double resonance
rf	radio-frequency
RFDR	radio-frequency driven dipolar recoupling
RPM	radical pair mechanism
S	singlet state
SPINAL	small phase incremental alternation
SW_f-TPPM	Swept-frequency two-pulse phase modulation
T_0	triplet state with magnetic quantum number 0
TEDOR	transferred-echo double resonance
TPPM	two-pulse phase modulated decoupling
TSM	electron-electron-nuclear three spin mixing
WAHUHA	Waugh-Huber-Haberlen Sequence
wPMLG	windowed phase-modulated Lee-Goldburg
WT	wild-type
XiX	X inverse-X decoupling
Φ_A	bacteriopheophytin *a* on the "active" branch A
Φ_B	bacteriopheophytin *a* on the "inactive" branch B

Chapter 1

General introduction

1.1 Bacterial reaction center

1.1.1 Photosynthesis

Life on Earth is predominantly due to photosynthesis, a process which consists of two different pathways namely anoxygenic and oxygenic. In anoxygenic photosynthesis only carbon dioxide is consumed, while in oxygenic photosynthesis along with that oxygen is also liberated. In general photosynthetic process produces food for living beings and provides the fossil fuels for human energy consumption. Photosynthesis has been well studied in higher plants, algae, cyanobacteria as well as in green and purple bacteria (Blankenship, 2002). These organisms utilize sunlight to power their cellular processes and derive their biomass through chemical reactions driven by light. Photosynthesis is initiated by photon absorption in an antenna pigment. A wide variety of different antenna complexes are found in different photosynthetic systems (Blankenship, 2002) using pigments such as (bacterio)chlorophylls (B)Chl, carotenoids and bilins (*i.e.*, open-chain tetrapyrroles). Antennas allow to increase the spectral range of the photons as well as the absorption cross section without having to build an entire reaction center. Due to the functional organisation of the antenna, excitations are transferred into the photosynthetic reaction center (RC) in which the charge separation occurs. The RC is an integral membrane pigment-protein complex that carries out light-driven electron transfer reactions. One or more electronically excited BChl molecules transfer an electron to nearby acceptor molecules, thereby creating an ion pair state consisting of the oxidized primary donor and a reduced acceptor. After this initial electron transfer event, a series of electron transfer reactions takes place that eventually stabilizes the stored energy in forms that can be used by the cell. The RC complex from the anoxygenic purple bacteria namely

Rhodobacter sphaeroides is the best understood of all photosynthetic RCs, from both a structural and a functional point of view (Deisenhofer & Norris, 1993; Blankenship *et al.*, 1995). These were the first reaction center complexes to be purified and studied by picosecond kinetic methods and the first even to have X-ray structures resolved (Hunter *et al.*, 2008). Much of the molecular level understanding of the early events in photosynthesis is based on the information derived from this system.

1.1.2 Overview of Purple Bacteria

Purple bacteria are photosynthetic gram-negative prokaryotes that convert light energy into chemical energy by the process of anoxygenic photosynthesis. Purple bacteria contain photosynthetic pigments–bacteriochlorophylls and carotenoids—and can grow using inorganic materials as a source of nutrients, with CO_2 as sole carbon source and using photosynthesis or chemosynthesis as a source of energy. Purple sulfur bacteria differ from purple nonsulfur bacteria on both metabolic and genetic basis. The species of two major groups often coexisted under light and anoxic places in nature. Purple sulfur bacteria are poorly equipped for metabolism and growth in the dark, while the purple nonsulfur bacteria possess diverse capacities for dark metabolism and growth. Purple nonsulfur bacteria are a physiologically versatile group of purple bacteria that can grow well both phototrophically and in darkness. Many genera of purple nonsulfur bacteria are known and one of the most widely studied is *Rhodopseudomonas sphaeroides*. This was first identified and named by van Niel (van Niel, 1944). Later this generic name has been changed to *Rhodobacter* (*R.) sphaeroides* and continued to hold the same name (Hunter *et al.*, 2008). These bacteria contain complexes that catalyze light-induced electron and proton transport across the photosynthetic membrane and have been optimized by nature to perform with quantum efficiency close to unity. They grow most rapidly with N_2 as sole nitrogen source and show the highest rates of *in vivo* nitrogenase activity (Madigan, 1984). Purple nonsulfur bacteria occasionally form dense blooms in habitats where levels of sulfide are

either low or undetectable. They are also present in sewage(Holm & Vennes, 1970; Siefert *et al.*, 1978) and waste lagoons (Jones, 1956; Cooper *et al.*, 1975).

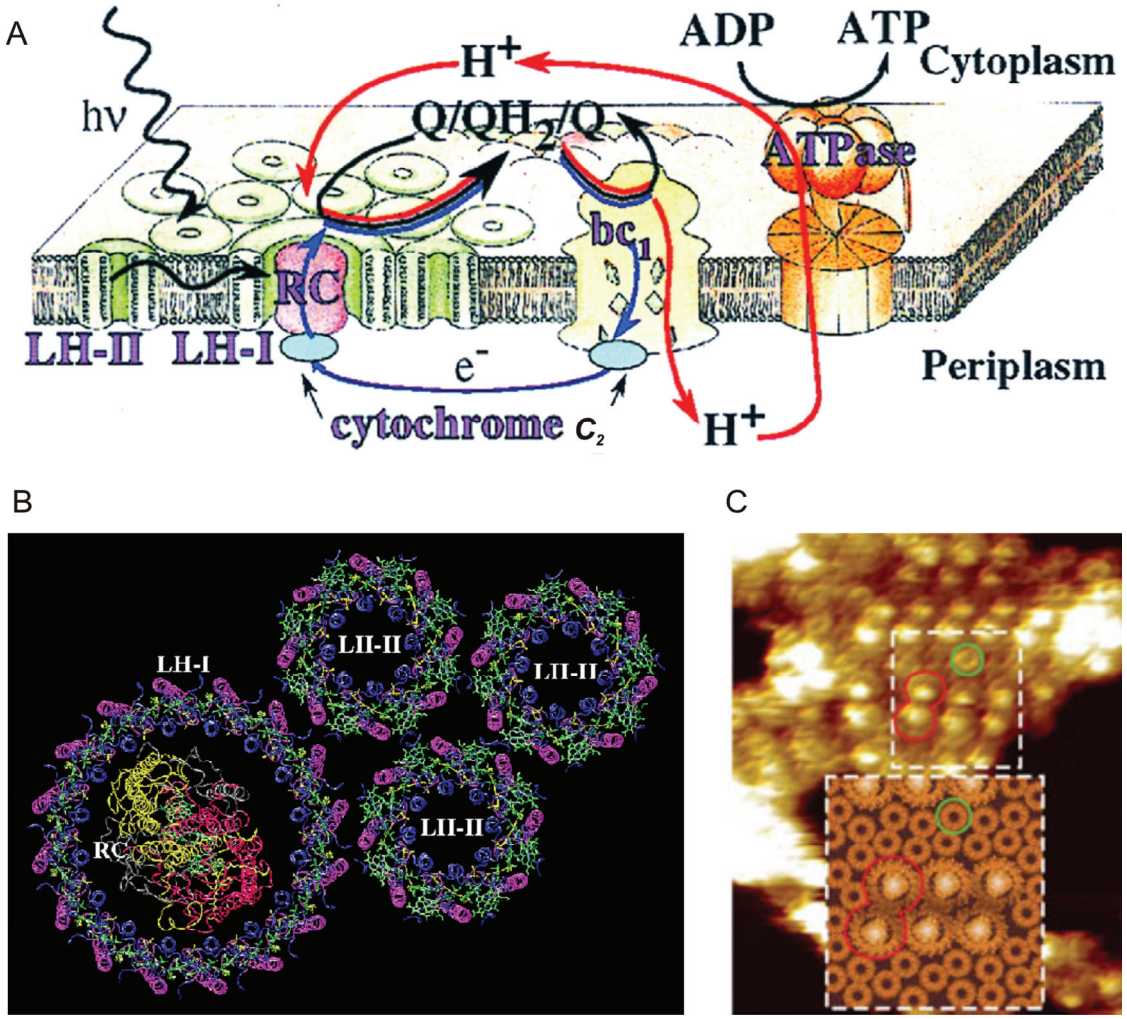

Figure 1.1 (A) Schematic representation of the photosynthetic apparatus in the intracytoplasmic membrane of purple bacteria. The RC (red) is surrounded by the light-harvesting complex I (LH-I, green) to form the LH-I–RC complex, which is surrounded by multiple light-harvesting complexes LH-II (green), forming altogether the PSU. Photons are absorbed by the light-harvesting complexes and excitation is transferred to the RC initiating a charge (electron-hole) separation. The RC binds quinone, reduces it to hydroquinone and releases the latter. This hydroquinone is oxidized by the bc_1 complex, which uses the exothermic reaction to pump protons across the membrane; electrons are shuttled back to the RC by the cytochrome c_2 complex (blue) from the ubiquinone–cytochrome bc_1 complex (yellow). The electron transfer across the membrane produces a large proton gradient that drives the synthesis of ATP from ADP by the ATPase (orange). Electron flow is represented in blue, proton flow in red, and quinone flow, likely confined to the intramembrane space, in black (Hu *et al.*, 1998) Copyright (© 1998) National Academy of Sciences, U.S.A. (B) Arrangement of pigment–protein complexes in the modeled bacterial PSU of *R. sphaeroides*. (Hu *et al.*, 1998) Copyright (© 1998) National Academy of Sciences, U.S.A. (C) AFM picture of photosynthetic membrane, LH2 complexes (green) funnel light energy to RC-LH1 complexes (red) as seen by AFM (small square) or by molecular modeling (bigger square) Reprinted by permission from Macmillan Publishers Ltd: Nature, ref (Bahatyrova *et al.*, 2004) © 2004.

1.1.3 The photosynthetic membrane of purple bacteria

The photosynthetic apparatus of these purple bacteria (Figure 1.1) consists of light harvesting antenna complexes (LH), the RC protein, an ubiquinone-cytochrome *b/c* oxidoreductase complex and ATP synthase (Hu *et al.*, 1998). The energy flow is facilitated by the peripheral light-harvesting complex, LH2, the core light-harvesting complex, LH1 (Karrasch *et al.*, 1995; McDermott *et al.*, 1995; Hu & Schulten, 1998; Bahatyrova *et al.*, 2004) and the RC (Deisenhofer *et al.*, 1985; Allen *et al.*, 1987; Ermler *et al.*, 1994; Camara-Artigas *et al.*, 2002a). The RC reduces quinone to hydroquinone as a result of electron transfer; subsequently the ubiquinol-cytochrome c_2 oxidoreductase (bc_1 complex) (Crofts *et al.*, 1983; Valesco & Crofts, 1991; Gennis *et al.*, 1993; Xia *et al.*, 1997) oxidizes hydroquinone and reduces cytochrome c_2, which completes the cycle by shuttling electrons back to the RC. The ATP-synthase (Junge *et al.*, 1997; Fillingame, 2000; Fillingame *et al.*, 2000) makes use of the resulting proton gradient. The purple bacterial photosynthetic unit displays a certain simplicity in contrast to its counterpart in plants and the supramolecular organization of the constituent proteins is difficult to determine and must be ascertained by combining atomic force microscopy (Bahatyrova *et al.*, 2004; Scheuring *et al.*, 2004; Scheuring & Sturgis, 2005; Scheuring *et al.*, 2005), cryo-electron microscopy (Jungas *et al.*, 1999; Siebert *et al.*, 2004; Qian *et al.*, 2005) and linear dichroism (Frese *et al.*, 2004) studies.

1.1.4 Structure and function of purple bacterial RCs

The structure and function of purple bacterial RCs have been studied over many decades. The crystallographic determination of the RC structure was the first of a membrane protein and has been awarded by the Nobel prize of Chemistry in 1994 to Deisenhofer, Huber and Michel (Deisenhofer *et al.*, 1985).

The RC of *R. sphaeroides* is a transmembrane protein complex made of three major polypeptides, L, M and H (for light, medium and heavy) (Yeates *et al.*, 1987; Ermler *et al.*, 1994; Camara-Artigas *et al.*, 2002a), see Figure 1.2A. The L and M subunits contain five transmembrane α-helices, which are packed together in a

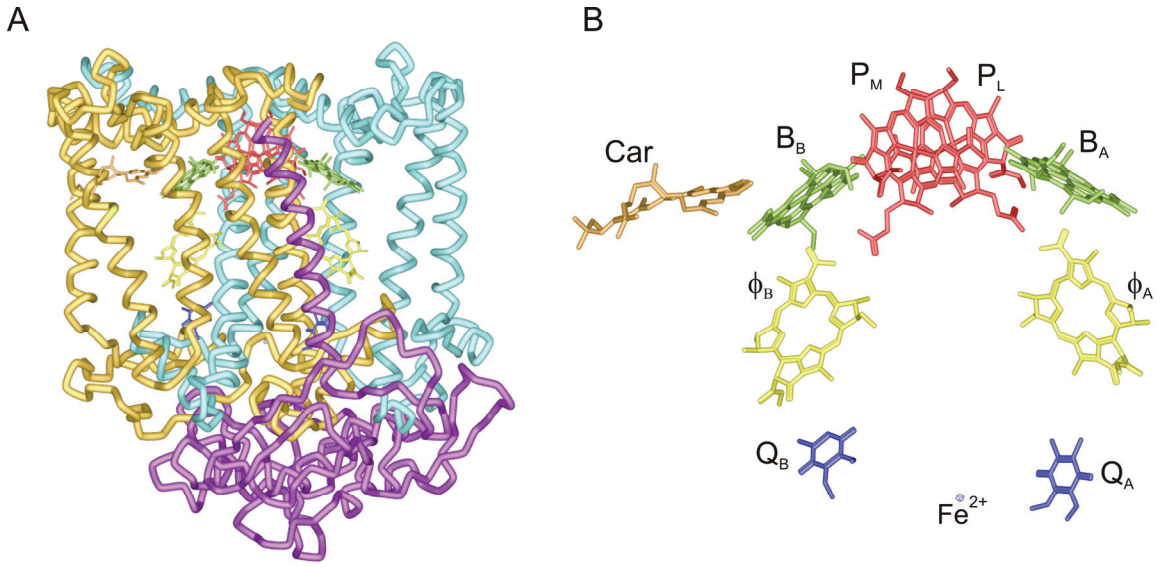

Figure 1.2: (A) The complex arrangement of 3 polypeptide subunits are represented in different colors with a ribbon representation, L (blue), M (yellow) and H (violet) with RC. (B) Clear view of cofactors in the reaction center (RC) of *R. sphaeroides* wild type (WT). The primary electron donor, the special pair, is formed by the two bacteriochlorophyll a (BChl) molecules P_L and P_M. B_A and B_B are accessory BChl cofactors. Φ_A and Φ_B are bacteriopheophytin (BPhe) cofactors. On the acceptor side, two ubiquinone-10 cofactors Q_A and Q_B with a non-heme iron in between are localized. Side chains are omitted for sake of clarity. The symmetry of the cofactor arrangement is broken by a carotenoid cofactor (Car). The light-induced electron transfer occurs selectively via branch A. [PDB entry 1M3X, the figure has been made with Accelrys Discovery Studio] (Camara-Artigas *et al.*, 2002b).

nearly symmetrical way. Subunit H is more globular in shape and is located mainly in the cytoplasmic side of the membrane. The L and M subunits bind the cofactors. Four molecules of bacteriochlorophyll *a* (BChl *a*), two molecules of bacteriopheophytin *a* (BPhe *a*), two ubiquinone-10 molecules (Q), a non-heme iron (Fe^{2+}) and a carotenoid molecule (Car) form the cofactors of the RC protein. The arrangement of the cofactors is shown in Figure 1.2B.

The cofactors form two nearly symmetric branches, the "active" A-branch and the "inactive" B-branch. Two BChls form the primary donor (P), a tightly interacting dimer called the "Special Pair" (P_L and P_M). On either side of the special pair an additional BChl molecule is located, known as the accessory BChl (B_A and B_B). The two BPhe (Φ) are positioned at an edge-to-edge distance of ~14 Å from the special pair.

Situated below the BPhe are the ubiquinones-10, (Q_A and Q_B). Finally, the non-heme Fe^{2+} ion is located in the center of the two branches near the cytoplasmic

side of the membrane. The tenth cofactor, the carotenoid molecule, breaks the apparent symmetry of the cofactor arrangement and is located near B_B. In the RC of *R. sphaeroides* R26, a mutant strain, the carotenoid molecule is not present.

1.1.5 Spectroscopy of RCs

The purple bacterial RC has been studied with many spectroscopic techniques (Hoff & Deisenhofer, 1997). The BChl and BPhe cofactors in particular have distinctive absorbance spectra that provide a very sensitive probe of the structural and functional integrity of the complex, and provide a means to follow the route and rate of light-driven electron transfer.

The absorbance spectrum of the purified *R. sphaeroides* RC is shown in Figure 1.3. Owing to their electronic structure, the BChl and BPhe cofactors give rise to three sets of absorbance bands in the so-called Soret (300–420 nm), Q_x (500–630 nm) and Q_y (650–950 nm) regions. Molar absorption coefficients (ε) for the prominent bands in the Q_y region allow the concentration of RCs to be monitored. A particularly useful feature of the spectrum is that the purity of the complex can be measured from the ratio of protein absorbance at 280 nm to BChl absorbance at 802 nm, with a ratio of 1.3 or less indicating RCs of sufficient purity for crystallization (Okamura *et al.*, 1974). The structural integrity of the RC can be checked through characteristic spectral changes that take place as the protein

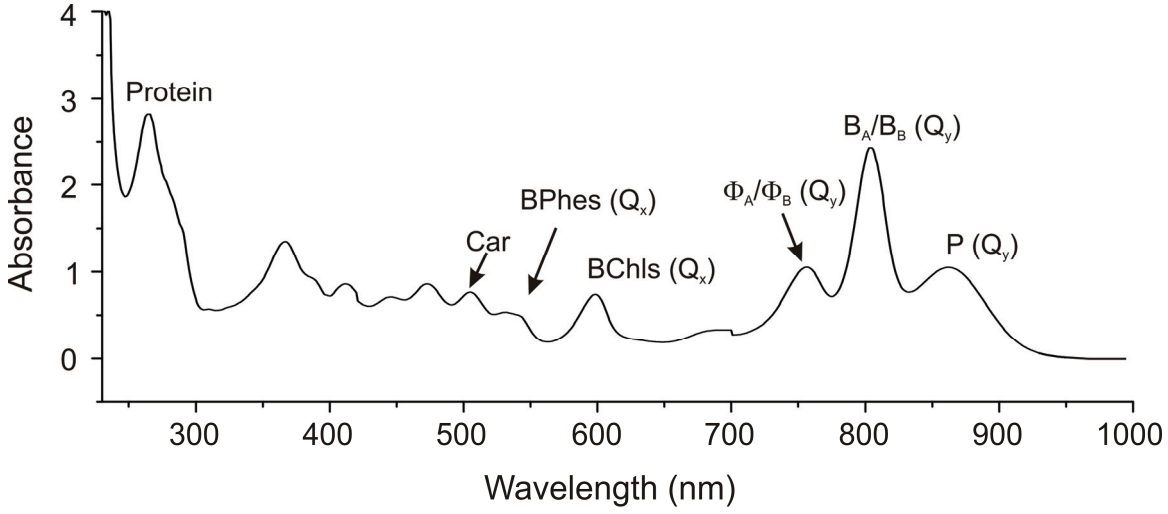

Figure 1.3 The absorbance spectrum of the purified RC of *R. sphaeroides* (WT).

unfolds and the cofactors are released from their native binding sites (Hughes *et al.*, 2006). Photo-oxidation of the RC is accompanied by respective changes in its absorbance spectrum, and especially the Q_y absorbance band attributed to the P BChls at 870 nm vanishes (the term 'bleached' is often used to describe this). The primary donor BChls were first identified through photobleaching of the absorbance band of a BChl species at 870 nm.

1.1.6 Energy and Kinetics of RCs

Though many spectroscopic techniques have been applied, the technique of picosecond-absorbance transient-difference spectroscopy has been very informative with respect to finding the path of the electron flow in these complexes (Blankenship, 2002). Figure 1.4 A and B summarizes the kinetics and energetics of the electron transfer process. After photochemical excitation of P to P*, one electron is transferred to the primary electron acceptor Φ_A within 4 ps, forming the primary radical pair state $P^+\Phi_A^-$ (Martin *et al.*, 1986). The Φ_A^- anion radical decays in about 200 ps and transfers the electron to the ubiquinone Q_A. The

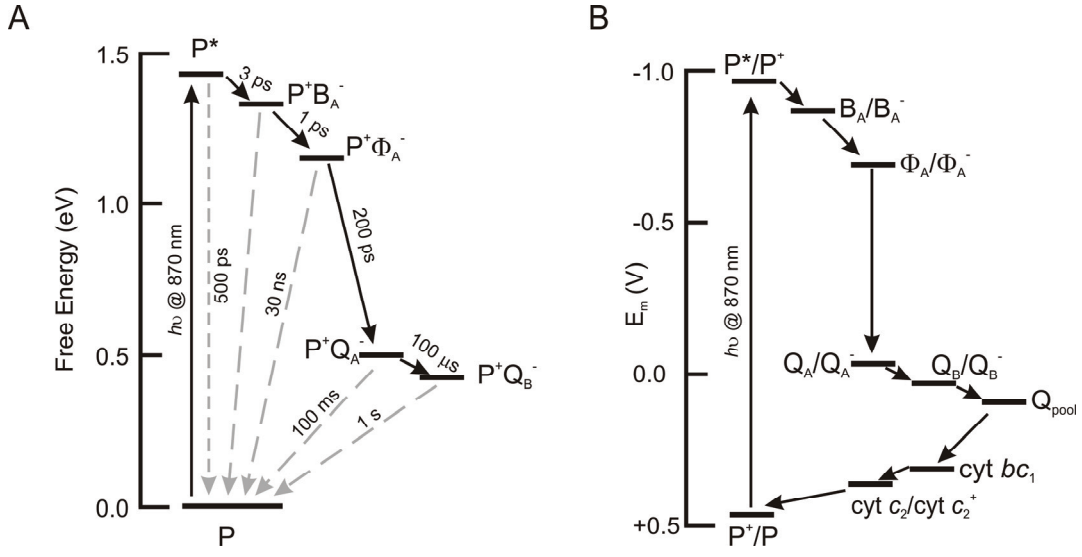

Figure 1.4 (A) Free energies of the states involved in light-activated charge separation in the RCs. (B) Midpoint redox potentials of centres involved in light-driven cyclic electron transfer. Centres are labelled using the convention reactant/product. Cyt bc_1 refers to electron transfer through the high-potential chain formed by the iron–sulfur centre and cytochrome c_1. "This research was originally published in Biochemical Society Transactions. Jones, M. R., The petite purple photosynthetic powerpack. Biochemical Society Transactions. 2009; 37: 400-407 © the Biochemical Society".

electron subsequently moves from Q_A to Q_B in 100 μs reducing Q_B once. Meanwhile, the oxidized primary electron donor P is re-reduced by accepting an electron from cytochrome *c* at the periplasmic side of the protein. The RC can be excited again and Q_A can give a second electron to Q_B. The doubly reduced and protonated Q_B leaves the RC to the ubiquinone pool. New ubiquinone from the ubiquinone pool of the membrane replaces the ubiquinol leading to the initial state of the RC. The movement of charge through the RC proceeds with extremely high quantum efficiency, and at each stage in electron transfer the productive forward reaction (black arrows) is much faster than competing reactions such as recombination of radical pairs to the ground state (grey arrows). To achieve this, movement of the electron through the RC involves the formation of radical pairs with progressively decreased free energies (Figure 1.4B). The P* excited state is a strong reductant, with an estimated excited state redox potential of -940 mV *vs* normal hydrogen electrode (Jones, 2009).

1.1.7 The Solid-state photo-CIDNP effect

The discovery of the solid-state photo-CIDNP effect (for reviews, (Jeschke & Matysik, 2003; Daviso *et al.*, 2008b) by Zysmilich and McDermott in 1994 in frozen and quinone-blocked bacterial RCs of *R. sphaeroides* R26 by ^{15}N magic-angle spinning (MAS) NMR under continuous illumination with white light offered NMR access to the electron-nuclear processes during the charge separation (Zysmilich & McDermott, 1994). By induction of a non-Boltzmann nuclear spin order upon photo-reaction in rigid samples, a signal enhancement of a factor of more than 10,000 has been observed by ^{13}C MAS NMR in several RCs (Prakash *et al.*, 2005; Prakash *et al.*, 2006). In the meantime, the solid-state photo-CIDNP has been observed also on *Rhodopseudomonas acidophila* (Diller *et al.*, 2008) of the green sulphur bacterium *Chlorobium tepidum*, (Roy *et al.*, 2007) of the heliobacterium *Heliobacillus mobilis* (Roy *et al.*, 2008) as well as of the photosystems I and II of plants (Matysik *et al.*, 2000a; Alia *et al.*, 2004; Diller *et al.*, 2007b) and algae (Janssen *et al.*, 2010). The signal enhancement provided by the solid-state photo-CIDNP

effect may thus be considered an intrinsic property of natural photosynthetic RCs and allows directly resolving the signals of ^{13}C atoms within the RC (Matysik *et al.*, 2009).

Under continuous illumination on RCs of *R. sphaeroides* WT, two solid-state mechanisms run in parallel to induce net nuclear polarization which remains under steady-state conditions (Jeschke & Matysik, 2003; Daviso *et al.*, 2008b): (i) Electron–electron–nuclear three-spin mixing (TSM) breaks the balance by coherent evolution of the correlated radical pair state in interaction with the nuclear spins and the applied magnetic field, depending on the signs of the electron–electron and of the anisotropic electron–nuclear interactions (Jeschke, 1997, 1998). (ii) In the electron-nuclear differential decay (DD) mechanism (Polenova & McDermott, 1999) only a single matching condition with a dependence of secular part of the hyperfine coupling is required and the difference of singlet and triplet radical pair lifetimes must be of the order of the inverse hyperfine coupling (Jeschke & Matysik, 2003). The mechanism has been summarized and explained in Chapter 2 (this thesis). Understanding of the spin-chemical processes (Daviso *et al.*, 2009a) allowed to apply photo-CIDNP MAS NMR as an analytical tool for elucidating electronic structures of the cofactors forming radical pairs (Daviso *et al.*, 2009c).

1.2 Theoretical background of Solid State NMR

1.2.1 Basic interactions in solid state NMR

Nuclear magnetic resonance (NMR) has established its own importance starting from structural characterization of liquids, compounds in solution and solids, further to polymers, proteins and also membrane proteins (Schmidt-Rohr & Spiess, 1994). The advances in multidimensional NMR have been exploited in many fields in physics, chemistry, material science and also in biology.

Lorentz predicted the splitting of spectral lines of an atom placed in an external magnetic field on the basis of classical theory. This splitting was first observed by Zeeman. The Zeeman interaction in NMR describes the interaction

between the nuclear magnetic moment (μ) of a spin with an external static magnetic field B_0 in the spin Hamiltonian, and is expressed as

$$H_0 = -\mu \cdot B_0 . \qquad 1.1$$

The magnetic moment (μ) can be expressed in terms of a nuclear spin operator I as $\mu = \gamma\hbar I$, and equation 1.1 can be rewritten as

$$H_0 = -\gamma\hbar I_z B_0 \qquad 1.2$$

assuming that B_0 points in the Z-direction. Although the Zeeman interaction is the most dominant interaction in NMR and generally determines the quantization z-axis of the spins, it contains little structural information in itself (Abragam, 1961).

In NMR, relevant chemical and structural information originates from the local fields that the nuclear spins experience. These fields are due to the shielding of the B_0 field by the electron clouds and from all the interactions between the spins. For an ensemble of nuclear spins placed in a large magnetic field containing two types of nuclei, *i.e.* abundant spins *I* (e.g., ^{1}H) with a gyromagnetic ratio γ^I and a resonant frequency of ω_I and a rare spin *S* (e.g., ^{13}C, ^{15}N) with a gyromagnetic ratio of γ^S and a resonance frequency of ω_S, the interactions can be described in the spin Hamiltonians by the chemical shift term H_{CS}, and the homonuclear and heteronuclear dipolar terms, H_D^{II} and H_D^{IS} respectively. In the lab frame all the interactions can be represented by the spin Hamiltonian

$$H = H_0 + H_{CS} + H_D^{II} + H_D^{IS} . \qquad 1.3$$

1.2.2 Chemical shielding Hamiltonian

The chemical shielding Hamiltonian describing the electron distribution acting on a spin *I*, is expressed by

$$H_{CS} = -\gamma\sigma_{zz} I_z B_0 , \qquad 1.4$$

where $\sigma_{pq}(p,q = x,y,z)$ are the components of chemical shielding tensor, in the laboratory frame where the z axis is along the static magnetic field.

The electronic distribution around a nucleus in a molecule is rarely spherically symmetric. Since the chemical shielding arises from the electronic surroundings of a nucleus, its value depends on the orientation of the molecule in the magnetic field B_0. This orientation dependence is best described in terms of a chemical shielding tensor, which is a 3×3 matrix with elements σ_{pq} determined by the orientation of the laboratory frame with respect to a molecular principle axes frame where $\sigma_{PQ} = 0$ for $P \neq Q$ and by σ_{XX}, σ_{YY} and σ_{ZZ} themselves.

In solid-state NMR, the three principal axis tensor elements are often replaced by

$$\sigma_{iso} = \frac{1}{3}\left(\sigma_{XX} + \sigma_{YY} + \sigma_{ZZ}\right), \qquad 1.5$$

$$\delta = \sigma_{ZZ} - \sigma_{iso}, \qquad 1.6$$

$$\eta = \frac{\sigma_{XX} - \sigma_{YY}}{\delta} \qquad 1.7$$

Here, σ_{iso} is the isotropic value, while δ and η are the chemical shift anisotropy (CSA) and asymmetry parameter, respectively (Schmidt-Rohr & Spiess, 1994; Duer, 2004).

The expression for the anisotropic frequency shift of a single site in a static sample can be derived from the values δ, η and the polar angles (θ,ϕ) of the B_0 field in the principal axis system

$$\omega(\theta,\phi) = \frac{1}{2}\delta(3\cos^2\theta - 1 - \eta\sin^2\theta\cos(2\phi))\gamma B_0 . \qquad 1.8$$

And the chemical shielding Hamiltonian H_{CS} in the principal axis system becomes

$$H_{\mathrm{CS}} = \{\sigma_{\mathrm{iso}} + \frac{1}{2}\delta[3\cos^2\theta - 1 - \eta\sin^2\theta\cos(2\phi)]\}\gamma B_0 I_z . \qquad 1.9$$

1.2.3 Dipolar coupling Hamiltonian

The heteronuclear coupling is responsible for much of the broadening observed in the solid-state NMR spectrum. Since each spin represents a nuclear magnetic moment that produces a small magnetic field, every spin "feels" the magnetic field

produced by the nearby spins. The strength of the heteronuclear dipolar coupling is represented by the truncated dipolar Hamiltonian

$$H_{\mathrm{D}}^{IS} = -\frac{\mu_0}{4\pi}\hbar\sum_i\sum_j \frac{\gamma^I\gamma^S}{r_{ij}^3}\frac{1}{2}(3\cos^2\theta_{ij}-1)2I_z^iS_z^j, \qquad 1.10$$

where r_{ij} represents the internuclear distance, μ_0 is the vacuum permeability, γ^I and γ^S are the gyromagnetic ratios of the interacting *I* and *S* spins, respectively, and I_z^i and S_z^j are the z-components of the nuclear spin angular momentum operators respectively. The angle θ_{ij} describes the orientation of the internuclear vector with respect to the orientation of the external magnetic field. Since the magnitude of the coupling between two nuclear spins has a r^{-3} distance dependence, the dipolar coupling is a long-range through space interaction. Spins also experience a homonuclear dipolar coupling, which results from an interaction between spins of the same species. The homonuclear dipolar Hamiltonian of the *I* spins is given by

$$H_{\mathrm{D}}^{II} = -\frac{\mu_0}{4\pi}\hbar\sum_i\sum_j \frac{\gamma^{\mathrm{I}}\cdot\gamma^{\mathrm{I}}}{r_{ij}^3}\frac{1}{2}(3\cos^2\theta_{ij}-1)(3I_z^iI_z^j-\mathbf{I}^i\cdot\mathbf{I}^j). \qquad 1.11$$

There again r_{ij} and θ_{ij} represent the internuclear distance and the angle between this internuclear vector and the external magnetic field, respectively. Two equivalent spins are able to undergo an energy-conserving "flip-flop" transition in which one spin flips up while the other spin flips down (Schmidt-Rohr & Spiess, 1994).

1.3 High resolution NMR Techniques for solids

In liquid-state NMR, spectra consist of a series often resolved lines that are due to the averaging of the anisotropic NMR interactions by rapid tumbling of the molecules. In contrast, in solid-state NMR the effects of anisotropic interactions are observed and hence the resulting signals are generally very broad. Therefore special techniques for coherent averaging of the couplings "in spin space" and "in real space" by sample rotations and pulse sequence are essential for high resolution solid state NMR spectra (Schmidt-Rohr & Spiess, 1994).

1.3.1 Magic angle spinning

Magic-angle spinning (MAS) is routinely used in the majority of solid-state NMR experiments. As discussed in earlier sections 1.2.2 and 1.2.3, the dependence on the molecular interaction is of the form $\left(3\cos^2\theta - 1 - \eta\sin^2\theta\cos(2\phi)\right)$, where the angle (θ,ϕ) describes the orientation of the interacting tensors, in particular the chemical shielding and dipolar coupling $(\eta = 0)$ tensors. In the MAS experiment, the sample is spun rapidly in a cylindrical rotor around a spinning axis oriented at the magic angle $\left(\theta_m = \arccos\left(1/\sqrt{3}\right) = 54.74^0\right)$ with respect to the applied magnetic field B_0 (Andrew *et al.*, 1958; Lowe, 1959). MAS makes the average of the heteronucelar dipolar coupling and CSA interactions zero. Thus at fast sample rotation, the inhomogeneous anisotropic line broadenings are removed resulting in narrow central lines flawed by narrow sidebands. The spinning also partially removes homonuclear dipolar-coupling effects. For a detailed mathematical description of MAS, see (Duer, 2004).

1.3.2 Cross-polarization

Cross-polarization (CP) is the most important signal enhancement technique in solid-state NMR. It was introduced in 1962 by Hartmann and Hahn for static samples. Here nuclear polarization is transferred from abundant spins (I = ^{1}H) to rare spins (S = ^{13}C, ^{15}N) relying on the heteronuclear dipolar interaction (Figure 1.5). The maximum possible enhancement factor for the signals of the rare spins is given by γ_I / γ_S, which is 4 for ^{1}H and ^{13}C (Schmidt-Rohr & Spiess, 1994). The

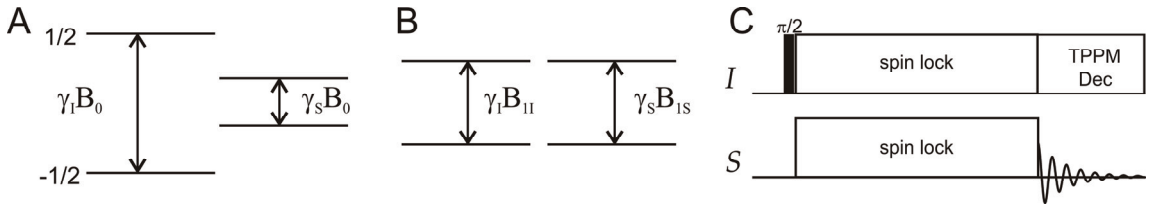

Figure 1.5 Energy levels of the I (^{1}H) and S (^{13}C) spins. (A) In the laboratory frame the transfer of magnetization is not possible. (B) In the rotating frame the transfer of magnetization is possible as the energy separation is determined by the rf-field. The matching condition is then fulfilled. (C) Pulse sequence for HH-CP.

transfer can be described in the doubly rotating frame, that is, one in which the ^{1}H spins are considered in a frame in which all the rf irradiation fields during ^{1}H pulses appear static, and the *S* spins are considered in a frame in which all the rf fields appear static. Here we assume that all pulses are exactly on resonance for the spins to which they are applied. The simple pulse sequence is shown in Figure 1.5B. An initial $\pi/2$ pulse is applied on the *I* spins and the resulting magnetization is locked at an rf field B_{1I}. Simultaneously another spin-lock field of B_{1S} is applied to the *S* spins that has the same nutation frequency $\omega_{1S} = \gamma_S B_{1S}$ as the one on the *I* spins $\omega_{1I} = \gamma_I B_{1S}$, thus satisfying the Hartmann-Hahn (HH) condition (Hartmann & Hahn, 1962)

$$\omega_{1I} = \omega_{1S} . \qquad 1.12$$

The transfer depends on how well the HH condition is fulfilled. Typical rf-field strengths for the HH CP are between 50 kHz and 100 kHz. The optimal CP contact time depends on the size of the heteronuclear dipolar coupling and on rotating frame relaxation times $T_{1\rho}$ of the two spins.

Advantages of the CP over the direct excitation of low abundant spins are the increase in polarization and faster repetition delays due to shorter relaxation times of abundant spins. CP can be combined with MAS leading to modified HH matching conditions

$$\pm\left(\omega_{1I} - \omega_{1S}\right) = n\omega_r . \qquad 1.13$$

Here the difference between the rf-field amplitudes must be an integral multiple of the spinning frequency (Stejskal *et al.*, 1977; Stejskal *et al.*, 1984).

1.3.3 Spin decoupling

Although MAS removes the main effects of the anisotropic dipolar interactions on the linewidths, higher order effects must be still removed by spin decoupling. This can be achieved through the application of rf-frequency irradiation schemes on the non-observed spins for heteronuclear interactions and on the observed spins for homonuclear interactions. There are several techniques either for heteronuclear decoupling, such as CW and gated decoupling, TPPM, SPINAL, XiX, SW$_f$-TPPM

or for homonuclear decoupling such as LG, WAHUHA, MREV-8, BR-24, FSLG, PMLG, DUMBO etc. A few of the mentioned techniques are discussed below.

1.3.3.1 Continuous wave (CW) decoupling

For a spin system, where a single spin *S* is coupled to a number N of *I* spins, continuous high power rf-field irradiation on the *I* spins eliminates the effect of the heteronucelar couplings on the observed *S* spin, regardless of the states of its magnetization (Sarles & Cotts, 1958).

1.3.3.2 Two-pulse phase modulated decoupling (TPPM)

TPPM was the first multiple-pulse decoupling sequence (Bennett *et al.*, 1995) which improved heteronuclear decoupling efficiency compared to CW decoupling. This sequence consists of a continuous repetition of two pulses of length τ_p and phase $\pm\phi$. The phase and the angle of the pulses are 15^0 and 180^0, but in practice the exact phase and length values are best optimized experimentally. At slow spinning speeds, the variation of these values of efficient decoupling is quite large, but at high MAS frequencies, the sequence needs to be optimized very carefully in order to obtain narrow lines.

1.3.3.3 Lee-Goldburg (LG) decoupling

MAS can be used to remove the effects of the homonuclear dipolar couplings on NMR spectra, provided the spinning frequency is much faster than the strength of the dipolar interactions, which for protons are usually of the order of tens of kHz. Thus spinning frequencies up to 70 kHz are not sufficient to decouple and multiple-pulse sequences must be applied to suppress the homonuclear dipolar line-broadening effects. The Lee-Goldburg scheme is shown in Figure 1.6. The basic principle of this technique is to irradiate the protons continuously with an off-resonance rf-field of intensity $\omega_1 = -\gamma B_1$ and off resonance value $\Delta\omega_{LG} = \omega_{rf} - \omega_0$, in such a way that the total effective field B_{eff} in the rotating frame is inclined at the magic angle $\theta_m = 54.74^0$ with respect to the static magnetic

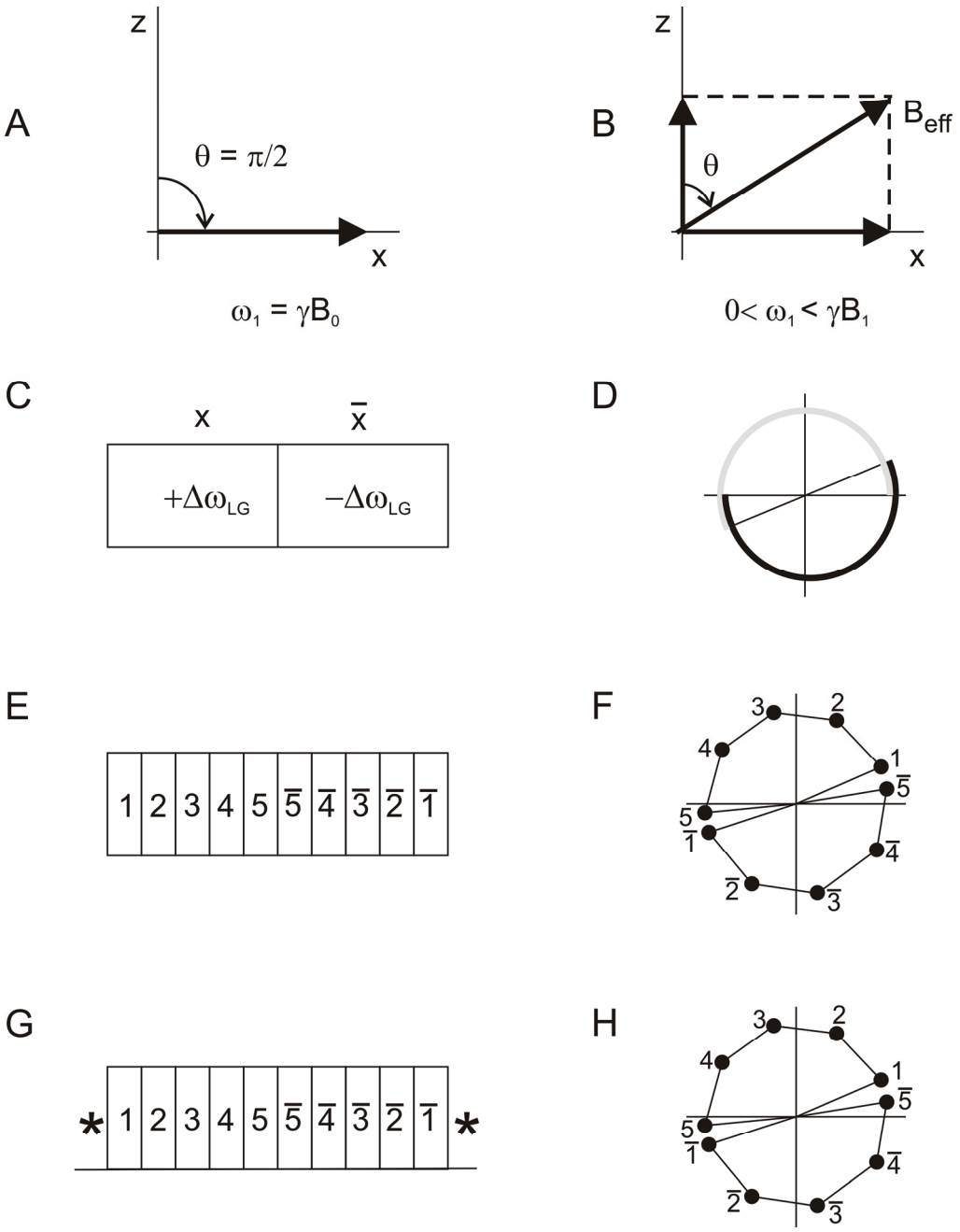

Figure 1.6 The Lee-Goldburg scheme, viewed from rotating frame, where $\omega_{frame} = -\omega_{RF}$ around the z-axis. (A) on-resonance, (B) off-resonance with rf-fields. The pulse schemes and time dependent rf irradiation field profiles in the xy-plane of the on-resonance rotating frame of FSLG (C, D), PMLG5 (E, F) and *w*PMLG5 (G, H). Asterisks denote possible data sampling points. The rotation frequencies ΔLG (grey) and −ΔLG (black) of the irradiation vector in the case of FSLG obey the relation ΔLG = $\omega_1/\sqrt{2}$, where ω_1 is the rf intensity. The continuous time-dependent phase in FSLG is replaced in PMLGn by n discrete phases (shown by dots in E – H). The set of phase values for both PMLG5 and for *w*PMLG5 are given below

$$\phi_1 = 20.78^0, \phi_2 = 62.34^0, \phi_3 = 103.9^0, \phi_4 = 145.46^0, \phi_5 = 187.02^0, \phi_{\bar{5}} = 7.02^0, \phi_{\bar{4}} = 325.46^0,$$
$$\phi_{\bar{3}} = 283.9^0, \phi_{\bar{2}} = 242.34^0, \phi_{\bar{1}} = 200.78^0$$

field direction. The LG condition is given by

$$\pm \Delta\omega_{LG} = \pm \frac{1}{2}\sqrt{2}|\omega_1| \qquad 1.14$$

(Lee & Goldburg, 1965).

The LG irradiation scheme averages the homonuclear dipolar interaction to zero-order, and a scheme can be incorporated with standard HH-CP to suppress the proton-proton interactions during the CP transfer experiment. This is referred to as LG-CP. Several variations and modifications of the LG scheme, to improve the averaging of spin-space interactions are in use. For example: (i) Frequency-switched LG (FSLG): This involves application of an off-resonance rf-field at $+\Delta\omega_{LG}$ for a duration of τ_{LG} with phase x, immediately followed by the application of another off-resonance rf-field at $-\Delta\omega_{LG}$ for a duration of τ_{LG} with phase $\bar{x}$ (Mehring & Waugh, 1972; Bielecki *et al.*, 1989; Levitt *et al.*, 1993). This involves simultaneous switching of both the phase and the frequency of the rf-irradiation as shown in Figure 1.6 (C & D). (ii) Phase-modulated LG (PMLG): This consists of a series of pulses in which the phase is changed, while their frequencies are kept constant. Hence, in both FSLG and PMLG, both the zero- and the first-order homonuclear dipolar interactions are averaged. A PMLG*n* cycle approximates an LG unit by *n* on-resonance pulses, each with duration of τ_{LG}/n, with n= 3,5,9… and a phase increment of $\Delta\Phi = 207.8/n$ between successive pulses, again followed by the same set of pulses in the reverse order with an overall phase shift of 180^0 with respect to the first set. The pulse sequence and the rf profile in the on-resonance rotating frame are shown in Figure 1.6 (E & F). High-resolution ^{1}H spectra can then be obtained in a 1D way by inserting observation windows in the PMLG cycle, *w*PMLG*n* (Vinogradov *et al.*, 2002). The rf-schematic of this approach is shown in Figure 1.6 (G & H) (Vinogradov *et al.*, 2005). Implementing such sequences is experimentally challenging since the free-induction decay (FID) data points are collected at particular points in between sets cycle of pulses. High power with short pulse lengths is required to achieve maximum decoupling efficiency.

1.3.4 Recoupling techniques

Fast MAS averages the inhomogeneous and partly the homogeneous anisotropic interactions present in the solid-state, giving rise to narrow lines in the spectra. As a result, the structural information about the distance and orientation content of these interactions is lost. Using recoupling techniques, it is possible to reintroduce homonuclear and heteronuclear dipolar couplings even under MAS conditions. Recoupling reintroduces the anisotropic interactions under MAS by interfering with the averaging of the spatial part through manipulations of the spin part. Such techniques are based on the fact that the dipole-dipole coupling between nuclei that are spatially close permits the build-up of zero-quantum or double-quantum coherences. These can be classified into heteronuclear and homonuclear recoupling sequences.

1.3.4.1 Heteronuclear recoupling sequence

CP and phase- or frequency- switched LG-CP under MAS conditions are examples for heteronuclear recoupling of dipolar interactions. Examples of other well known solid-state NMR recoupling techniques are R3, REDOR and TEDOR (Oas *et al.*, 1988; Gullion & Schaefer, 1989; Hing *et al.*, 1992). In particular we should mention that the symmetry theory of recoupling (Levitt, 2002) has facilitated the plan of designing rotor-synchronized radio-frequency pulse sequences which selectively restore subsets of spin interactions, and suppress others (Eden & Levitt, 1999; Carravetta *et al.*, 2000; Brinkmann & Levitt, 2001).

1.3.4.2 Homonuclear recoupling sequences

A number of sequences for broadband ^{13}C–^{13}C dipolar recoupling under MAS conditions have been developed, such as PDSD, RFDR and DARR (Szeverenyi *et al.*, 1982; Bennett *et al.*, 1992; Takegoshi *et al.*, 2001). PDSD (Proton-Driven Spin Diffusion) was one of the first experiments used for dipolar-mediated polarization transfer under MAS. The transfer of magnetization from ^{13}C to ^{13}C occurs directly through space and is mediated by the interaction with the protons. The polarization transfer is inefficient when the ^{13}C-^{13}C dipolar coupling is smaller

than the difference of their resonance frequencies. Since no rf radiation is applied during the PDSD mixing time in 2D experiments, the recoupling is most efficient at low spinning frequencies. Typical mixing times in protonated compounds are in the order of 10 ms for ^{13}C-^{13}C transfer via direct bonds up to several 100 ms for long range transfer (Szeverenyi *et al.*, 1982; Grommek *et al.*, 2006). However, in such long-range transfers, the ^{13}C-^{13}C correlations tend to be lost due to the so-called dipolar truncation effect. The strong dipolar coupling for a pair of adjacent ^{13}C–^{13}C spins tends to suppress weaker couplings between a ^{13}C spin in the pair and remote ^{13}C spins (Baldus & Meier, 1997; Hoshino *et al.*, 1998; Hohwy *et al.*, 1999).

In DARR (^{13}C–^{1}H dipolar-assisted rotational resonance), broadband recoupling is achieved by ^{13}C–^{13}C spectral overlap, made possible by ^{13}C-^{1}H interactions. The ^{13}C–^{1}H dipolar interaction is recovered by suitable rf irradiation on the protons. This sequence recouples ^{13}C–^{13}C dipolar interactions broadbandly but non-uniformly. This unique feature makes it possible to suppress the dipolar truncation effects even though the sample is extensively ^{13}C labeled (Takegoshi *et al.*, 2001; Takegoshi & Terao, 2002; Crocker *et al.*, 2004).

1.3.5 Spin diffusion

The term "spin diffusion" was first introduced by Bloembergen to describe the phenomenon of polarization transfer through homonuclear dipolar couplings in solids which on a macroscopic level looked like a diffusion process (Bloembergen, 1949). In general, spin diffusion can be observed on two different physical scales, either as spatial spin diffusion or as spectral spin diffusion. Spatial spin diffusion describes the flow of magnetization in space between equivalent nuclei due to a non-equilibrium distribution of the initial longitudinal magnetization (Abragam, 1961). Spectral spin diffusion is the flow of polarization between spins of different resonance frequencies (Suter & Ernst, 1982). Real systems often show both aspects of spin diffusion. Spin diffusion has two important application aspects in solid-state NMR namely, (i) as a transport mechanism to transfer magnetization in a

two-dimensional correlation experiment which then establishes the relative orientation of tensorial interactions (Linder *et al.*, 1985) and (ii) measuring distances between spins, e.g., between domains in a heterogeneous polymer (Cheung, 1981; Heinen *et al.*, 1998; Mulder *et al.*, 2000).

Spin diffusion between protons can be used to measure domain sizes in polymers. Usually, these systems have a dense network of homonuclear dipolar couplings resulting in a fast spin-diffusion rate constant. Here, the diffusion rate constants are in the order of about 1 nm^2/ms, allowing to probe distances up to 200 nm (Schmidt-Rohr & Spiess, 1994). Such true ^1H spin diffusion has revealed long-range inter-molecular distance restraints in a self-aggregated Chl *a* samples (de Boer *et al.*, 2002). Recently, similar experiments have been applied to chlorosomes to determine the orientation of BChls (Ganapathy *et al.*, 2009).

Proton-driven spin diffusion between rare nuclei is a "classical" spin diffusion experiment applied to obtain distance constraints. Biosynthetically site-directed, ^{13}C and ^{15}N labelled samples allowed the observation of long-range distance correlations up to 7Å in the α-spectrin SH3 domain (Castellani *et al.*, 2002). Such spin diffusion experiments also allow the observation of polarization transfer across small couplings even in the presence of strong coupling without severe dipolar-truncation effects (Grommek *et al.*, 2006). Recently, complex formation and light activation in membrane-embedded sensory rhodopsin II has been observed by such experiments (Etzkorn *et al.*, 2010).

1.4 Aim and scope of this thesis

Light-induced charge transfer in photosynthetic RCs is highly efficient, having a quantum yield for the entire electron transfer chain close to unity. Artificial systems have not yet reached such yield, and it is not clear how to improve their efficiency. In RCs of *R. sphaeroides*, the electron transfer is selective on one of the two symmetric branches of cofactors. It is observed that electron transfer in structurally similar RCs, as that of photosystem I, occurs equally over both branches, to make the mechanism of charge separation even more mysterious. To solve these questions, the first goal to reach will be to construct a complete picture

of the orbitals involved in electron transfer. A second goal is to complement such a static orbital picture with dynamic information. Since electron transfer is coupled to phonons, it is related to local mobility, which might be crucial for directing the transfer and for dissipating efficiently the energy. A third aspect is to which degree and by what means the environment of the protein tunes the properties of the entire electron transfer pathway.

The solid-state photo-CIDNP effect with its dramatic enhancement of local NMR signals provides an analytical tool that is especially suited for studying electron transfer in photosynthetic RCs. In fact, photo-CIDNP MAS NMR has been applied to explore the electronic structures of the electron donors. It was possible to obtain an almost complete picture of the electronic ground state of the donor in the mutant *R. sphaeroides* R26 (Daviso *et al.*, 2009c). Also other donors have been analyzed, for example the donor of photosystem II of plants, which has been identified to be monomeric and highly asymmetric (Matysik *et al.*, 2000a; Diller *et al.*, 2007b). In this thesis, the photo-CIDNP MAS NMR assessment of electronic structure of the donor of *R. sphaeroides* WT, the Special Pair in its ground state will be completed (**Chapter 2**). In addition, the electronic structure of the acceptor, the bacteriopheophytin, will be provided (**Chapter 4**).

For studying the dynamics of the Special Pair, a new strategy is introduced, aiming to further develop the methodology of photo-CIDNP MAS NMR. A spin-torch type experiment is applied here by transferring the photo-CIDNP polarization to nearby carbon atoms by using ^{13}C-^{13}C spin diffusion between different isotope labels. Thus, local mobility will be probed (**Chapter 3**).

To explore the protein pocket, which might tune to the Special Pair, an alternate spin-torch experiment using protons is proposed. In this concept, the strong polarization of the donor carbons is transferred to the pocket, which can be studied at atomic resolution. To this end, the possibility to use ^{13}C photo-CIDNP for ^{13}C-^{1}H transfer is explored (**Chapter 5**).

Chapter 2

Two-dimensional nanosecond laser-flash photo-CIDNP MAS NMR experiments provide direct access to the electronic structure of the donor in bacterial reaction centers

Abstract

Although the two branches of cofactors are apparently symmetrically arranged, electron transfer in photosynthetic reaction centers (RCs) of the photosynthetic purple bacteria *Rhodobacter (R.) sphaeroides* wildtype (WT) occurs exclusively via the redox chain formed by the cofactors on the A branch. Previous ^{13}C and ^{15}N photochemically induced dynamic nuclear polarization (photo-CIDNP) solid-state magic-angle spinning (MAS) NMR studies using selective isotope labelling patterns of the cofactors have shown that an electron distribution map of the ground state can be obtained. Here we present a complete mapping of the electronic ground state of the donor cofactors in RCs (WT). Following biosynthetic labelling of RCs from *R. sphaeroides* (WT), the increased selectivity of the novel time-resolved two-dimensional dipolar-assisted rotational resonance (DARR) MAS NMR experiment simplifies the signal assignment compared to complex spectra of the same RCs obtained by continuous illumination. The shielding pattern of the ^{13}C nuclei confirms that there is excess electron density towards pyrrole ring III of $P_{L^{\cdot}}$ compared with pyrrole ring III of P_M and the pattern of ^{13}C shifts for the ring carbons is well in line with $P_L^{\delta-}P_M^{\varepsilon-}$ charge transfer character, with $\delta > \varepsilon$. Hence symmetry breaking of the electronic structure with excess negative charge on the P_L is detected in the ground state, to mediate asymmetric electron transfer following excitation.

2.1 Introduction

The discovery of the solid-state photo-CIDNP (photochemically induced dynamic nuclear polarization) effect (for reviews, (Jeschke & Matysik, 2003; Daviso *et al.*, 2008b)) by Zysmilich and McDermott in frozen and quinone-blocked bacterial reaction centers (RCs) of *Rhodobacter (R.) sphaeroides* R26 by ^{15}N magic-angle spinning (MAS) NMR under continuous illumination with white light offers NMR access to the electron-nuclear processes during charge separation (Zysmilich & McDermott, 1994). By induction of a non-Boltzmann nuclear spin polarization upon photo-reaction in rigid samples, a signal enhancement of a factor of more than 10,000 has been observed by ^{13}C MAS NMR in several RCs (Prakash *et al.*, 2005; Prakash *et al.*, 2006; Roy *et al.*, 2008). The solid-state photo-CIDNP effect can now be produced routinely for the enhancement of the ^{13}C MAS NMR for various photosynthetic RCs, including those of the purple bacteria of *R. sphaeroides* wild type (WT) (Prakash *et al.*, 2005) and R26 (Zysmilich & McDermott, 1994; Prakash *et*

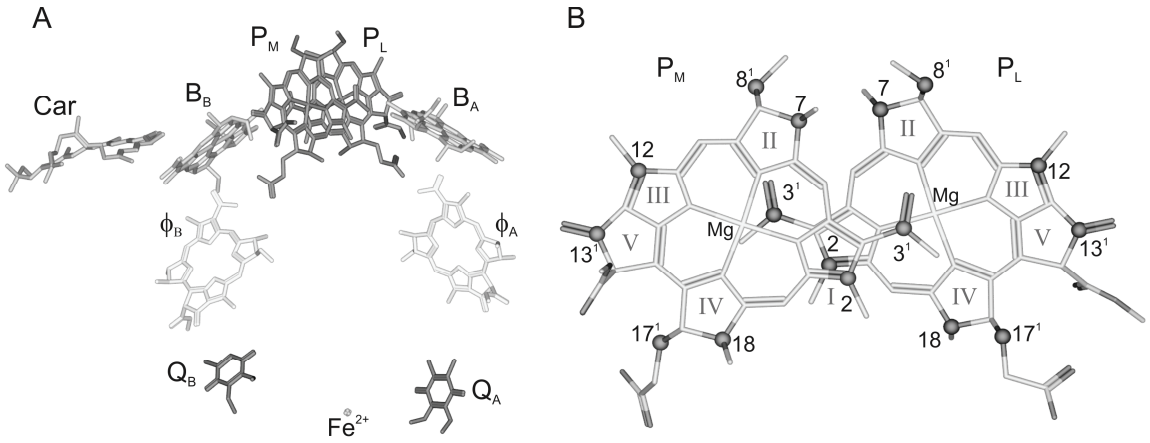

Figure 2.1 (A): Arrangement of cofactors in reaction centers (RCs) of *Rhodobacter (R.) sphaeroides* wildtype (WT). The primary electron donor, the special pair, is formed by the two bacteriochlorophyll *a* (BChl) molecules P_M and P_L. B_A and B_B are accessory BChl cofactors, Φ_A and Φ_B are bacteriopheophytin (BPhe) cofactors. On the acceptor side, two ubiquinone-10 cofactors Q_A and Q_B are located with a non-heme iron in between. The symmetry of the cofactor arrangement is broken by a carotenoid (Car) cofactor. The light-induced electron transfer occurs selectively via branch A. (B): The spatial arrangement of the two cofactors P_L (right, isotope labels in grey) and P_M (left, isotope labels in grey) forming the special pair. The pyrrole rings are numbered with Roman numbers. Pyrrole rings I are overlapping. The isotope labelling pattern has been obtained by feeding with 3-$^{13}C_1$-δ-aminolevulinic acid (3-ALA, see Figure 2.4). The long side chains are omitted to provide a better view on the arrangement of the active elements in the charge separation process. [pdb entry 1M3X, (Camara-Artigas *et al.*, 2002b) the figure has been made with Accelrys Discovery Studio]

al., 2006) and *Rhodopseudomonas acidophila* (Diller *et al.*, 2008), of the green sulphur bacterium *Chlorobium tepidum* (Roy *et al.*, 2007), of the heliobacterium *Heliobacillus mobilis* (Roy *et al.*, 2008) as well as of the photosystems I and II of plants (Matysik *et al.*, 2000a; Alia *et al.*, 2004; Diller *et al.*, 2007b) and algae (Janssen *et al.*, 2010). Hence there is converging evidence that the solid-state photo-CIDNP effect is an intrinsic property of natural photosynthetic RCs (Matysik *et al.*, 2009).

In RCs of *R. sphaeroides*, light absorption induces charge separation within 4 ps from the primary donor (P) to the primary acceptor, a bacteriopheophytin (Φ_A) (for review, see (Hoff & Deisenhofer, 1997)) (Figure 2.1A). The primary electron donor is a special pair formed by 2 bacteriochlorophyll *a* (BChl) cofactors called P_L and P_M (Figure 2.1B). The radical pair is initially in a pure spin-correlated singlet state (Figure 2.2). From this singlet state, photochemically induced dynamic electron polarization (photo-CIDEP) is observed as strongly enhanced absorptive and emissive signals in the EPR spectrum (Blankenship *et al.*, 1975; Hoff *et al.*, 1977). During the lifetime of the radical pair, the electron-spin system oscillates between the singlet ($\underline{S}$) of the radical pair state and the triplet state with magnetic quantum number 0 (T_0), with a frequency that depends on both the hyperfine tensor and the difference of the electron Zeeman interaction between the two electrons forming the radical pair.

The coherent interconversion from singlet to triplet radical pairs and back gives rise to spin sorting within the scheme of the well-known radical pair mechanism (RPM) (Figure 2.2) (Closs & Closs, 1969; Kaptein & Oosterhoff, 1969). Under continuous illumination (CI), the RPM does not induce signal enhancement because the reaction products of both decay branches are identical. Hence, no net nuclear polarization is induced by the RPM in RCs of *R. sphaeroides* WT. Transiently, using time-resolved experiments, however, this nuclear polarization can be observed (Daviso *et al.*, 2009a). Therefore, the sign of the transient light-induced signals follows Kaptein's sign rules (Kaptein, 1971).

In solid-state photo-CIDNP MAS NMR experiments under CI on RCs of *R.*

sphaeroides WT, two additional solid-state mechanisms run in parallel to induce net nuclear polarization which remains under steady-state conditions (Figure 2.2) (Jeschke & Matysik, 2003; Daviso *et al.*, 2008b): (i) Electron–electron–nuclear three-spin mixing (TSM) breaks the balance by coherent evolution of the correlated radical pair state in interaction with the nuclear spins and the applied magnetic field, depending on the signs of the electron–electron and of the anisotropic electron–nuclear interactions (Jeschke, 1997, 1998). (ii) In the electron-nuclear differential decay (DD) mechanism (Polenova & McDermott, 1999), the symmetry is broken by different lifetimes of the S and of the T_0 states. The dependence of

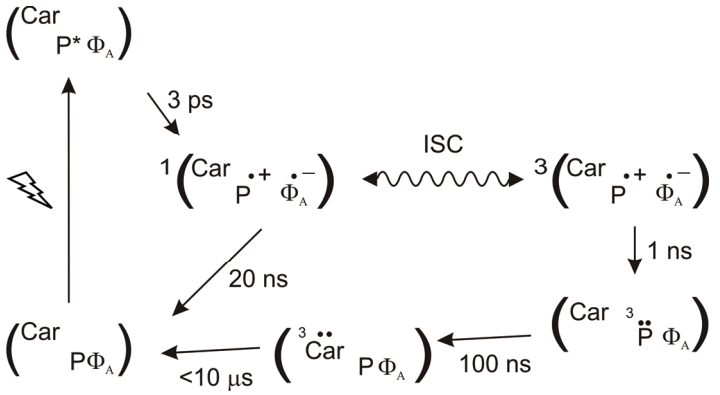

Figure 2.2 Kinetics and spin dynamics of electron transport in quinone-depleted RCs of *R. sphaeroides* wild type (WT). After absorption of a photon the photochemically excited state of the primary donor P* is formed and an electron is transferred to the primary acceptor Φ_A, a bacteriopheophytin cofactor. Initially, the radical pair is in its singlet state $^1(P^{\bullet+}\Phi_A^{\bullet-})$. It evolves into a triplet state $^3(P^{\bullet+}\Phi_A^{\bullet-})$ due to the electronic interactions and hyperfine coupling with nearby nuclei, a process which is known as intersystem crossing (ISC). The radical-pair mechanism (RPM) leads to sorting of nuclear spins via the isotropic hyperfine coupling, but without a net increase of the population difference of the spin up and the spin down nuclear states. In the TSM, hyperfine coupling, nuclear and electronic Zeeman interactions, and anisotropic interactions involving electrons and nuclei lead to symmetry breaking and net nuclear polarization that can be observed both in laser excitation experiments and under steady-state conditions. The lifetime for recombination from the singlet state to the ground state is 20 ns, while charge recombination from the $^3(P^{\bullet+}\Phi_A^{\bullet-})$ radical pair state forms a donor triplet state ^3P with a time constant of 1 ns. With continuous illumination the difference in recombination rates from the singlet and triplet states to the neutral ground state also break the symmetry when they match the inverse of the pseudosecular component of the hyperfine interaction, a process which is known as the DD mechanism. For the WT, the ^3P is rapidly converted (100 ns) in a carotenoid triplet (^{3}Car) and followed by a much slower decay from the carotenoid triplet state to the ground state. Time-resolved experiments have shown that a large fraction of the excited state decays via ^{3}Car, in competition with back conversion to the $^3(P^{\bullet+}\Phi_A^{\bullet-})$ that decays rapidly with 20 ns to establish the steady state. Before reaching this steady state, however, transient effects from RPM, TSM and DD can be observed with time-resolved photo-CIDNP, on a timescale of 10 µs and different mechanisms can be resolved by adjusting the time between the photo-CIDNP excitation and the NMR detection scheme.

secular part of the hyperfine coupling is the only single matching of interactions $2|\omega_I| = |A|$ is required and the difference of singlet and triplet radical pair lifetimes must be of the order of the inverse hyperfine coupling (Jeschke & Matysik, 2003).

In time-resolved experiments on RCs of *R. sphaeroides* WT, transient nuclear polarization has been observed up to 10 μs (Daviso *et al.*, 2009a). The decay from the singlet state to the ground state is 20 ns, much faster than the pathway via the three triplet states, which is rate limited by the decay from the carotenoid triplet state to the ground state, 10 μs (Figure 2.2). Thus, transient nuclear polarization can be observed, originating from the nuclear polarization associated with rapid decay of the $^1(P^{\bullet+}\Phi_A^{\bullet-})$ state while the polarization associated with the decay of the T_0 channel is hidden by dipolar dephasing from the paramagnetic triplet on the carotenoid (^{3}Car) during its lifetime. As a result, the nuclear polarization of the triplet decay channel cannot be detected on the nearby nuclei in experiments with a short delay <10 μs between optical excitation and NMR detection (Figure 2.2) (Daviso *et al.*, 2008b; Daviso *et al.*, 2009a).

Time-resolved photo-CIDNP MAS NMR has also been demonstrated to map the electron spin density on the donor with atomic selectivity since the transient nuclear polarization intensities reflect the local electron spin densities on the donor (Daviso *et al.*, 2009c). Interpretation of one-dimensional envelope of transient nuclear polarization however requires chemical shift assignments, which need to be obtained in separate experiments. Here we show that two-dimensional nanosecond laser-flash photo-CIDNP MAS NMR experiments allow for direct measurement of both chemical shifts and local electron spin densities in a single experiment.

2.2 Methodology

2.2.1 Dipolar assisted rotational resonance (DARR) spectroscopy

To explore connectivities between carbons, ^{13}C-^{13}C homonuclear shift-correlation experiments are necessary. In solid state NMR, different pulse sequences have been developed for use with MAS, such as DRAMA (Tycko & Dabbagh, 1990),

RFDR (Bennett *et al.*, 1992; Bennett *et al.*, 1998) , C7 (Lee *et al.*, 1995), PDSD (Szeverenyi *et al.*, 1982; Grommek *et al.*, 2006) and DARR (Takegoshi *et al.*, 2001). With DARR (Dipolar assisted rotational resonance), In the DARR experiment, nuclear polarization transfer is driven by a spin-diffusion-type mechanism while the heteronuclear (^{1}H-^{13}C) dipolar couplings are re-established by continuous ^{1}H rf irradiation on a rotary resonance condition. The pulse program for a DARR experiment is shown in Figure 2.3A. As in any two-dimensional experiment, there are four periods: i) preparation, ii) evolution, iii) mixing and iv) acquisition. In the preparation period, a standard cross polarization (CP) step is used mainly to enhance the ^{13}C polarization, by factor of ~ 4 by transfer of magnetization from the protons. During the evolution period (t_1) the ^{13}C nuclei precess according to their chemical shift. For a well resolved spectrum, efficient heteronuclear ^{1}H-^{13}C decoupling as TPPM is required during this period. After the evolution period, the magnetization is put along the z-axis with a $\pi/2$ pulse and mixing (t_{mix}) occurs longitudinally with low power irradiation on ^{1}H. The ^{1}H rf field strength is set to the n=1 rotary resonance condition (Nielsen *et al.*, 1992). During the acquisition, TPPM (Bennett *et al.*, 1995) is applied in the ^{1}H channel for optimum decoupling.

^{13}C signal assignments can be obtained by analyzing ^{13}C–^{13}C cross peaks in data sets collected with a short mixing time, where polarization transfer by ^{13}C–^{13}C dipolar interactions occurs mostly within directly bonded ^{13}C–^{13}C pairs. At longer mixing times, long range correlations may also be observed. In broadband dipolar recoupling experiments, however, such long-range correlations are quenched by dipolar truncation (Takegoshi, 2008). The strong dipolar coupling for a pair of adjacent ^{13}C–^{13}C spins tends to obscure weaker couplings between a ^{13}C spin in the pair and remote ^{13}C spins (Baldus & Meier, 1997; Hoshino *et al.*, 1998; Hohwy *et al.*, 1999). However, DARR produces broadband recoupling of weakly interacting ^{13}C spins without appreciable dipolar truncation effects even though the sample is extensively ^{13}C labelled (Takegoshi *et al.*, 2003; Crocker *et al.*, 2004; Igumenova *et al.*, 2004). In addition to broadband recoupling, DARR has other features that

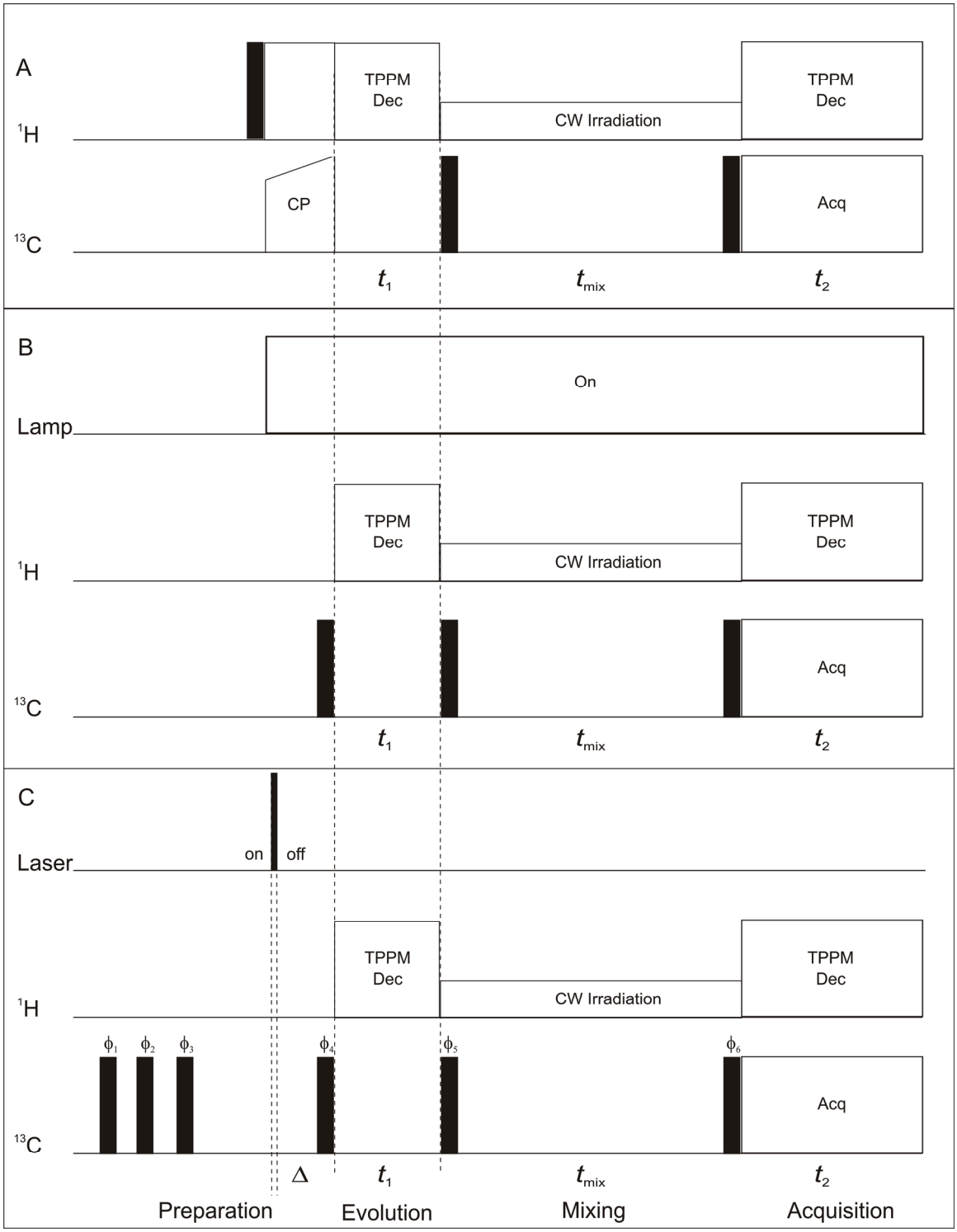

Figure 2.3 Two-dimensional ^{13}C-^{13}C CP DARR MAS NMR pulse program. Solid bars indicate the π/2 pulses and CP is cross polarization, TPPM and CW are different types of decoupling methods that can be applied, while Acq is the acquisition. t_1 and t_2 are the indirect and direct dimensions of the 2D experiment and t_{mix} is the spin diffusion mixing time. (A) Standard DARR experiment, (B) modified DARR experiment with CI setup, (C) Two-dimensional ^{13}C-^{13}C photo-CIDNP laser DARR MAS NMR pulse program used for the experiment. Solid bars indicate the π/2 pulses, Δ is the delay between the laser pulse and the π/2 pulse on the carbon channel, here Δ= 0 μs, during the ^{13}C mixing time ^{1}H was irradiated under the rotational resonance condition ($\omega_{1H} = n\omega_R$). The phase cycling used in the pulse program is Φ_1 = 0 2, Φ_2 = 0, Φ_3 = 2, Φ_4 = 0 0 0 0 0 0 0 0 2 2 2 2 2 2 2 2, Φ_5 = 0 0 0 0 2 2 2 2, Φ_6 = 0 2 1 3 and receiver Φ_R= 0 2 1 3 2 0 3 1 2 0 3 1 0 2 1 3. Here definitions are: 0 = +X, 1 = +Y, 2 = -X, 3 = -Y.

make it very suitable for homonuclear shift-correlation experiments: (i) tolerance with respect to the spinning speed and its stability, (ii) low rf-power requirements, (iii) tolerance to rf inhomogeneity, and (iv) good signal strength when a long mixing time is applied, comparable to the spin-lattice relaxation time of ^{13}C. Finally, cross peak intensities in DARR experiments at lower spinning frequencies correlate well with internuclear distances (Takegoshi *et al.*, 2003).

2.2.2 Modified DARR for photo-CIDNP under continuous illumination

The modified pulse program using the strong initial ^{13}C polarization provided by the solid-state photo-CIDNP effect is displayed in Figure 2.3B. The preparation period has been modified from the standard DARR experiment (Figure 2.3A) by replacing the CP segment with a simple ^{13}C $\pi/2$ pulse. Light is obtained from a 1000-W xenon arc lamp (Matysik *et al.*, 2000b).

2.2.3 Modified DARR for photo-CIDNP under laser-flash illumination

The modified pulse program using the strong initial ^{13}C polarization provided by the solid-state photo-CIDNP effect is displayed in Figure 2.3C. The preparation period has been modified from the standard DARR experiment (Figure 2.3A) by removing the CP segment to enhance the ^{13}C signal. Advanced photo-CIDNP techniques are used here for selective excitation of the source for the nuclear polarization, and the laser-flash photo-CIDNP segment (Daviso *et al.*, 2008a) is incorporated, using a laser flash and a subsequent $\pi/2$ pulse. The presaturation of ^{13}C pulses allows for accelerating the experiment by destroying any residual polarization from the previous $\pi/2$ pulse.

2.3 Materials and Methods

2.3.1 Sample preparation

The selective isotopic labelling in RCs of *R. sphaeroides* is achieved by feeding of selectively labelled 3-$^{13}C_1$-δ-aminolevulinic acid (3-ALA), which is a precursor for the formation of BChl and BPhe (Figure 2.4), and leads to a ^{13}C enrichment of

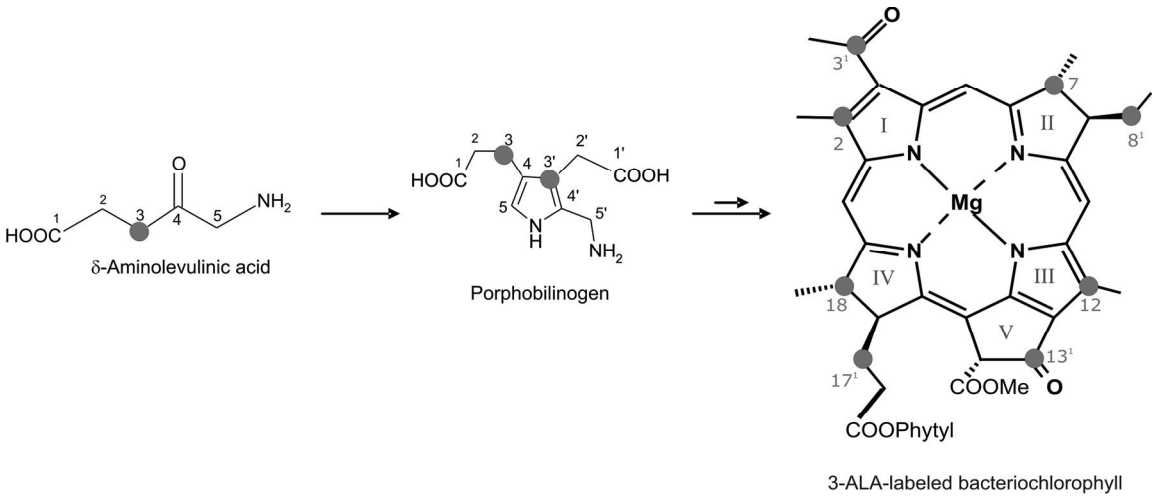

Figure 2.4 Biosynthetic pathway for the formation of selectively ^{13}C isotope labelled bacteriochlorophyll *a* (BChl) by feeding the bacteria with 3-$^{13}C_1$-δ-aminolevulinic acid (3-ALA).

~60% (Schulten *et al.*, 2002). The 3-ALA has been purchased from Buchem B.V. (Apeldoorn, The Netherlands).

The RCs were isolated as described earlier (Shochat *et al.*, 1994) and the quinones were removed by incubating the RCs at a concentration of 0.6 µM in 4% LDAO, 10 mM *o*-phenanthroline, 10 mM Tris buffer, pH 8.0, containing 0.025% LDAO and 1 mM EDTA (Okamura *et al.*, 1975). Approximately 15 mg of RC protein complex embedded in LDAO micelles were used for a NMR experiment.

2.3.2 MAS NMR experiments

NMR experiments were performed with an Avance DMX-200 NMR spectrometer equipped with a double resonance CP/MAS probe (Bruker-Biospin, Karlsruhe, Germany). The sample was loaded into a clear 4-mm sapphire rotor and inserted into the MAS probe. It was frozen slowly at a low spinning frequency of 600 Hz to ensure a homogeneous sample distribution against the rotor wall (Fischer *et al.*, 1992). The light and dark spectra were collected using a Hahn echo pulse sequence with the CYCLOPS phase cycle of the (π/2) pulse. The data were collected with TPPM carbon-proton decoupling (Bennett *et al.*, 1995) at a temperature of 223 K under continuous illumination with white light (Matysik *et al.*, 2001). The optimum length of the (π/2) carbon pulse, determined on uniformly ^{13}C labelled tyrosine, is ~4.0 µs at a strength of 62.5 kHz. The rotational frequency for MAS was

8 kHz. A total number of 128 scans were collected with a recycle delay of 4 s and a line broadening of 10 Hz was applied prior to Fourier transformation. The ^{13}C-MAS NMR spectra were referenced to the ^{13}COOH response of solid tyrosine·(HCl) at 172.1 ppm. All the spectra were phased by using only the zeroth order phase correction.

2.3.3 Lamp set up

The continuous illumination setup for the MAS NMR experiments comprises a 1000-Watt xenon arc lamp with collimation optics, a liquid filter and glass filters, a focusing element and a light fiber. Since the emission spectrum of a Xe lamp is similar to sunlight, the full range of radiation from UV to IR is available for illumination. Disturbance of the spinning frequency counting, which operates from a weak light source in the near-IR region, was avoided by water and also by various glass filters such as W27 and K3G. A fiber bundle was used to transfer the radiation from the collimation optics to the sample (Matysik *et al.*, 2000b; Daviso *et al.*, 2008b).

2.3.4 2D ^{13}C-^{13}C photo-CIDNP DARR MAS NMR under continuous illumination

All the two-dimensional (2D) ^{13}C-^{13}C photo-CIDNP DARR MAS NMR experiments were recorded with a DMX-200 (4.7 Tesla) magnet system. The sample has been frozen in the dark. Samples were kept spinning at 8 kHz at a temperature of 223 K under continuous illumination with white light (Matysik *et al.*, 2000b). The DARR pulse program was modified to incorporate the excitation with light (Figure 2.3B). For DARR experiments, all spectra were collected with 200 t_1 increments and 64 scans, with a recycle delay of 4 s. A spin diffusion mixing time of 1 second was applied.

2.3.5 Laser setup

Using 1064-nm flashes of a Nd:YAG laser (SpectraPhysics Quanta-Ray INDI 40-10, Irvine CA, USA), and frequency-doubling with a second harmonic generator, 532-

nm laser flashes were generated with pulse lengths of 6-8 ns and an energy between 20 to 270 mJ. The laser was operating with repetition rates between 1 and 4 Hz. Time-resolved photo-CIDNP MAS NMR data were acquired with NMR detection immediately after light excitation, using a presaturation pulse sequence to erase the polarization and coherence from previous scans as described in Daviso *et al.* (Daviso *et al.*, 2008a).

2.3.6 2D ^{13}C-^{13}C photo-CIDNP laser DARR MAS NMR experiments

The 2D ^{13}C-^{13}C photo-CIDNP laser-flash DARR MAS NMR experiment was recorded with the sample spinning at 8 kHz at a temperature of 223 K using a DMX-200 (4.7 Tesla) magnet system. The sample was frozen in the dark. The pulse program was modified to incorporate the triggering of the laser pulse CIDNP excitation (Figure 2.3C). For laser-flash DARR experiments, all spectra were collected with 100 t_1 increments in 3024 scans, with a recycle delay of 4 s. A spin diffusion mixing time of 1 second was applied.

2.3.7 Data processing

All spectra were processed using the TopSpin (version 1.2) software package (Bruker-Biospin, Karlsruhe, Germany). The Qsine window function was applied along with zero-filling to 1024 data points in both the t_1 and the t_2 dimensions.

2.4 Results

2.4.1 1D ^{13}C MAS NMR experiments

Figure 2.5 shows the one-dimensional ^{13}C MAS NMR spectra of 3-ALA labelled RCs of *R. sphaeroides* WT. The data were obtained in a magnetic field of 4.7 Tesla and at a temperature of 223 K with a MAS frequency of 8 kHz. Figure 2.6 provides a detailed view on the carbonylic and aliphatic regions.

Spectrum A in Figure 2.5 is collected in the dark, and no signal is observed. Upon CI with white light, strong polarization is established (Spectrum B in Figure 2.5 and 2.6). All signals are light-induced and emissive (negative). The sign of the signal has been explained by the dominance of the TSM over the DD mechanism (Prakash *et al.*, 2005). The two strongest signals at 119.4 and 134.2 ppm have been assigned to the C-12 and C-2 carbons, respectively. The strong solid-state photo-CIDNP effect confirms that these aromatic carbons obtain direct strong enhancement from the electron spin that is delocalized over the special pair (Daviso *et al.*, 2008b). All other signals are considerably weaker. At least four signals can be distinguished in the carbonyl region. The carbonyl carbon atoms are labelled and may gain intensity from the nearby C-2 and C-12 that are strongly polarized. The intensity of the signals in the aliphatic region between 0 and 60 ppm is less than for the signals in the aromatic region. Since for unlabelled RCs

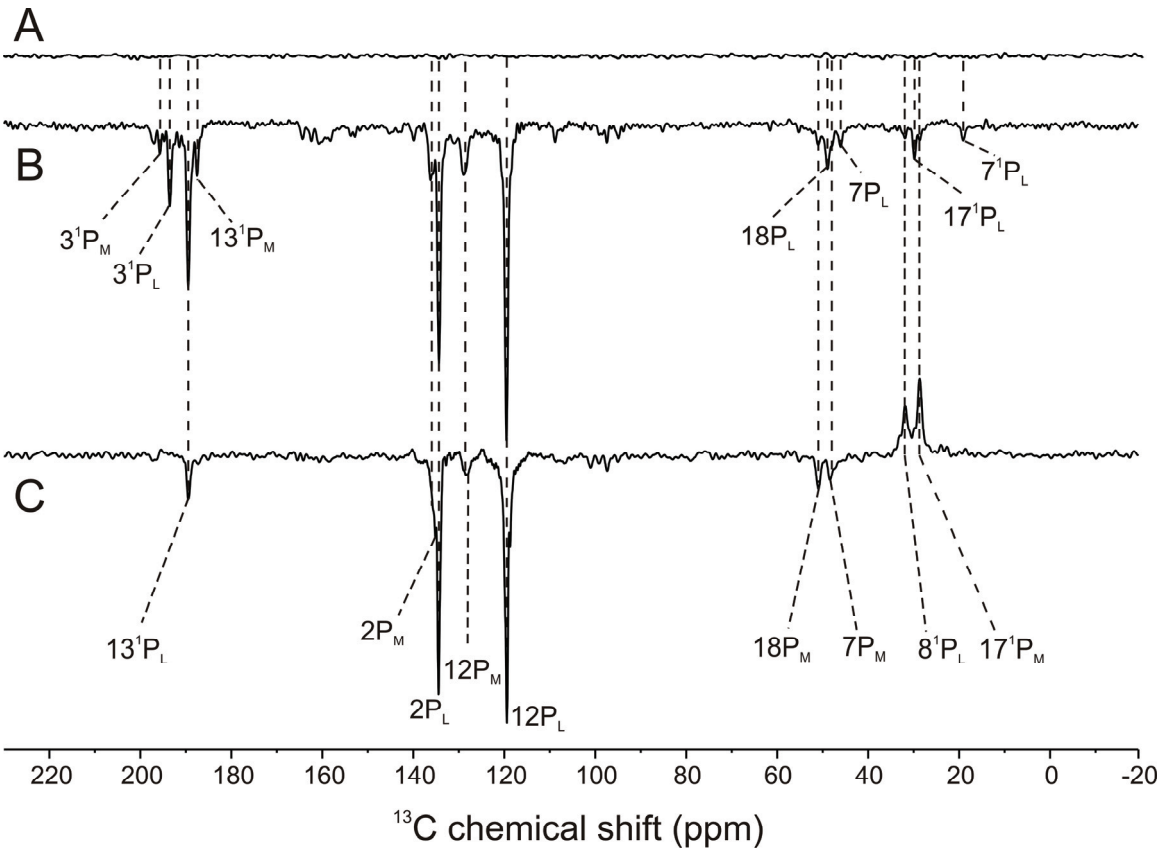

Figure 2.5 One-dimensional ^{13}C photo-CIDNP MAS NMR spectra of 3-ALA labelled RCs of *R. sphaeroides* WT (A) in the dark, (B) under continuous light and (C) under nanosecond laser-flash with $\Delta = 0$ µsec.

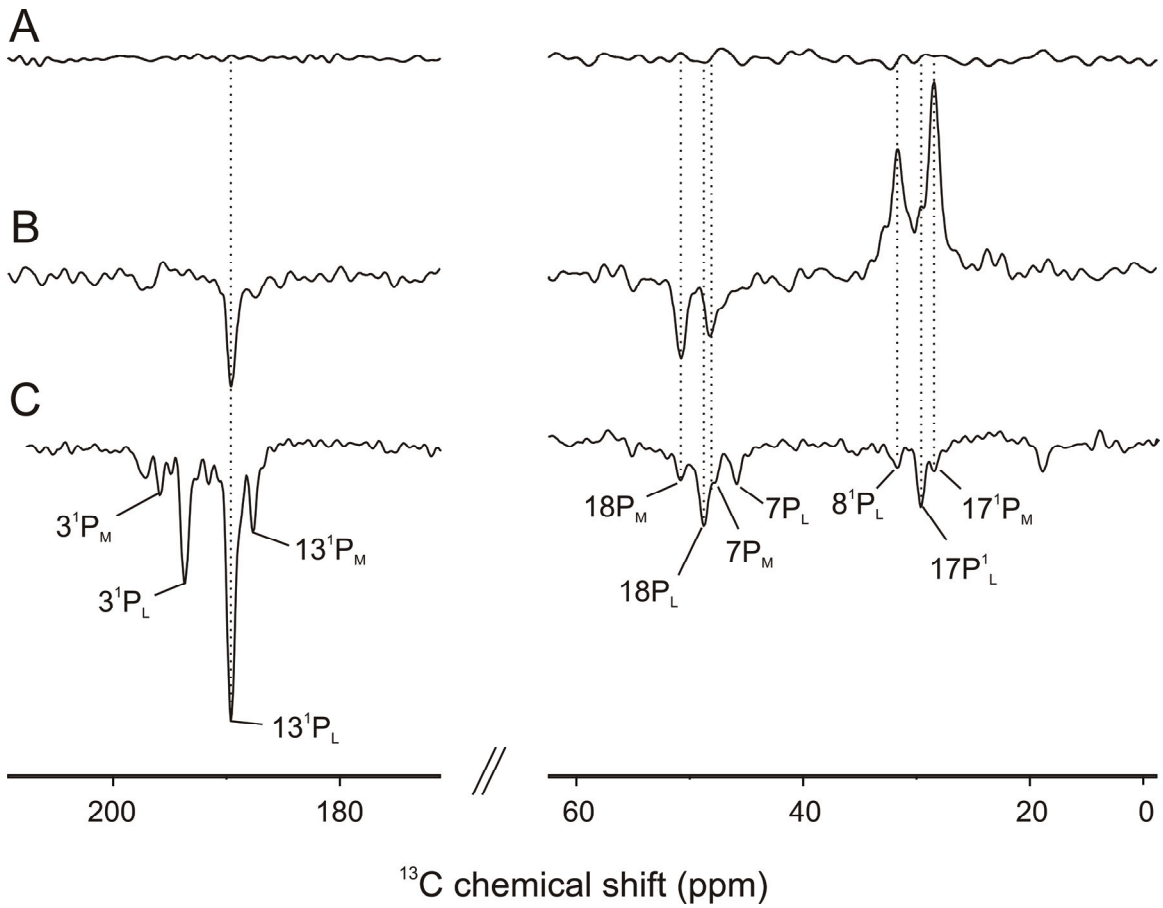

Figure 2.6 Carbonyl and aliphatic regions of one-dimensional ^{13}C photo-CIDNP MAS NMR spectra of 3-ALA labelled RCs of *R. sphaeroides* WT (A) in the dark, (B) under nanosecond laser-flash with Δ = 0 µsec and (C) under continuous light.

under continuous illumination, very little photo-CIDNP arises at aliphatic carbons (Prakash *et al.*, 2005), the observed intensity gain in the 1D experiments is attributed to transfer from strongly polarized aromatic carbons by ^{13}C spin diffusion.

In Spectrum C in Figure 2.5 and 2.6, photo-CIDNP is induced by laser flashes, immediately followed by NMR detection. This spectrum's signs are from the RPM, and the signals are both absorptive and emissive (Kaptein, 1971). As discussed in the above theory section, the sign and intensities of the transient response provides direct access to isotropic hyperfine values.

2.4.2 Continuous illumination 2D ^{13}C-^{13}C photo-CIDNP DARR MAS NMR spectrum

In Figure 2.7A, the two-dimensional ^{13}C-^{13}C photo-CIDNP DARR MAS NMR spectra of 3-ALA labelled RCs of *R. sphaeroides* WT obtained under continuous illumination with white light are shown. The spin-diffusion mixing time is 1 s. In addition to the diagonal peaks, several cross peaks are observed. In such 2D experiments, generally spins are allowed to evolve at their characteristic frequency during the t_1 and t_2 time intervals. During the mixing period (t_{mix}), between t_1 and t_2, magnetization is transferred between spins via the dipolar coupling. In general, spins that are close in space will interact. Thus, a two-dimensional dataset is collected as a function of both t_1 and t_2. Two-dimensional Fourier transformation of this time domain dataset leads to a two-dimensional frequency spectrum, with frequency axes labelled f_1 and f_2, corresponding with the t_1 and t_2 axes in the time domain, respectively. Signals along the $f_1 = f_2$ diagonal are autocorrelation peaks and arise from magnetization that did not transfer between spins during the mixing period. Additionally, there are cross peaks present as a result of transfer of magnetization by the dipolar coupling during the t_{mix} period between the interacting spins. Hence, the intensity and the sign of the cross peaks depends on the state obtained after the preparation, at the start of the evolution period t_1, and reflect the strength and sign of correlated diagonal peaks along the f_2 dimension.

Many carbons of the BChl cofactors of the special pair have been already assigned in previous studies on unlabelled (Prakash *et al.*, 2005; Prakash *et al.*, 2006), 4-ALA (Schulten *et al.*, 2002; Daviso *et al.*, 2009a) and 5-ALA (Prakash *et al.*, 2007) labelled WT RCs. While the 4- and 5-ALA label patterns allow to study the aromatic carbons of the BChl and BPhe macrocycles, 3-ALA labelling leads to isotope enrichment of the more peripheral carbon positions (Figure 2.1 and 2.4). This label pattern is particularly suitable for observation of spin diffusion since it combines a range of internuclear distances for the bacteriochlorin rings and some side chains with a good dispersion of chemical shifts that facilitates the detection of transfer between pairs of labels.

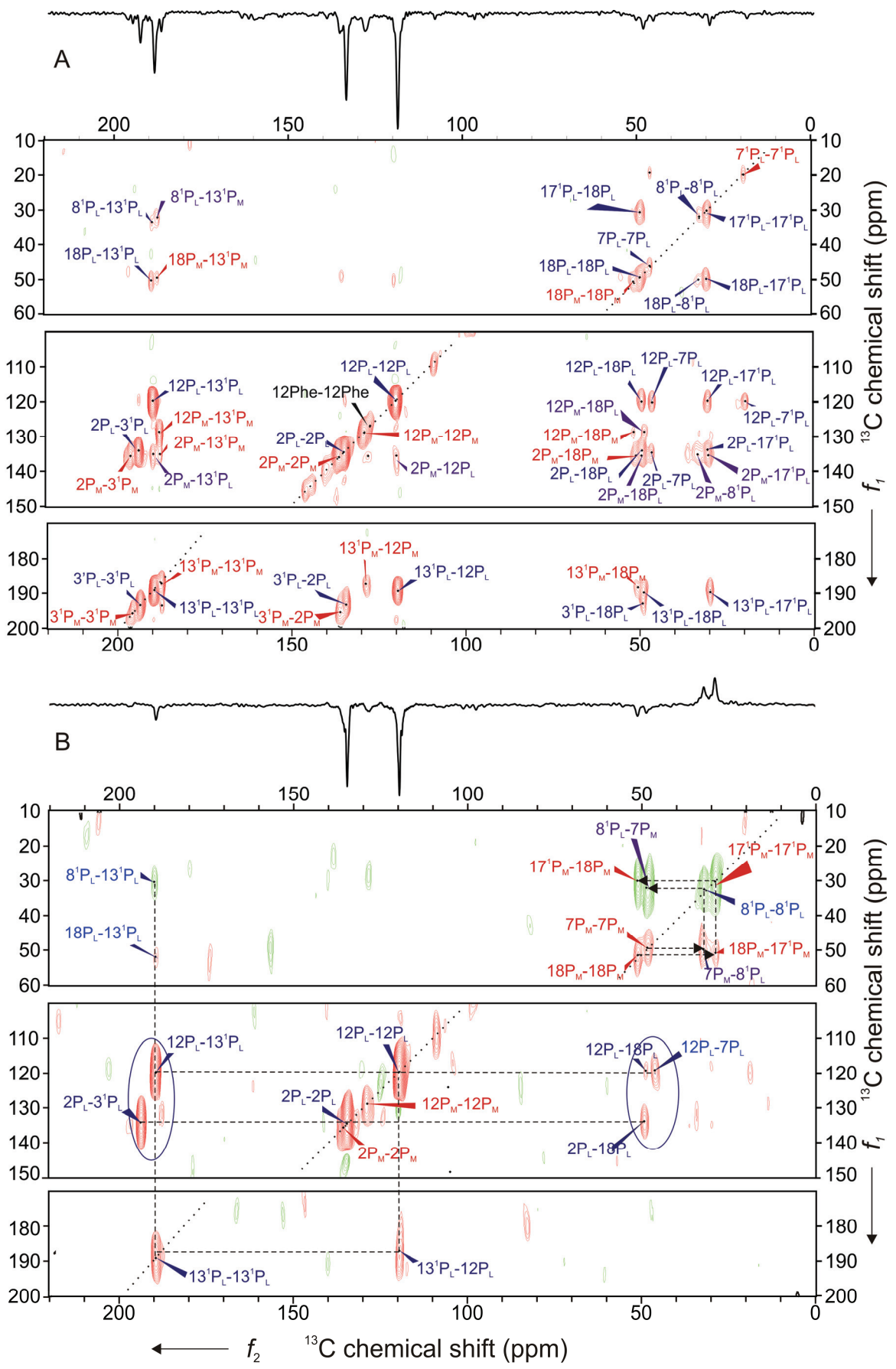

Figure 2.7 Two-dimensional ^{13}C-^{13}C photo-CIDNP DARR MAS NMR spectra of 3-ALA labelled RCs of *R. sphaeroides* WT with a spin-diffusion mixing time of 1 s, collected with a spinning frequency of 8 kHz at a temperature of 223 K. (A) Light source used is a 1000 W xenon lamp. (B) Data obtained with the laser setup. Circled region displayed less number of cross peaks in laser experiment compared to the same regions with CI experiment.

In photo-CIDNP MAS NMR on RCs of *R. sphaeroides* WT, signals from three cofactors are enhanced, the two BChl cofactors of the special pair and the primary electron acceptor BPhe in the active A branch. In the DARR spectrum of Figure 2.7, however, only two networks are observed. The more extended network is labelled in blue and is assigned to cofactor P_L of the special pair. It represents a complete set of correlation signals for eight carbon nuclei, including the responses from the C-2 and the C-12 with the strongest intensities. From this network, all chemical shift assignments have been obtained (Table 2.1). A second network, labelled in red, is from a spin system comprising five ^{13}C nuclei, and is assigned to cofactor P_M. As observed previously, most of the signals assigned to P_L are shielded compared to the signals of P_M (Schulten *et al.*, 2002; Prakash *et al.*, 2005; Prakash *et al.*, 2007; Daviso *et al.*, 2009c). In particular the difference between the chemical shifts of the C-12 atoms of 9.0 ppm is remarkable.

2.4.3 Time-resolved 2D ^{13}C-^{13}C photo-CIDNP DARR MAS NMR spectrum

Figure 2.7B shows the two-dimensional ^{13}C-^{13}C photo-CIDNP laser DARR MAS NMR spectra of 3-ALA labelled RCs of *R. sphaeroides* WT collected at 223 K with a spin-diffusion mixing time of 1 s and a MAS frequency of 8 kHz. In time-resolved experiments on RCs of *R. sphaeroides* WT without a delay between laser flash and NMR detection, the light-induced signals are mainly due to the transient polarization as explained in (Figure 2.2) (Daviso *et al.*, 2009a). Hence, the ^{13}C-^{13}C correlation experiment provides both a view on the electronic structure and the chemical shift assignments of the labelled atoms in the special pair.

In the time-resolved two-dimensional spectrum, mainly peaks from P_L appear and only a few from P_M. In the one-dimensional dataset collected with laser excitation, the signals in the aliphatic region are strong compared to the CI experiment and the signals from C-17^1 P_M, C-17^1 P_L and C-8^1 P_L are absorptive. In Figure 2.7, selected regions of 2D spectra are displayed. Since Figure 2.7A is obtained with CI, all diagonal peaks are emissive, which leads to a completely emissive sets of cross peaks. The cross peak intensities confirm that the signal

Table 2.1 Assignment of the signals from 3-ALA-labelled BRCs obtained with continuous illumination and nanosecond laser-flash excitation, with their respective signs of polarization. For the continuous illumination experiment all the polarization is emissive. (E = emissive; A = absorptive).

Carbon's position in BChl *a*	P_L	Sign in laser expt	P_M	Sign in laser expt	BPhe
2	134.3	E	136.2	E	
3^1	193.5	-	195.6	-	
7	46.1	-	48.3	E	
8^1	32.1	A			
12	119.5	E	128.8	E	126.9
13^1	189.4	E	187.5	-	
17^1	29.9	A	28.4	A	
18	49.1	-	50.9	E	
7^1	19.1	-		-	

strength is transferred along the f_2 dimension. For example, the cross peak, C12 (P_L) / $C7^1$ (P_L) is very pronounced, as the corresponding diagonal peak in the f_2 direction is also strong. In Figure 2.7B, laser flashes were used as source of the photo-CIDNP enhancement and both absorptive and emissive signals occur. The cross peaks in the aliphatic region, for example, C18 (P_M) / $C17^1$ (P_M) show the same sign as the diagonal peaks along the f_2 dimension (see dashed arrows).

Compared to the continuous illumination experiment, less diagonal peaks occur due to the selectivity of the RPM, therefore also less cross peaks are observed for the same mixing time of 1 s. Hence, the enhancement mechanism in the 2D Laser-DARR acts as a filter for correlation experiments. The higher selectivity also allows for clarifying the assignments for C7 (P_M), C7 (P_M), C8 (P_L) and C18 (P_M) (Table 2.1).

2.4.4 Experimental reconstruction of the electronic structures of the Special Pair

Nearly complete sets of ^{13}C assignments for the macrocyles of both the P_L and P_M cofactors are presented in Table 2.2 and 2.3, respectively, compiling the results of this work using the 3-Ala label pattern (Table 2.1) with that of previous work using 4- and 5-Ala label patterns (Schulten *et al.*, 2002; Prakash *et al.*, 2007; Egorova-Zachernyuk *et al.*, 2008; Daviso *et al.*, 2009a). After correction for ring current effects, the comparison of ^{13}C chemical shifts of the special pair with chemical shifts obtained from a BChl in solution in chloroform provide the full signature of the ground state electronic structure with great detail (Figure 2.8). Apparently the formation of the supermolecule leads to a concentration of electronic shielding, indicated with yellow spheres in the overlap region of pyrrole rings I of P_L and P_M (Figure 2.8). These results validate the earlier observations for RCs of the carotenoid-less mutant R26 (Daviso *et al.*, 2009c) and show that the presence of the carotene has little effect on the ground state electronic properties and the structure of the Special Pair. In addition, theoretical studies indicate that accumulation of negative charge on the P_L and P_M can be established by partial charge transfer from the axial histidines HisL173 and HisM202 (Alia *et al.*, 2009; Wawrzyniak *et al.*, 2011).

Figure 2.8 compiles the differences in chemical shift, reflecting the shielding and deshielding by the electronic distribution for the ground state of the Special Pair. This has been experimentally obtained in the present study by the laser-flash experiment (Table 2.1). In line with earlier time-resolved photo-CIDNP studies, the P_L is more shielded than the P_M (Zysmilich & McDermott, 1994; Schulten *et al.*, 2002; Prakash *et al.*, 2007; Daviso *et al.*, 2009c). For both cofactors, considerable shielding is observed for the ^{13}C on pyrrole rings I, indicating accumulation of electron density in the overlap region. The shift pattern also points to more relative electron density on the pyrrole ring III of P_L , while the pyrrole ring III of P_M is deshielded, indicating accumulation of positive charge in the region.

Table 2.2 ^{13}C positions in P_L and their NMR chemical shifts [1].

Carbon's position in BChl *a*	Chemical shift (ppm) of BChl *a* in acetone solution [a]	Chemical shift (ppm) of P_L			
		Measured by MAS NMR	Calculated ring current	Real CS Corrected (observed -calculated ring current)	Corrected (corr CS-CS in liquid)
	δ_{Model}	δ_{PL}	δ_{RC}	$\delta_{PL(Corr)}= \delta_{PL}- \delta_{RC}$	$\Delta_{(Corr)}= \delta_{PL(Corr)}- \delta_{Model}$
1	151.2	143.5 [b]	-1.3	144.8	-6.4
2	142.0	134.3 [c]	-2.3	136.6	-5.4
3	137.7	127.4 [b]	-3.3	130.7	-7.0
3[1]	199.3	193.5 [c]	-4.2	197.7	-1.6
4	150.0	136.8 [b]	-2.0	138.8	-11.2
5	99.9	103.0 [b]	-1.1	104.1	4.2
6	168.9	165.9 [b]	-0.1	166.0	-2.9
7	48.3	46.1 [c]	0.3	45.8	-2.5
7[1]	23.4	19.1 [c]	0.0	19.1	-4.3
8	55.8	54.7 [b]	0.2	54.5	-1.3
8[1]	30.8	32.1 [c]	0.4	31.7	0.9
9	158.5	162.6 [b]	0.2	162.4	3.9
10	102.4	100.4 [b]	0.2	100.2	-2.2
11	149.5	153.6 [b]	0.2	153.4	3.9
12	124.0	119.5 [c]	0.2	119.3	-4.7
13	130.6	130.8 [b]	0.2	130.6	0.0
13[1]	189.0	189.4 [c]	0.2	189.2	0.2
14	160.8	157.2 [b]	0.2	157.0	-3.8
15	109.7	108.7 [b]	0.2	108.5	-1.2
16	152.0	145.6 [b]	0.2	145.4	-6.6
17	50.5	50.0 [b]	0.2	49.8	-0.7
17[1]	30.5	29.9 [c]	0.3	29.6	-0.9
18	49.5	49.1 [c]	0.1	49.0	-0.5
19	167.3	161.0 [b]	-0.1	161.1	-6.2
20	96.3	104.1 [b]	-0.5	104.6	8.3

[a] Egorova-Zachernyuk (2008); ([b]) earlier works; ([c]) This work

[1] NMR chemical shifts of P_L (δ_{PL}) , its monomeric chlorophyll in acetone (δ_{Model}) and respective differences in chemical shift after the subtraction of estimated ring current effects ($\Delta_{(Corr)}$).

Table 2.3 ^{13}C positions in P_M and NMR chemical shifts [2].

Carbon's position in BChl *a*	Chemical shift (ppm) of BChl *a* in acetone solution [a]	Chemical shift (ppm) of P_M			
		Measured by MAS NMR	Calculated ring current	Real CS Corrected (observed - calculated ring current)	Corrected (corr CS-CS in liquid)
	δ_{Model}	δ_{PM}	δ_{RC}	$\delta_{PM(Corr)}= \delta_{PM}- \delta_{RC}$	$\Delta_{(Corr)}= \delta_{PM(Corr)} - \delta_{Model}$
1	151.2	148.5 [b]	-1.1	149.6	-1.6
2	142.0	136.2 [c]	-2.1	138.3	-3.7
3	137.7	129.7 [b]	-3.2	132.9	-4.8
3^1	199.3	195.6 [c]	-4.2	199.8	0.5
4	150.0	144.5 [b]	0.1	144.4	-5.6
5	99.9	101.2 [b]	-1.3	102.5	2.6
6	168.9	166.5 [b]	-0.2	166.7	-2.2
7	48.3	48.3 [c]	0.2	48.1	-0.2
7^1	23.4	22.6 [b]	-0.1	22.7	-0.7
8	55.8	52.7 [b]	0.3	52.4	-3.4
8^1	30.8	29.5 [b]	0.6	28.9	-1.9
9	158.5	158.5 [b]	0.3	158.2	-0.3
10	102.4	98.3 [b]	0.1	98.2	-4.2
11	149.5	149.8 [b]	0.3	149.5	0.0
12	124.0	128.8 [c]	0.2	128.6	4.6
13	130.6	132.8 [b]	0.1	132.7	2.1
13^1	189.0	187.5 [c]	0.1	187.4	-1.6
14	160.8	160.1 [b]	0.1	160.0	-0.8
15	109.7	106.6 [b]	0.1	106.5	-3.2
16	152.0	151.5 [b]	0.1	151.4	-0.6
17	50.5	47.4 [b]	0.1	47.3	-3.2
17^1	30.5	28.4 [c]	0.1	28.3	-2.2
18	49.5	50.9 [c]	0.1	50.8	1.3
19	167.3	164.4 [b]	0.0	164.4	-2.9
20	96.3	102.0 [b]	-0.3	102.3	6.0

[a] Egorova-Zachernyuk (2008); ([b]) earlier works; ([c]) This work

[2] NMR chemical shifts of P_M (δ_{PM}) , its monomeric chlorophyll in acetone (δ_{Model}) and respective differences in chemical shift after the subtraction of estimated ring current effects ($\Delta_{(Corr)}$).

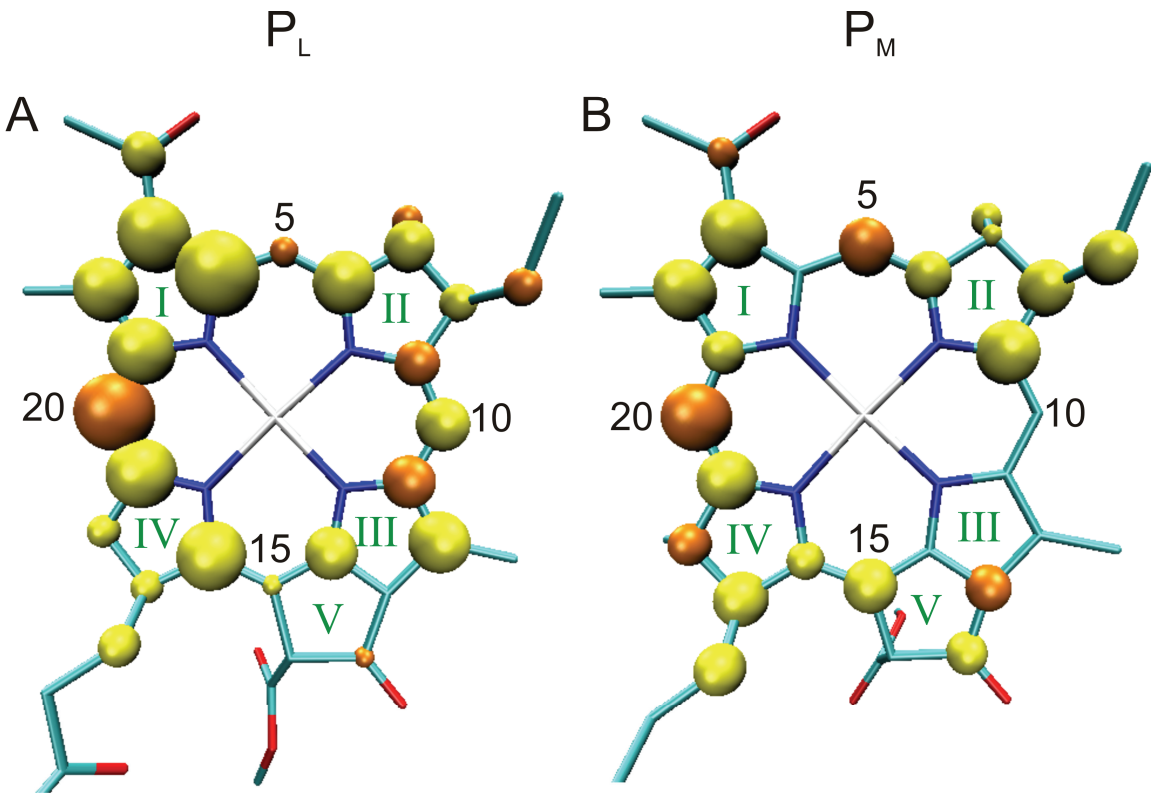

Figure 2.8 The cofactors P_L and P_M of the Special Pair, with the numbering of pyrrole rings and meso carbon atoms. The spheres correspond with the difference in chemical shifts after the correction by the estimated ring current effects, which reflect the relative electronic distribution for P_L and P_M in the electronic ground state derived experimentally. Yellow and orange colored spheres represent negative (shielding) and positive (deshielding) differences in chemical shifts, respectively.

This character of the special pair could be well represented as $P_L^{\delta-}P_M^{\varepsilon-}$, from the photo-CIDNP analysis of the ground state chemical shifts. We find $\delta > \varepsilon$ which would imply that there is some dipole character in the ground state, superimposed on a overall negative charge and is well in line with earlier NMR studies that indicate balancing of the special pair charge state by the protein surroundings (Alia *et al.*, 2009). The electronically excited state and the radical cation state have been studied by other spectroscopic methods. From the absorption and Stark spectroscopy, it has been concluded that the excited state has $P_L^+P_M^-$ charge transfer character, while the radical cation state has more negative charge on the P_L, which parallels the findings in this chapter (Lendzian *et al.*, 1993; Daviso *et al.*, 2009c). The $P_L^{\delta-}P_M^{\varepsilon-}$ charge transfer character and associated symmetry breaking of the electronic structure can possibly mediate asymmetric electron transfer following excitation, which will be further explored in chapter 3.

Chapter 3

Dynamic asymmetry in the Special Pair of *Rhodobacter sphaeroides* observed by photochemically induced dynamic nuclear polarization ^{13}C NMR

Abstract

Electron transfer in photosynthetic reaction centers (RCs) of the photosynthetic purple bacteria *Rhodobacter (R.) sphaeroides* wild type (WT) occurs almost exclusively via the A branch. The primary electron donor, the Special Pair (P), is constituted by two bacteriochlorophyll *a* (BChl) cofactors. Here we investigate the internal dynamics of P by ^{13}C photochemically induced dynamic nuclear polarization (photo-CIDNP) solid-state magic-angle spinning (MAS) NMR dipolar correlation spectroscopy and site-selective ^{13}C isotope enrichment of P in the ground state. Solid-state photo-CIDNP excitation leads to strong signal enhancement in two-dimensional dipolar-assisted rotational resonance (DARR) MAS NMR experiments. 2D spectra collected with different mixing times allow for both the assignment of signals and mapping of rapid oscillatory motion of P around its ground state equilibrium structure with atomic selectivity from the kinetics of the ^{13}C spin-diffusion processes. With a rate matrix analysis the dynamic partial averaging of dipolar interactions is resolved for individual ^{13}C spin pairs. The data provide convincing evidence that the collective modes are localized towards the P_M bacteriochlorophyll that is connected to the active branch accessory bacteriochlorophyll via His M202 and a water molecule and possible implications of the localized dynamics for symmetry breaking and charge transfer are discussed.

3.1 Introduction

In photosynthetic reaction centers (RCs) of the purple bacterium *Rhodobacter (R.) sphaeroides* WT (for reviews, see (Hoff & Deisenhofer, 1997; Hunter *et al.*, 2008)), the primary electron donor is a bacteriochlorophyll *a* (BChl) dimer, called the Special Pair P, comprising two dimer halves P_L and P_M (Figure 3.1A). Two additional BChl cofactors called accessory BChls (B_A & B_B), two bacteriopheophytins (Φ_A & Φ_B), two quinones and a non-heme iron are organized into two pseudo-symmetric branches named A and B (Figure 3.1B). It was found that collective nuclear motion on the potential energy surface of the excited state of the primary electron donor P* enables the charge transfer in the RC which is initiated by $P_L^+P_M^-$ internal charge transfer character, followed by the formation of $P^+B_A^-$ and $P^+\Phi_A^-$ intermediates over the active A branch (Moore *et al.*, 1999; Yakovlev *et al.*, 2010a). Excitations that enter the RC from the antenna are thought to lose excitonic character and gain polaronic character by coupling to two specific collective nuclear modes, a higher frequency intradimer mode of around 130 cm^{-1} and a low frequency protein mode of ~30 cm^{-1} (Novoderezhkin *et al.*, 2004). This

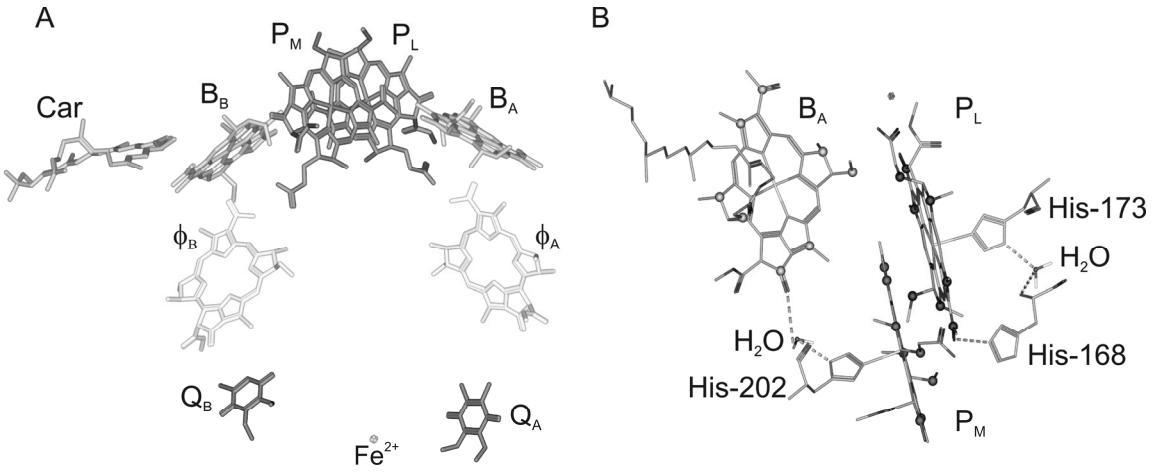

Figure 3.1 (A) The arrangement of cofactors in reaction centers (RCs) of *Rhodobacter (R.) sphaeroides* wild type (WT). The primary electron donor, the special pair, is formed by the two bacteriochlorophyll *a* (BChl) molecules P_L and P_M. B_A and B_B are accessory BChl cofactors. Φ_A and Φ_B are bacteriopheophytin (BPhe) cofactors. The two ubiquinone-10 cofactors Q_A and Q_B are localized on the acceptor side with a non-heme iron in between. Side chains are omitted to provide a clear view on the active parts. The apparent symmetry of the cofactor arrangement is broken by a carotenoid cofactor (Car). The light-induced electron transfer occurs selectively via branch A. (B) Another view of spatial arrangement of the cofactors P_L (top, right, isotope labels in blue), P_M (bottom, middle, isotope labels in red) forming the Special Pair and an accessory bacteriochlorophyll on the A branch (B_A) along with hydrogen bondings with nearest water molecules. [PDB entry 1M3X, the figure has been made with Accelrys Discovery Studio].

low frequency mode has been proposed to be connected to a protic species, *e.g.* the reorganization of the phenolic OH of Tyr M210 between P and B_A or the water molecule that is hydrogen bonded to the B_A ring V keto functionality and the N_π of the HisM202 that is axially coordinated with the N_τ to the Mg^{2+} of the P_M. Such hydrogen bondings can stabilize a $P^+B_A^-$ charge transfer contribution in a collinear proton coupled electron transfer (PCET)-type process from the P* to the B_A along the chain of polar groups Mg(P_M)–N–C–N(HisM202)–HOH(55)–O=(B_A) (Moore *et al.*, 1999; Yakovlev *et al.*, 2002; Potter *et al.*, 2005; Grondelle & Novoderezhkin, 2006; Alia *et al.*, 2009; Yakovlev *et al.*, 2010b; Wawrzyniak, 2011).

Stark effect measurements on RCs of *R. sphaeroides* that are sensitive to changes in the electronic charge distribution following excitation reveal a large change in dipole moment, 8.6 D, and the excited state of the Special Pair contains significant $P_L^+P_M^-$ charge-transfer character (Deleeuv *et al.*, 1982; Lockhart & Boxer, 1987, 1988). These observations are consistent with hole-burning experiments (Johnson *et al.*, 1991; Purchase & Völker, 2009), where large values for the total Huang-Rhys factor of ~1.5 and the Special Pair marker mode of ~120 cm^{-1} have been reported and attributed to a geometry change in the excited state induced by the primary charge separation (Reddy *et al.*, 1992; Lyle *et al.*, 1993).

As demonstrated also by differences in vibrational frequencies (Palaniappan *et al.*, 1993), the structure of the two cofactor halves (Camara-Artigas *et al.*, 2002a) and their chemical shifts (see chapter 2), the symmetry between the two cofactors is already broken in the ground state (Schulten *et al.*, 2002; Daviso *et al.*, 2009c). In addition, theoretical calculations indicate that the axial histidines donate electron density to P_L and P_M and that the orientation of the 3^1 acetyl group in P_L and protein surrounding modulate the distribution of the excess electron density over the two halves of the special pair (Alia *et al.*, 2004; Wawrzyniak *et al.*, 2011). For the radical cation state, it has been shown by ^1H ENDOR (Lendzian *et al.*, 1993) that the electron-spin density is asymmetrically distributed in favor of P_L in the Special Pair. Recent ^{13}C and ^{15}N laser-flash photo-CIDNP MAS NMR (Daviso *et al.*, 2009b; Daviso *et al.*, 2010) allowed to determine the electronic

structure of the HOMO at atomic resolution. In this study it has also been shown that there is excess spin density on the P_L in the radical cation state. Hence the asymmetry of the HOMO is an intrinsic property of the Special Pair complex with its axial histidines and is caused by small differences between the thermally averaged geometries of the two cofactors in their surrounding protein matrix. Here we explore a new avenue by probing the dynamics of the BChl in the Special Pair by labelling of the macrocycle rings at various positions (Figure 3.1B). These positions were ^{13}C labelled by culturing *R. sphaeroides* in a medium containing a selectively isotope labelled precursor of the tetrapyrrole synthesis, 3-$^{13}C_1$-δ-aminolevulinic acid (3-ALA) (Figure 3.2).

The solid-state photo-CIDNP effect (for reviews, (Jeschke & Matysik, 2003; Daviso *et al.*, 2008b; Matysik *et al.*, 2009)) has been observed for the first time in 1994 by Zysmilich and McDermott (Zysmilich & McDermott, 1994) in RCs of *R. sphaeroides* and allows enhancement of ^{13}C signals of the Special Pair by a factor of more than 10,000 (Prakash *et al.*, 2005; Prakash *et al.*, 2006). Upon illumination, a highly electron spin-ordered radical pair is formed, and nuclear polarization is established in nearby nuclei by up to three mechanisms, called three-spin mixing (Jeschke, 1997, 1998), differential decay (Polenova & McDermott, 1999) and differential relaxation (Goldstein & Boxer, 1987; McDermott *et al.*, 1998). The combined operation of these mechanisms in generating photo-CIDNP is now well understood (for a review, see (Daviso *et al.*, 2009a)). In the meanwhile, the effect has also been observed in RCs of plants, of green sulfur bacteria and of purple non-sulfur bacteria (Matysik *et al.*, 2009). The signal enhancement provided by the solid-state photo-CIDNP effect may thus be considered an intrinsic property of natural photosynthetic RCs and allows directly resolving the signals of ^{13}C atoms within the RC (Matysik *et al.*, 2009). In chapter 2 an experimental scheme is introduced for two-dimensional chemical-shift correlation spectroscopy using dipolar-assisted rotational resonance (DARR) following excitation by photo-CIDNP (Takegoshi *et al.*, 2001). In the DARR experiment, nuclear polarization transfer is driven by a spin-diffusion-type mechanism while the heteronuclear (^1H-

^{13}C) dipolar couplings are re-established by continuous ^{1}H rf irradiation on a rotary resonance condition $\omega_1 = n\omega_r$, with ω_1 the nutation frequency of the ^{1}H rf irradiation, ω_r the spinning frequency, and n= 1 or 2 (Levitt *et al.*, 1988; Oas *et al.*, 1988). Such an irradiation leads not only to a broadening of the ^{13}C lines but also to an active recoupling at second-order resonance conditions which is based on the matching of the nutation frequency of the I spins to the isotropic chemical-shift difference of S-spin pairs ($\omega_1 = n\omega_r \pm \Delta\ \omega_{iso}$) (Scholz *et al.*, 2008). DARR spectra can provide ^{13}C assignments and provide information about the local mobility. The decay rates of the diagonal peaks are related to local mobility, and the build-up of the cross peaks depends on the magnitude of the dipolar couplings, which are maximum if the molecule is rigid.

In an analogy to other dipolar processes, such as the Förster transfer of optical excitations (Förster, 1948), spin diffusion in static samples can be described phenomenologically by a rate constant W_{ij} that characterizes transfer of magnetization between two nuclei *i* and *j* and is given by (Abragam, 1961)

$$W_{ij} = \frac{1}{2}\pi * g_o^{ij}(0) * \omega_{ij}^2, \qquad (3.1)$$

with the dipolar coupling constant ω_{ij} between the two spins being given by

$$\omega_D^{ij} = -2\left(\frac{\mu_0}{4\pi}\right)\left(\frac{\hbar\gamma_i\gamma_j}{r_{ij}^3}\right). \qquad (3.2)$$

The function $g_0^{ij}(0)$ describes the intensity of the normalized zero-quantum line at frequency zero, which can be approximated by the overlap between the two NMR single-quantum lines of spins *i* and *j*, assuming that the broadening mechanisms are uncorrelated. Since the dipolar coupling constant between the two spins depends on the inverse third power of the distance r, spin diffusion is a short- to intermediate-range effect with $W_{ij} \propto r_{ij}^{-6}$. Using this distance dependence, solid-state NMR experiments based on spin diffusion have been introduced to obtain distance information in solids (Douglass & McBrierty, 1978; McBrierty, 1979; Caravatti *et al.*, 1982; Szeverenyi *et al.*, 1982; Henrichs & Linder, 1984; Caravatti *et*

al., 1985) in analogy to the nuclear Overhauser effects in liquids (Hull & Sykes, 1975; Kalk & Berendsen, 1976; Gordon & Wüthrich, 1978; Kumar *et al.*, 1980; Kumar *et al.*, 1981).

Although dipolar couplings are in zeroth-order approximation averaged by MAS (Andrew *et al.*, 1959; Lowe, 1959), spin diffusion has also been observed in polycrystalline solids under MAS (Kubo & McDowell, 1988), opening the possibility to use distance restraints derived from spin-diffusion data as a tool for protein structure determination (Griffiths *et al.*, 2000; Mulder *et al.*, 2000; van Rossum *et al.*, 2000; Castellani *et al.*, 2002; de Boer *et al.*, 2002; Hiller *et al.*, 2005; van Gammeren *et al.*, 2005; De Paepe *et al.*, 2008; Gardiennet *et al.*, 2008; Loquet *et al.*, 2008). With MAS, spin diffusion is promoted not directly by the dipolar-coupling Hamiltonian. It involves higher-order terms in the average Hamiltonian expansion that have a form similar to the static dipolar Hamiltonian (Grommek *et al.*, 2006). Since the spin-diffusion rate constant is proportional to the square of the effective dipolar-coupling strength, dynamic processes will lead to a slowdown of the spin-diffusion process due to the reduction in the strength of the dipolar couplings.

3.2 Materials and Methods

3.2.1 Sample preparation

The selective isotope labelling in RCs of *R. sphaeroides* is achieved by feeding the bacteria with selectively labelled 3-$^{13}C_1$-δ-aminolevulinic acid (3-ALA), which is a

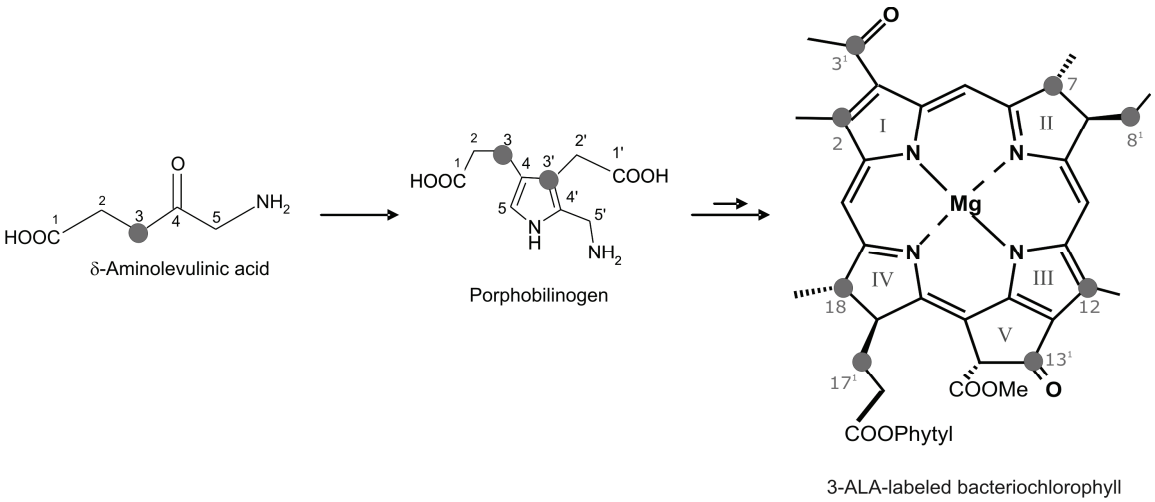

Figure 3.2 Biosynthetic pathway for the formation of selectively ^{13}C isotope labelled bacteriochlorophyll a (BChl) by feeding the bacteria with 3-^{13}C-δ-aminolevulinic acid (3-ALA).

precursor for the formation of BChl and BPhe, and leads to a ^{13}C enrichment of ~60%. The 3-ALA (Figure 3.2) has been purchased from Buchem B.V. (Apeldoorn, The Netherlands). The RCs were isolated as described earlier (Shochat *et al.*, 1994) and the quinones were removed by incubating the RCs at a concentration of 0.6 µM in 4% LDAO, 10 mM o-phenanthroline, 10 mM Tris buffer, pH 8.0, containing 0.025% LDAO and 1 mM EDTA (Okamura *et al.*, 1975). Approximately 15 mg of RC protein complex embedded in LDAO micelles were used for a NMR experiment.

3.2.2 MAS NMR experiments

NMR experiments were performed with an Avance DMX-200 (4.7 Tesla) NMR spectrometer equipped with a 4 mm MAS probe (Bruker BioSpin GmbH, Karlsruhe, Germany). The sample was loaded into a clear 4 mm sapphire rotor and inserted into the MAS probe. It was frozen slowly at a low spinning frequency of 600 Hz to ensure a homogeneous sample distribution against the rotor wall (Fischer *et al.*, 1992).

All two-dimensional (2D) ^{13}C-^{13}C photo-CIDNP DARR MAS NMR experiments were recorded with a MAS frequency of 8 kHz and at a set temperature of 223 K using continuous illumination with white light (Matysik *et al.*, 2000b). The spectra were measured in 64 scans with 200 t_1 increments and a recycle delay of 4 s, resulting in a total experiment time of 11 h for a mixing time of 2 s. Spin-diffusion mixing times between 0.02 to 10 s were used. The FID was detected with proton decoupling using the TPPM sequence (Bennett *et al.*, 1995). The optimum length of the ($\pi/2$) carbon pulse, determined on uniformly ^{13}C labelled tyrosine, was ~4.0 µs, corresponding with the nutation frequency of 62.5 kHz. All ^{13}C-MAS NMR spectra were referenced to the carbonyl resonance of solid tyrosine•(HCl) set to 172.1 ppm.

2D spectra were processed using the TopSpin (version 2.1) software package (Bruker BioSpin GmbH, Rheinstetten, Germany). A sine-squared window function was applied along with zero filling to 1024 data points in both

dimensions. All 2D data sets were deconvoluted using the mixed line shape function with a 90% Gaussian and 10% Lorentzian contribution to obtain integrated intensities.

3.2.3 The rate-matrix approach

To obtain quantitative data for the spin-diffusion rate constants of Eq. (3.1), a rate-matrix approach has been applied. The diagonal peaks were normalized with the sum of the respective cross peak intensities. These integrated and normalized diagonal and cross-peak intensities were used to determine the spin-diffusion rate constants using Matlab scripts (Matlab, The MathWorks, Natick, Massachusetts, USA). The time evolution of the spin-diffusion process is described by the differential equation

$$\frac{d}{dt}\vec{p}(t) = W\vec{p}(t), \qquad (3.3)$$

where $\vec{p}(t)$ is the time-dependent vector of all the polarizations of the involved resonances and the matrix W contains the rate constants W_{ij} in the off-diagonal elements while the diagonal elements are given by (Ernst & Meier, 1998)

$$W_{jj} = -\sum_{i \neq j} W_{ij} - R_1^{(j)}. \qquad (3.4)$$

Here, $R_1^{(j)}$ is the longitudinal relaxation rate constant of the resonance *j*. A sparse rate matrix with non-zero elements for all ^{13}C spin pairs that are separated by a distance less than 6 Å was used. Non-linear least-square fitting was used to optimize the spin-diffusion rate constants and the relaxation-rate constants in order to obtain information about the possible polarization-transfer pathways. For the fit, a series of 2D photo-CIDNP DARR MAS NMR spectra with spin-diffusion mixing times from 0.02 s to 10 s (not shown) were used. Figure 3.3, showing a spectrum with a mixing time of 2 s, is an example of this series of spectra. The obtained rate constants are shown in Table 3.2 & Table 3.3 and plots of some of the experimental cross-peak and diagonal-peak intensities together with the best fitted curves are shown in Figure 3.4 and Figure 3.5. The intensity of the diagonal peak at zero mixing time has been normalized to unity.

3.3 Results & discussion

3.3.1 Signal assignment

Many ^{13}C resonances of the BChl cofactors of the Special Pair have already been assigned in previous studies on unlabelled (Prakash *et al.*, 2006; Daviso *et al.*, 2009b), and selectively with 4-ALA (Schulten *et al.*, 2002; Daviso *et al.*, 2009a) and 5-ALA (Prakash *et al.*, 2007) labelled WT RCs. While the 4-ALA and 5-ALA label patterns allow the study of the aromatic carbons of the BChl and BPhe macrocycles, 3-ALA labelling leads to isotope enrichment of the more peripheral carbon positions (Figure 3.1A and 3.2). This labelling pattern is particularly suitable for observation of spin diffusion because it provides a broad range of distances as well as chemical-shift differences between pairs of labels. Figure 3.3 shows a 2D photo-CIDNP DARR MAS NMR spectrum of a selectively labelled 3-ALA (WT) RC sample.

In this experiment, the spin-diffusion mixing time was set to 2 s to observe as many cross peaks as possible. In Chapter 2, similar experiment had been performed but with a mixing time of 1 s. The corresponding 1D spectra shown on the top and on the side demonstrates that all signals are emissive (negative). The negative sign of the signal has been explained by the dominance of the three-spin mixing mechanism which involves a symmetry breaking process by the nuclear Zeeman, hyperfine and anisotropic interactions. This leads to emissive signals, independent of the sign of all other interactions involved.

Only ^{13}C nuclei from the two BChl cofactors of the Special Pair and the primary electron acceptor BPhe of the A branch that form the primary radical pair are observed with photo-CIDNP MAS NMR on RCs of *R. sphaeroides* WT (Prakash *et al.*, 2005; Prakash *et al.*, 2006; Daviso *et al.*, 2009a; Daviso *et al.*, 2010). The earlier studies have demonstrated that P_L carries a higher electron spin density and shows generally higher signal intensities than P_M. Further, the two-dimensional spectrum displayed in Figure 3.3, we observe two correlation networks; and they have been assigned in the similar way *i.e.*, the one with the higher signal intensities is from P_L and labelled in blue, while the second one is assigned to P_M

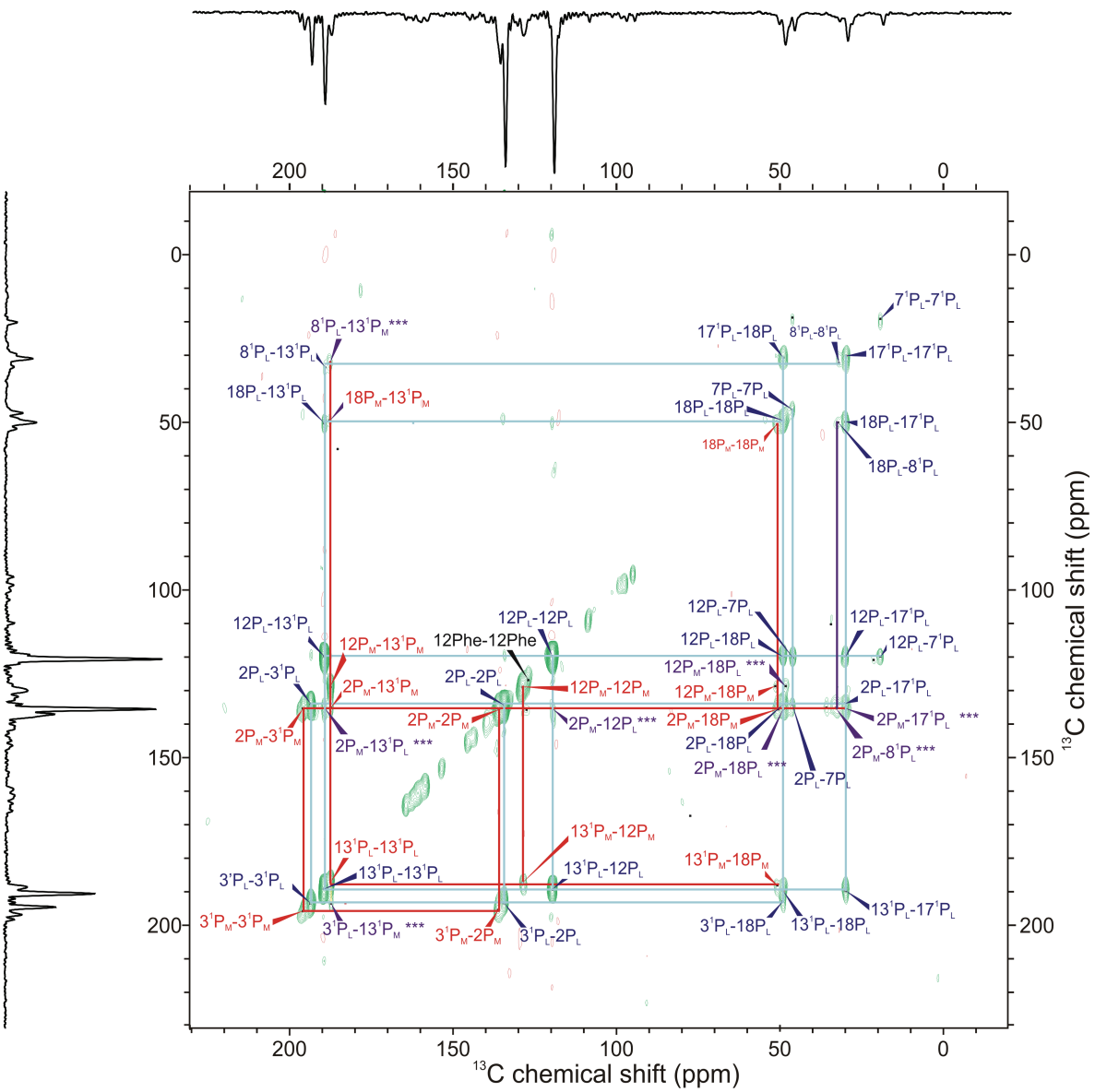

Figure 3.3 Two-dimensional photo-CIDNP DARR MAS NMR spectra of 3-ALA labelled RCs of *R. sphaeroides* WT obtained at a temperature of 223 K with a spin-diffusion mixing time of 2 s and a MAS frequency of 8 kHz. Two correlation networks are distinguished: One network is assigned to P_L (blue) while the other is assigned to P_M (red). Intermolecular cross peaks are shown in purple.

and is labelled red. The isolated C7/C8 pair can be conveniently added into the red network. In addition, at 126.9 ppm (C12 Phe), a signal occurs without any correlation, and is therefore assigned to the primary acceptor.

The strategy applied for assigning the spectrum in chapter 2 as been applied here. Starting point for the assignments can be the C3^{1} resonances, which appear in the carboxylic region at lowest field, *i.e.*, at 195.6 ppm for the red and at

Table 3.1 Assignment of the signals from 3-ALA-labelled from Special Pair in BRCs obtained with continuous illumination.

^{13}C position	P_L (ppm)	P_M (ppm)
2	134.3	136.0
3'	193.5	195.6
7	46.1	48.3
8'	32.1	-
12	119.5	128.8
13'	189.4	187.5
17'	29.9	28.4
18	49.1	50.9

193.5 ppm for the blue network. Alternatively, the signals of the two aromatic carbon positions, C2 and C12, provide a starting point, since these carbons obtain the strongest enhancement by the TSM photo-CIDNP effect (Prakash *et al.*, 2005). Aliphatic carbons C7 and C18, located on the macrocycle, resonate with a chemical shift around 50 ppm. Two labelled side chain carbons, $C8^1$ and $C17^1$, resonate around 30 ppm. Table 3.1 summarizes the assignments. Since the photo-CIDNP polarization transfer among the labelled ^{13}C atoms is mediated by spin diffusion, which operates through space providing access to the intermolecular distances and thus acting as a "Spin-torch" experiment. In addition to the two intramolecular networks, there are few cross-peaks, labelled purple, that arise from correlations between P_L and P_M. Examples of such correlations between P_L and P_M are $C3^1(P_L)$ / $C13^1(P_M)$ (7.1 Å), $C8^1(P_L)$ / $C13^1(P_M)$ (7.1 Å) and from P_M to P_L: $C12(P_M)$ / $C18(P_L)$ (13.1 Å), $C2(P_M)$ / $C18(P_L)$ (5.5 Å), $C2(P_M)$ / $C8^1(P_L)$ (7.9 Å), $C2(P_M)$ / $C17^1(P_L)$ (6.3 Å), $C2(P_M)$ / $C12(P_L)$ (8.4 Å), $C2(P_M)$/ $C13^1(P_L)$ (8.8 Å).

3.3.2 Spin Diffusion Measurements

The spin-diffusion rate depends directly on the strength of the dipolar couplings. Local dynamics will lead to partial averaging of dipolar couplings and, therefore, also to a reduction of the spin-diffusion rate constants compared to the corresponding rigid spin configuration The rate constants extracted from the DARR spectra are shown in Table 3.2 and Table 3.3, while some characteristic experimental sets for the build up and decay of cross-peak and diagonal-peak intensities, together with the analysis from the nonlinear least squares fitting of the rate matrix in eq (3.4), are shown in Figure 3.4 and Figure 3.5. The intensity of the diagonal peak at zero mixing time has been normalized to unity.

Due to the sparse labelling pattern of the BChl rings (Figure 3.1 and 3.2), the shorter internuclear distances are optimal for direct transfer of polarization within pairs of labels. The distances for intramolecular pairs are equal in P_L and P_M: $C17^1/C18$ (2.5 Å), $C7^1/C8^1$ (2.5 Å), $C2/C3^1$ (2.8 Å), and $C12/C13^1$ (2.8 Å). In addition, for the overlap region of P_L and P_M, the intramolecular distances for the $C2/C3^1$ pairs (2.8 Å) are significantly shorter than the shortest intermolecular distance between pairs of labels in the ring and in the side chain positions, C2 (P_L)/$C2^1$ (P_M) (3.8 Å). Polarization transfer between the nearby ^{13}C nuclei is mainly direct and can provide information about the local mobility.

The DARR spectra (Figure 3.3) also reveal correlation peaks for long range transfer up to 13 Å. Examples of long distance correlations between P_L and P_M are $C8^1(P_L)$ / $C13^1(P_M)$ (7.1 Å), $C2(P_M)$ / $C8^1(P_L)$ (7.9 Å), $C2(P_M)$ / $C12(P_L)$ (8.4 Å) and $C12(P_M)$ / $C18(P_L)$ (13.1 Å). Very little direct polarization transfer over such a long distance is possible and these cross peaks are attributed to relayed multi-step polarization transfer. The quantitative analysis of the spin-diffusion pathways with the relaxation matrix confirms that these long distance correlation events are mediated by relayed transfer involving various nuclei in the network of labels. Figure 3.6 shows four examples of such networks of multi-step transfers. In Figure 3.6A, the correlation network linking $C2(P_M)$ and $C8^1(P_L)$, over a distance of 7.9 Å,

Table 3.2 ^{13}C-^{13}C correlation pairs (diagonal peaks) with calculated rate constants for decay of the peaks obtained by nonlinear least squares fitting of the relaxation matrix.

No	Correlation pair	Calculated rate constant (sec^{-1})	Displayed
1	$C2(P_M)$	0.07	A
2	$C3^1(P_M)$	0.84	B
3	$C12(P_M)$	0.35	C
4	$C13^1(P_M)$	0.00	D
5	$C18(P_M)$	0.09	-
6	$C2(P_L)$	0.31	A
7	$C3^1(P_L)$	0.12	B
8	$C7(P_L)$	0.81	-
9	$C8^1(P_L)$	0.02	-
10	$C12(P_L)$	0.37	C
11	$C13^1(P_L)$	0.21	D
12	$C17^1(P_L)$	0.00	I
13	$C18(P_L)$	0.23	J

Table 3.3 ^{13}C-^{13}C correlation pairs (cross peaks) with distances and calculated rate constants for the rise of the peaks obtained by nonlinear least squares fitting of the relaxation matrix.

No	Correlation pair	Distance (Å)	Calculated rate constant (sec^{-1})	Displayed
1	$C2(P_M)$ / $C\text{-}3^1(P_M)$	2.8	3.02	E,F
2	$C2(P_M)$ / $C18(P_M)$	5.1	0.18	-
3	$C2(P_M)$ / $C2(P_L)$	3.8	0.00	-
4	$C2(P_M)$ / $C3^1(P_L)$	5.1	0.00	-
5	$C2(P_M)$ / $C18(P_L)$	5.5	0.08	-
6	$C3^1(P_M)$ / $C2(P_L)$	4.9	0.22	-
7	$C3^1(P_M)$ / $C3^1(P_L)$	6.0	0.00	-
8	$C3^1(P_M)$ / $C7(P_L)$	5.4	0.33	-
9	$C3^1(P_M)$ / $C8^1(P_L)$	5.6	1.93	-
10	$C3^1(P_M)$ / $C12(P_L)$	5.9	0.35	-
11	$C3^1(P_M)$ / $C17^1(P_L)$	5.8	0.00	-
12	$C3^1(P_M)$ / $C18(P_L)$	5.6	0.19	-
13	$C12(P_M)$ / $C13^1(P_M)$	2.8	0.61	G,H
14	$C12(P_M)$ / $C3^1(P_L)$	6.0	0.08	-
15	$C13^1(P_M)$ / $C18(P_M)$	6.0	0.14	-
16	$C18(P_M)$ / $C2(P_L)$	5.9	0.04	-
17	$C2(P_L)$ / $C\text{-}3^1(P_L)$	2.8	1.61	E,F
18	$C2(P_L)$ / $C18(P_L)$	5.0	0.41	-
19	$C3^1(P_L)$ / $C7(P_L)$	5.6	0.15	-
20	$C7(P_L)$ / $C8^1(P_L)$	2.5	0.00	-
21	$C8^1(P_L)$ / $C12(P_L)$	5.2	0.00	-
22	$C12(P_L)$ / $C13^1(P_L)$	2.9	2.19	G,H
23	$C13^1(P_L)$ / $C17^1(P_L)$	4.9	0.51	-
24	$C17^1(P_L)$ / $C18(P_L)$	2.5	10.00	K,L

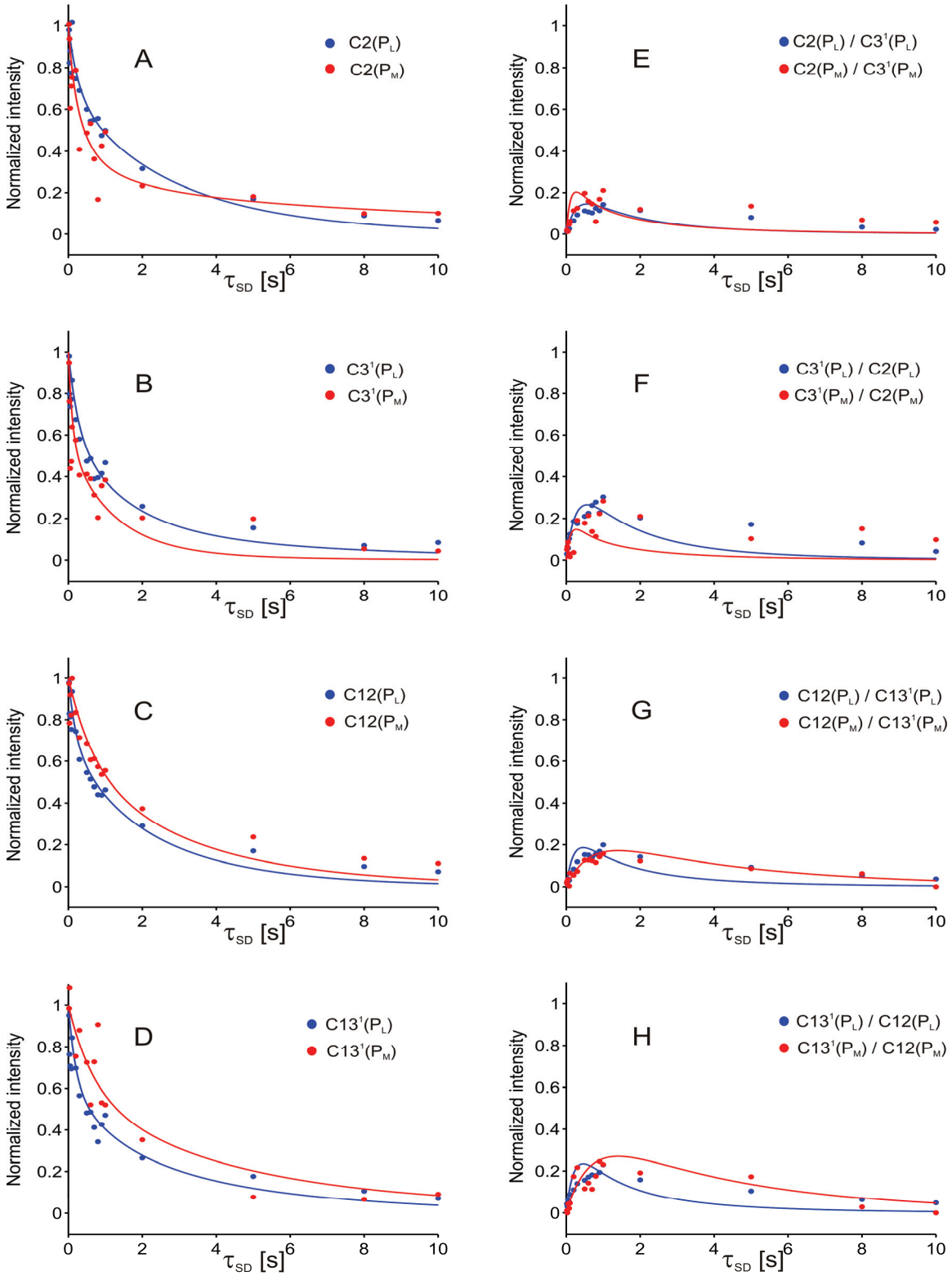

Figure 3.4 Decay of normalized diagonal peaks of P_L (blue) and P_M (red) and evolution of corresponding cross peaks of P_L (blue) and P_M (red) for selected ^{13}C-^{13}C correlation pairs.

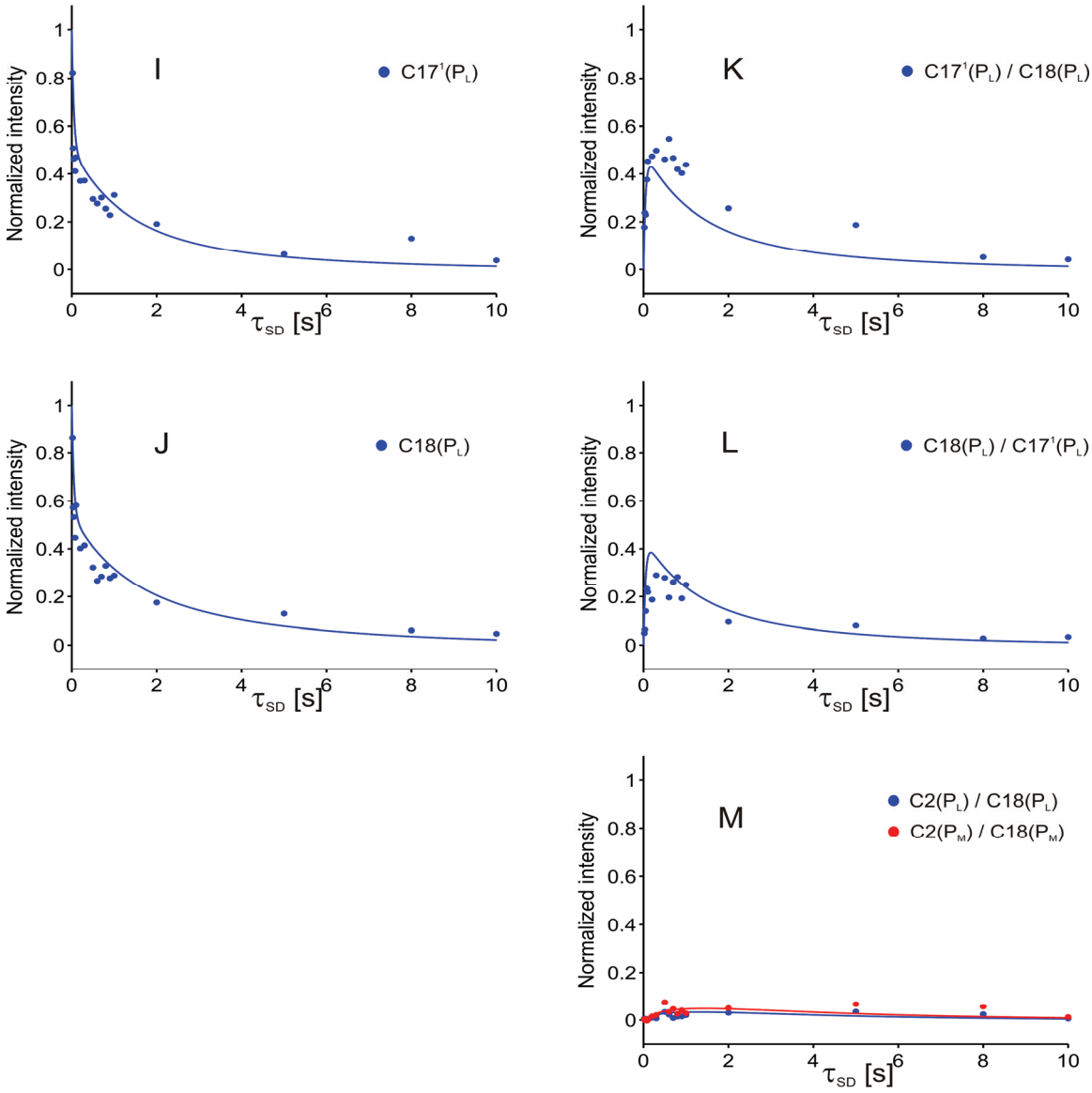

Figure 3.5 Decay of normalized diagonal peaks of P_L (blue) and P_M (red) and evolution of corresponding cross peaks of P_L (blue) and P_M (red) for selected ^{13}C-^{13}C correlation pairs.

is presented. The transfer occurs via two steps: first from C2(P_M) to C3^1(P_M) (2.8 Å), and then to C8^1(P_L) (5.6 Å). In Figure 3.6B, the most efficient pathway allowing for the correlation between C2(P_M) and C12(P_L), at a distance of 8.4 Å, is indicated. The transfer occurs via five steps, first from C2(P_M) to C2(P_L) (3.8 Å), then via C18(P_L) (5.0 Å), to C17^1(P_L) (2.5 Å), C13^1(P_L) (4.9 Å) and finally to C12(P_L) (2.9 Å). In this pathway, the C2(P_M) and C2(P_L) act as a bridge to transfer the polarization between the two cofactors of the Special Pair.

In Figure 3.6C, the transfer over a distance of 13.1 Å between C12(P_M) to C18(P_L) can proceed by several pathways. From the analysis of rate constants, we see that the polarization is transferred to C12(P_M) via C13^1(P_M) (2.8 Å), C18(P_M) (6.0 Å), C2(P_M) (5.1 Å), C3^1(P_M) (2.8 Å) and finally to C18(P_L) (5.6 Å). In Figure 3.6D, another example of long-distance transfer is presented. While the distance between C8^1(P_L) to C13^1(P_M) is 13.1 Å, the polarization is transferred via C3^1(P_M) (5.6 Å), C2(P_M) (2.8 Å), C18(P_M) (5.1 Å) and finally to C13^1(P_M) (6.0 Å). In any case, the occurrence of such long-distance contacts demonstrates that reduction of dipolar couplings by motional averaging is limited, and confirms that packing effects on the BChl comprising the Special Pair from the protein surrounding lead to a ground state potential energy surface that enhances the mobility of the rings for selective collective modes. A single, well defined and narrow NMR signal

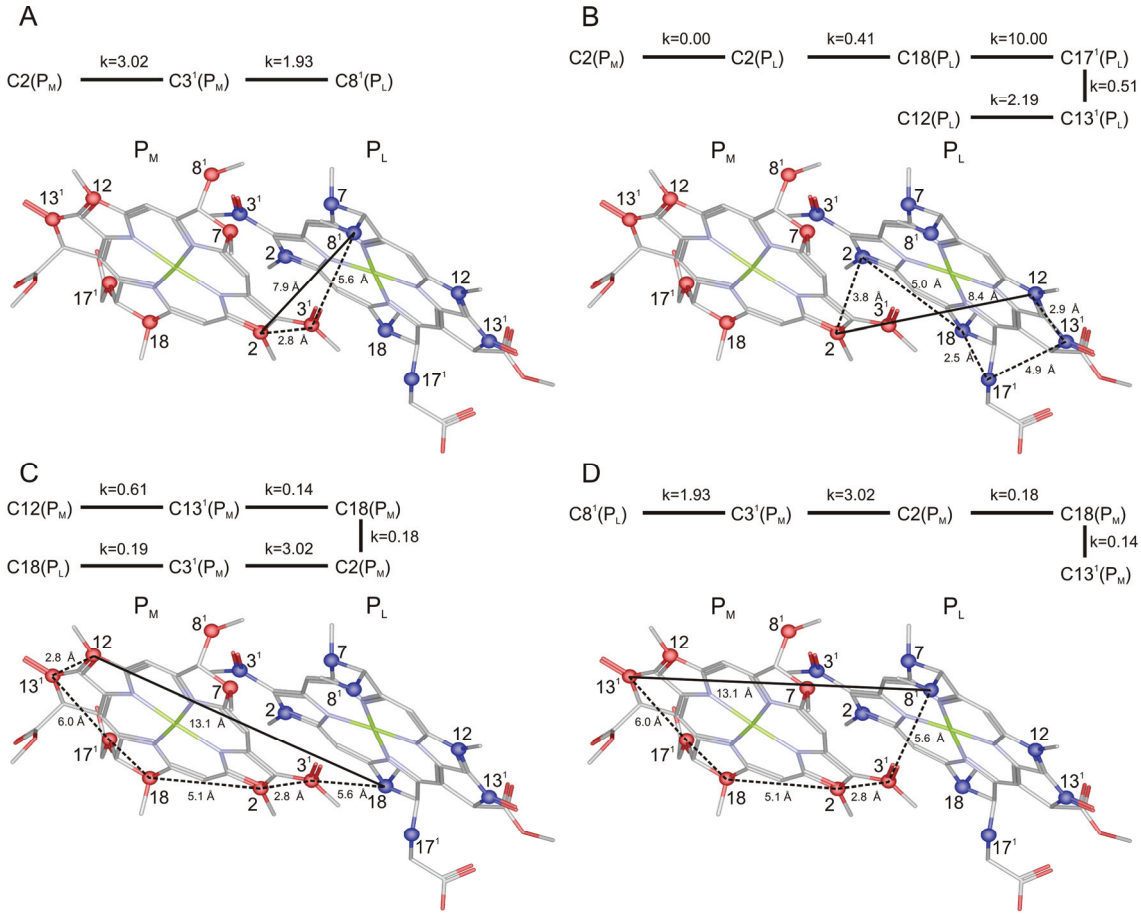

Figure 3.6 Selected polarization-transfer pathways obtained from the rate-matrix analysis. The solid line indicates the shortest distance between two carbons, while the dashed lines show the possible relay transfer between those two carbon atoms.

component is observed for every ^{13}C label of P by partial dynamic averaging of the supermolecular structure, instead of *e.g.* spectral doubling or gross inhomogeneous broadening due to polymorphism (Schulten *et al.*, 2002; Prakash *et al.*, 2005). This contrasts with optical spectroscopy that operates on a much shorter time scale and reveals quasi-static site disorder, variations of the structure of the special pair in the protein complex. In the optical experiments variations of the site energies lead to inhomogeneous broadening of the optical absorption profile (Hunter *et al.*, 2008).

The left part of Figure 3.4 (Plots A-D) compares the signal decay on selected carbons of both halves of the Special Pair. Those selected carbon atoms displayed there, show a different kinetics trend depending on their positions in the Special Pair. The difference is summarized in Figure 3.7, Table 3.2 and Table 3.3. The origin of this difference, however, is not clear. It may be due to enhanced mobility in low frequency collective vibrational modes that gives spectral density at the higher end of the T_1 NMR sensitivity region to drive spin-lattice relaxation. Alternatively, less dynamics can lead to an increase of the spin diffusion efficiency and more rapid decay. Hence, although plots A-D of Figure 3.4 clearly demonstrate that the symmetry in the Special Pair regarding the dynamics is broken, it is difficult to conclude for which of the two rings there is more constrained dynamics.

To determine which of the two sides is more flexible, the time dependence of the build up of the cross peaks is studied. This can be correlated with the spin diffusion efficiency, while T_1 relaxation of the carbons is not relevant on that short time scale. The kinetics of the decay of the diagonal-peaks is shown in the left parts of Figure 3.4 and 3.5. These two figures are summarized in Figure 3.7A and Table 3.2. Here the magnitude is visualized by the radius and color of the circle that matches the labelled position on Special Pair. The circles on the right side are larger than for the left hand side of the pseudo–C_2 axis. The kinetics of the build-up of the cross-peaks is shown in the right parts of Figure 3.4, 3.5 and is summarized in Figure 3.7B and Table 3.3**.** In this Figure 3.7B, the magnitude of the

spin-diffusion rate constants is visualized by the line width of an ellipse connecting the two ^{13}C labels involved. The spin diffusion in the right half of the Special Pair supermolecule is faster than the spin diffusion in the left half. Interestingly, this difference cannot be attributed to the two individual cofactors P_L and P_M, and is associated with the left and right half of the Special Pair supermolecule. All three pairs on the right half (C2/C18 and C12/C13^1 of P_L as well as C2/C3^1 of P_M) are significantly stronger coupled than the two pairs on the left half (C2/C18 and C12/C13^1 of P_M as well as C2/C3^1 of P_L). In addition the pair (C12/C13^1 of P_M) at the edge of the inactive branch appears to be rather mobile.

3.3.3 Possible implications for directed electron transfer

The Special Pair supermolecule is thus relatively rigid towards the P_L side, while the P_M side shows significantly more mobility that partially averages the dipolar couplings and leads to longer buildup times than for the corresponding pairs on the A side (Figure 3.7B). This shows that there is dynamic asymmetry in the Special Pair. The NMR detects a constrained but homogeneous structure with rapid averaging of dynamic disorder revealed by narrow lines in the spectra. In contrast, optical spectroscopy suggests heterogeneity which is revealed by inhomogeneous line broadening due to site disorder of the system (Reddy *et al.*, 1992; Reddy *et al.*, 1993). In addition, there is converging evidence for asymmetry of the average electronic structure, both for the ground- and the excited state, from distortions imposed upon the structure by geometric constraints and steric hindrance of the side chains. The protein environment also affects the electronic structure of the porphyrin ring via the electron-phonon coupling (Chapter.2; Lendzian *et al.*, 1993; Yamasaki *et al.*, 2008; Daviso *et al.*, 2009c).

To add to the structural basis for the asymmetry of the dynamics in the ground state observed with NMR, an analysis of polymorphism of the P_L and P_M in the available X-ray structures with resolution better than 3Å is shown in Figure 3.8, using the Normal-Coordinate Structural Decomposition (NSD) method (Jentzen *et al.*, 1997). A vibrating molecule moves along its normal coordinates,

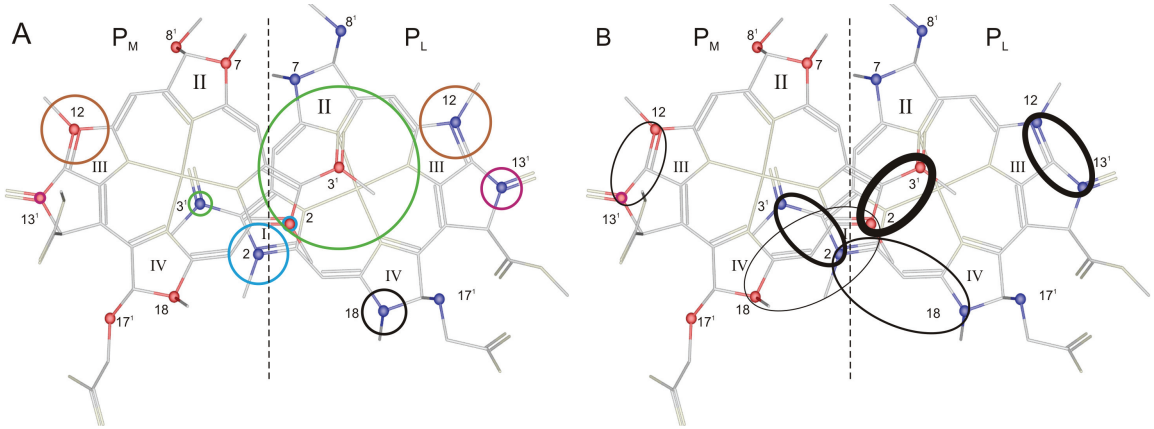

Figure 3.7 Spin-diffusion dynamics in the Special Pair. (A) The rate constants of carbon atoms from their diagonal peaks (The magnitude is visualized by the radius). (B) The rate constants of carbon atoms from their cross peaks (The magnitude of spin-diffusion-rate constants are visualized by the linewidth of an ellipse connecting the two ^{13}C labels).

and the molecular distortion is expressed as a sum of displacements along 3N-6 normal coordinates. For porphyrin systems, the macrocycle deformations are soft modes of distortion and correspond with the six lowest-frequency normal modes of the molecule. This method quantifies the nonplanarity of porphyrin structures by displacements along the lowest-frequency normal coordinates of the macrocycle (Jentzen *et al.*, 1998; Shelnutt *et al.*, 1998).

The bar graph of the displacements along the low frequency ring modes in Figure 3.8, indicates similarities and differences for the P_L and P_M in 3 different crystal structures. The largest variability is found for both BChls along the saddling and ruffling normal coordinates, which represent the softest modes of distortion and corresponds with the lowest frequency vibrations, usually around 65 cm^{-1} and 88 cm^{-1} in porphyrins (Shelnutt *et al.*, 1998). In P_L, the displacement along the doming mode coordinate is remarkably persistent and is ~ 1.1 Å in the three structures (Figure 3.8A). The doming mode has a characteristic frequency around 135 cm^{-1} in porphyrins (Shelnutt *et al.*, 1998). In contrast, the displacement for doming in P_M is small (Figure 3.8B). This makes it easier to deform the P_M ring than the P_L ring, in line with the NMR data that show enhanced dynamics for the P_M relative to the P_L. In addition, for the NSD analysis in Figure 3.8 the magnitude of the displacements along the saddling and ruffling coordinates for the P_M

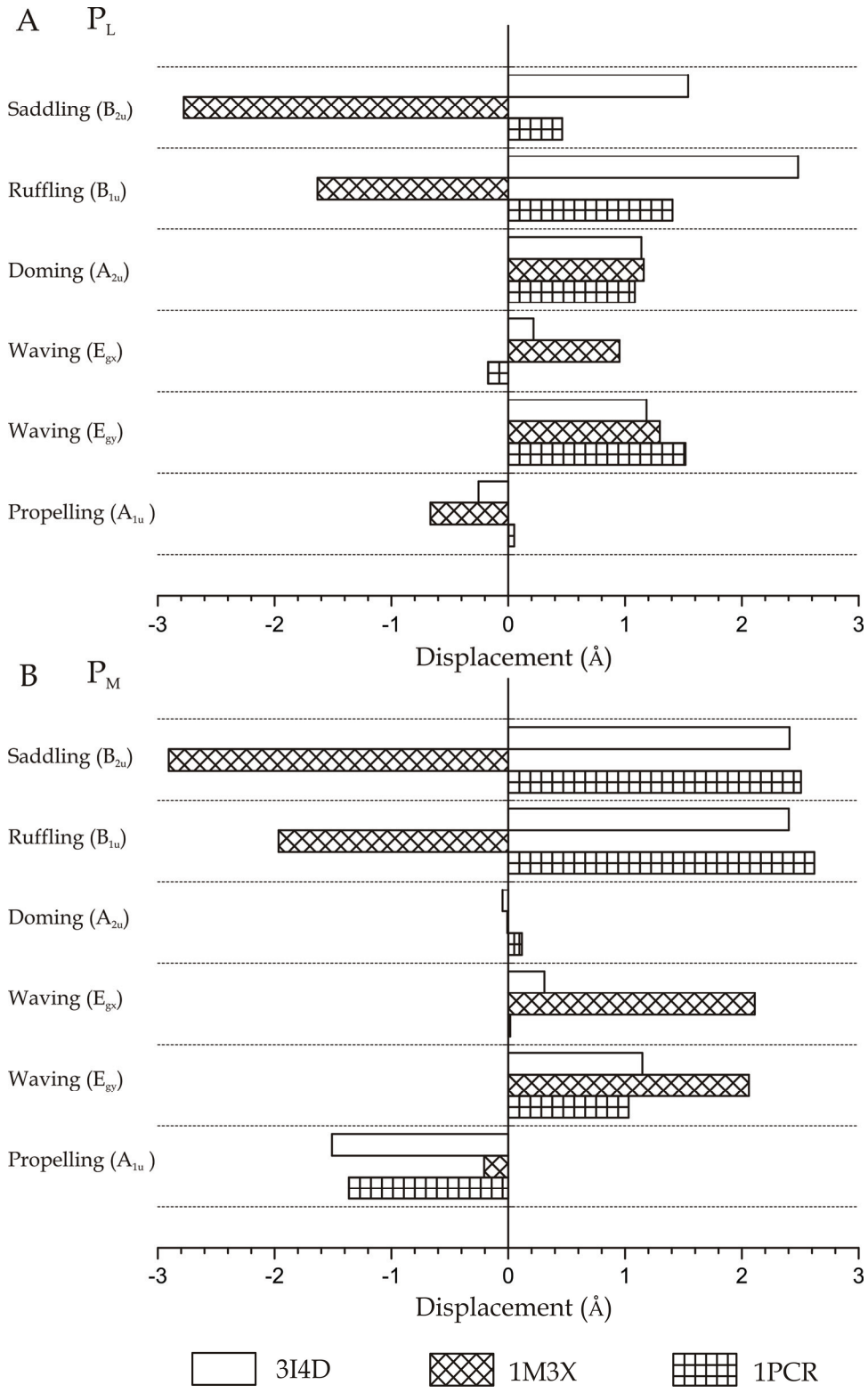

Figure 3.8 Nonplanarity of the P_L (A) and P_M (B) for three different X-Ray structures of *R. sphaeroides* RCs along the six lowest frequencies normal coordinates of the macrocycles.

appears larger than for the P_L. In this way the static structural variation in the X-ray data matches the dynamics observed in NMR data.

In early theoretical treatments of electron transfer in proteins, a coupling of the system to many thermal vibrational modes is invoked to obtain a rapid transfer process (Marcus, 1956b, 1965; Marcus & Sutin, 1985). In contrast with the Marcus treatment, in recent Redfield matrix analyses the charge separation dynamics is determined by the combined displacement along two selective vibrational modes to produce a high forward transfer rate and a low probability for back transfer. A 130 cm^{-1} collective mode connected with the intermolecular dynamics within the special pair governs the displacement along the first reaction coordinate (Novoderezhkin *et al.*, 2004). A planar ring structure is anomalous for a five-coordinated Mg^{2+}. NMR and modeling studies have provided evidence that the ground state exhibits HisL173$^{\delta+}$–$P_L^{\delta-}P_M^{\varepsilon-}$-HisM202$^{\delta+}$-$H_2O^{\delta-}$ charge transfer character (Schulten *et al.*, 2002; Prakash *et al.*, 2007; Alia *et al.*, 2009; Daviso *et al.*, 2009b; Wawrzyniak *et al.*, 2011; Wawrzyniak, 2011). In this scheme, the HisM202 is stabilizing both P_M and the attached water molecule by hydrogen bonding and partial charge transfer at both imidazole nitrogens (Alia *et al.*, 2009). In addition, EPR shows that after the release of an electron into the active branch the P_M carries excess positive charge. In contrast, the studies on RCs of *R. sphaeroides* by Stark spectroscopy indicate that the excited state of the Special Pair contains charge-transfer character of the form $P_L^+P_M^-$ (Lockhart & Boxer, 1987, 1988). In parallel hole-burning experiments showing a marker mode of ~120 cm^{-1}, indicate a persistent change upon excitation (Reddy *et al.*, 1992; Lyle *et al.*, 1993).

Our analysis suggests that the special pair dynamics involved in the initiation of charge transfer is asymmetric and restricted to the overlap region formed by the rings I of the P_L and the P_M, where most of the dynamics is in the P_M. According to the NMR and X-ray, the P_M is in an anomalous planar average structure with enhanced mobility in selective modes. The release of free energy in the excited state could then activate its deformation for mediating charge transfer by a geometry change, possibly towards a more domed conformation of the P_M and involving lowering of the free energy by the damping of vibrations. Finally, the dynamics detected with the NMR affects the ring structure and should give

rise to fluctuations in the $P_L^{\delta-}P_M^{\varepsilon-}$ charge transfer character. Indeed, in analyses of X-ray structures, charge density distributions depend on the polymorphism in the structure (Wawrzyniak *et al.*, 2011).

Chapter 4

Characterization of bacteriopheophytin *a* in the active branch of the reaction center of *Rhodobacter sphaeroides* by ^{13}C photo-CIDNP MAS NMR

Abstract

The electronic structure of the primary electron acceptor, bacteriopheophytin *a* (Φ_A), in photosynthetic reaction centers (RCs) of the purple bacterium *Rhodobacter (R.) sphaeroides* is investigated by photochemically induced dynamic nuclear polarization (photo-CIDNP) magic-angle spinning (MAS) NMR spectroscopy. Uniformly labelled RCs have been prepared for these experiments, by adding the u-$^{13}C_4$-δ-aminolevulinic acid as a precursor in the growing medium of *R. sphaeroides* wild type (WT). By using assignments from different selective labelling patterns, the ^{13}C observed chemical shifts attributed to the Φ_A have been compiled. These assignments are supported by theoretical calculations of ^{13}C chemical shifts of a bacteriopheophytin in two conformations, a fully relaxed geometry and in the x-ray structure found for Φ_A. The relative electronic densities of Φ_A in the ground state have been obtained by comparing these assignments with those of free bacteriopheophytin in acetone solution. From that analysis, it can be concluded that Φ_A in the active branch is not tuned in a special manner by its surrounding and appears to be electronically close to free bacteriopheophytin.

4.1 Introduction

Natural photosynthesis achieves the conversion of solar energy with a remarkably small set of cofactors, and the functional programming of the pigment chromophores is to a large extent encoded by their conformation, local environment, dynamics and mutual interactions. The photosynthetic apparatus of plants, algae and bacteria contain densely packed pigment-pigment and pigment-protein complexes for harvesting light and separating electrons and protons across the photosynthetic membrane (for reviews, (Hoff & Deisenhofer, 1997; Hunter *et al.*, 2008)). Both the photosynthetic reaction centers (RCs) and the light harvesting antennae of the purple bacterium *Rhodobacter (R.) sphaeroides* contain networks of interacting bacteriochlorophyll BChl *a*. In the RC, four BChl *a* and two bacteriopheophytin (BPhe) *a* are positioned in an apparent symmetric arrangement and use the energy absorbed by the BChls in LH2 and LH1 light harvesting antennae complexes. Two BChl *a* form an interacting dimer called the "Special Pair" (P). On either side of the special pair an additional BChl *a* molecule is located, the accessory BChls (B_A and B_B). In addition, two BPhe (Φ) are positioned at an edge-to-edge distance of ~14 Å from the special pair (Yeates *et al.*, 1988; Ermler *et al.*, 1994; Camara-Artigas *et al.*, 2002b).

Despite an approximate global symmetry in the arrangement of these six cofactors, their functioning is asymmetric, since charge separation proceeds almost exclusively over the A-branch. When excitations from the antennae are trapped by the special pair in the RCs, quantum delocalization by electron tunneling from the P* into the B_A and then into the Φ_A, leads to symmetry breaking of the excited state to establish the consecutive charge transfer contributions $P^+B_A^-$ and $P^+\Phi_A^-$. Hence, for the RC of *R. sphaeroides*, the charge transfer proceeds along the redox gradient represented by the cofactors of the A branch, and the functional mechanisms of this electron transfer process have been well studied. EPR, ENDOR and optical methods have provided insight into the electronic and spatial structure of the Special Pair donor and have clarified the role of the accessory BChls in the ET reaction (Feher *et al.*, 1972; Lubitz *et al.*, 1985; Shkuropatov & Shuvalov, 1993;

Schmidt *et al.*, 1994; Holzwarth & Muller, 1996; Franken *et al.*, 1997a, b; Lubitz & Feher, 1999; Moore *et al.*, 1999). The two halves of P are bound to the L and M subunits of the protein complex. MAS NMR in the dark and with photo-CIDNP enhancement has revealed packing effects on the cofactors induced by the folding and self-assembly of the RC complex. These packing effects produce structural deformation and electrostatic polarization of the BChl macrocycles and lead to electronic asymmetry of the form $P_L^{\delta-}P_M^{\varepsilon-}$ between the two BChl *a* of the P, (Prakash *et al.*, 2007; Alia *et al.*, 2009; Daviso *et al.*, 2009c; Wawrzyniak *et al.*, 2011). The variation of chemical shifts, also relative to the ^{13}C responses of BChl *a* in solution, cannot be explained by local side chain interactions, such as hydrogen bonding or nonplanarity of the $C3^1$ acetyl, but appears to be dominated by protein-induced macrocycle distortion (Daviso *et al.*, 2009c; Wawrzyniak *et al.*, 2011). Shaping of the macrocycle prominently affects the site energies, and this allows for dynamic structural tuning of the energy levels of the BChls by photosynthetic protein complexes (Daviso *et al.*, 2009c; Pandit *et al.*, 2010; Wawrzyniak *et al.*, 2011). In addition, ^{15}N and ^{13}C NMR data and DFT calculations have revealed an asymmetric electronic environment of P, which can facilitate thermodynamic control over the rate and direction of electron transfer (Alia *et al.*, 2009; Wawrzyniak *et al.*, 2011). Light enhanced DARR correlation spectroscopy of dynamic measurements in the ground state has shown that the protein environment induces strain on the BChls of P. The pair of BChls is subject to thermally activated dynamics along a few specific soft collective vibrational modes, which may lead to polymorphism in crystallization experiments and explain the inhomogeneous broadening of the optical absorption at ambient temperature (Huber *et al.*, 1998). The special pair dynamics is asymmetric, it is restricted to the overlap region formed by the rings I of the P_L and the P_M, and most of the dynamics is in the P_M (Chapter.2).

The excitation of P causes a change in the shape of P and its environment (Friesner & Won, 1989). The localized dynamics initiates directional charge transfer character in the special pair at the first stage of the photochemistry by symmetry breaking of excitons and increasing the polaronic character, leading to a

$P_L^+P_M^-$ charge transfer contribution to the product state (Moore *et al.*, 1999). The rate of formation of the $P^+\Phi_A^-$ primary product state depends on its free energy level relative to the $P^+B_A^-$ intermediate. When BPhe *a* is replaced by plant pheophytin *a* with a more negative redox potential, the free energy level of $P^+\Phi_A^-$ is ~ 200 cm^{-1} above $P^+B_A^-$, and this slows down the forward electron transfer (Franken *et al.*, 1997a, b). For such pheophytin-modified RCs of *R. sphaeroides* R-26, a coupling to collective nuclear modes in the development on the excited state potential energy surface leads to classically coherent control over the quantum delocalization in the formation of the charge separated states $P^+B_A^-$, $P^+\Phi_A^-$, and this has helped to resolve the mechanism of symmetry breaking in the first steps of the charge separation processes (Shuvalov & Yakovlev, 2003).

In contrast with the Marcus theory of electron transfer, the charge separation dynamics is apparently not coupled to random thermal motion in many nuclear modes (Marcus, 1956a, b, 1965). The strength of the coherence primarily depends on the displacement along two collective nuclear modes, an intradimer mode of around 130 cm^{-1} and a low frequency mode of ~32 cm^{-1} that is attributed to reorganization of a water molecule (Yakovlev *et al.*, 2002). This H_2O is hydrogen bonded to the B_A ring V keto functionality and the N_π of the HisM202 that is axially coordinated with its N_τ to the Mg^{2+} of the P_M. According to DFT modeling guided by MAS NMR data, this structural motif can stabilize a $P^+B_A^-$ charge transfer contribution by a release of free energy (Alia *et al.*, 2009; Wawrzyniak *et al.*, 2011). The 130 cm^{-1} collective mode is connected with the intermolecular dynamics within the special pair and its histidine ligands that develop the $P_L^+P_M^-$ charge transfer character upon excitation of the RC. Via the partially charged and polarizable His and the H_2O, the change in magnitude and angle upon excitation of the electric dipole moment of P that is governed by the intradimer displacement along the 130 cm^{-1} reaction coordinate can be coupled to $P^+B_A^-$ charge transfer, initially without a large structural displacement in the H_2O bridge (Alia *et al.*, 2009; Wawrzyniak *et al.*, 2011).

According to a recent Redfield density matrix analysis of a phenomenological model of the RC, comprising the P* and the $P^+B_A^-$ diabatic states strongly coupled to two modes, the electron transfer proceeds only after some passages through the crossing point of the P* and the $P^+B_A^-$ energy levels, by the displacement along the second reaction coordinate, the 32 cm^{-1} collective mode that is thought to be connected with the rotation of the water molecule . Thus, there is converging evidence that efficient photoproduct formation in a few picoseconds in the first steps of charge separation with a high forward transfer rate and a low probability for back transfer requires the combined displacement along a few selective vibrational modes coupled to symmetry breaking and charge transfer.

Thus, photosynthetic RC complexes represent complex dynamic topologies to promote charge separation on the excited state surface by easily accessible transition states and well-defined reaction coordinates for proceeding from the reactant to the product configurations $P_L^+P_M^-$ and $P^+B_A^-$. However, full charge separation requires transfer of an electron to the primary acceptor Φ_A to form the donor-acceptor radical pair state $P^+\Phi_A^-$ (Martin *et al.*, 1986).

The purpose of this study is to investigate by photo-CIDNP MAS NMR, the extent of functional preprogramming of the Φ_A, in its ground state, by charging, conformational tuning, or strain that produces thermal activation in specific modes. The discovery of the solid-state photo-CIDNP effect for *R. sphaeroides* R26 RCs under continuous illumination with white light, offers NMR access to the electronic and spatial structure of both the donor and the acceptor in the primary charge separation process (Zysmilich & McDermott, 1994). By induction of a non-Boltzmann nuclear spin polarization upon photoreaction in rigid samples, a signal enhancement of a factor of more than 10,000 has been observed by ^{13}C MAS NMR in several RCs (Prakash *et al.*, 2005; Prakash *et al.*, 2006; Roy *et al.*, 2008). The method is rapidly evolving, and solid-state photo-CIDNP is now routinely observed for virtually all types of photosynthetic RCs, including those of purple bacteria of *R. sphaeroides* wildtype (WT) (Prakash *et al.*, 2005) and of

Rhodopseudomonas acidophila (Diller *et al.*, 2008) of the green sulphur bacterium *Chlorobium tepidum* (Roy *et al.*, 2007), of the heliobacterium *Heliobacillus mobilis* (Roy *et al.*, 2008) as well as of the photosystems I and II of plants (Matysik *et al.*, 2000a; Alia *et al.*, 2004; Diller *et al.*, 2007a) and algae (Janssen *et al.*, 2010). The occurrence of the solid-state photo-CIDNP effect is an intrinsic property of natural photosynthetic RCs and Photo-CIDNP is a good method to resolve the local spatial and electronic structure both the donor and the acceptor, thereby providing access to intimate details of how the $P^{+}\Phi_{A}^{-}$ state is involved in the cascade of symmetry breaking mechanisms (Matysik *et al.*, 2009).

4.2 Materials and Method

4.2.1 Sample Preparation and specific isotopic labelling

The isotope labelling of cofactors in RCs is achieved by using labelled δ-aminolevulinic acid (ALA) that acts as a precursor for the biosynthesis of BChl and BPhe (Jordan, 1991; Matysik *et al.*, 2001). By enriching the growth medium with (u-^{13}C)-ALA labelled substrate, RCs that are labelled in the macroaromatic cycles of the cofactors are produced (Figure 4.1). The RCs were isolated as described previously (Shochat *et al.*, 1994). Quinones were removed by incubating the RCs at a concentration of 0.6 µM in 4% LDAO, 10 mM *o*-phenanthroline, 10 mM Tris buffer, pH 8.0, containing 0.025% LDAO and 1 mM EDTA (Okamura *et al.*, 1975).

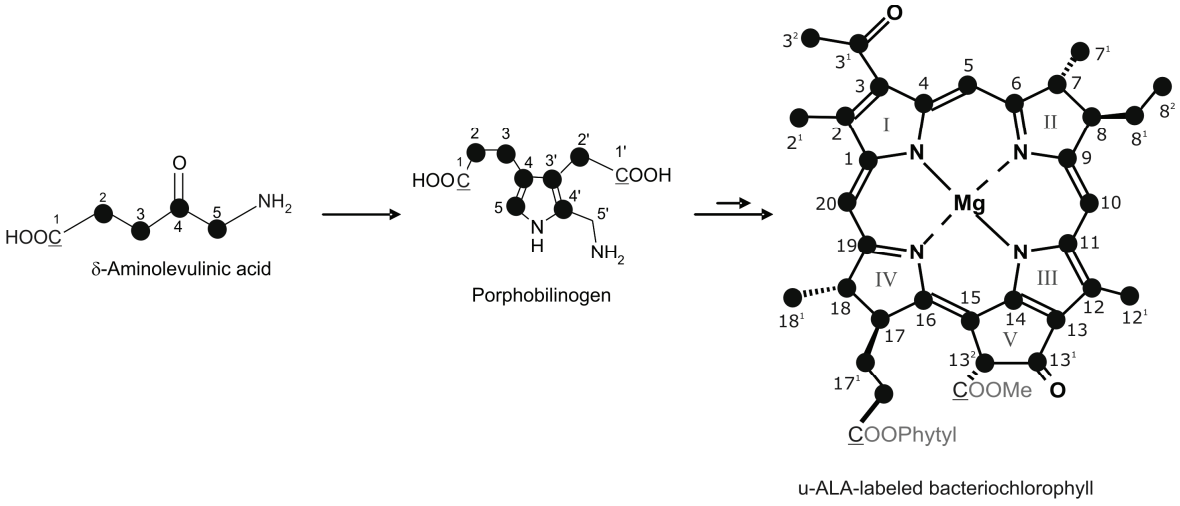

Figure 4.1 Biosynthetic pathway for the formation of selectively ^{13}C isotope labelled bacteriocholorophyll *a* (BChl) by feeding the bacteria with u-$^{13}C_4$-δ-aminolevulinic acid (u-ALA).

Approximately 15 mg of RC protein complex embedded in LDAO micelles was used for NMR experiments. Similarily with selective labeling of δ-aminolevulinic acid at different positions namely 3-^{13}C-ALA (chapter 3), 4-^{13}C-ALA (Daviso *et al.*, 2009a) and 5-^{13}C-ALA (Prakash *et al.*, 2007) RC's with sparse labeling in the cofactor rings were prepared (see: Figures in Appendix-A).

4.2.2 MAS-NMR experiments

NMR experiments were performed with an Avance DMX-200 NMR spectrometer equipped with a MAS probe (Bruker, Karlsruhe, Germany). The sample was loaded into a clear 4-mm sapphire rotor, inserted into the MAS probe and frozen slowly at a low spinning frequency of 600 Hz to ensure a homogeneous sample distribution against the rotor wall (Fischer *et al.*, 1992) . The light and dark spectra were collected with a Hahn echo pulse sequence with the CYCLOPS phase cycle of the (π/2) pulse and detection under proton decoupling using the TPPM sequence (Bennett *et al.*, 1995) at a temperature of 223 K under continuous illumination with white light (Matysik *et al.*, 2001). The optimum length of the (π /2) carbon pulse, determined on uniformly ^{13}C labelled tyrosine, is ~4 μs under our experimental conditions using a rf strength of 62.5 kHz. A recycle delay of 4 s was used. The sample was spinning at a MAS frequency of 8 kHz. A total number of 6240 scans (approximately 7 hrs) were collected for u-ALA RCs, while for 3-ALA, 4-ALA and 5-ALA labelled bacterial RCs around 256 scans (approximately 20 mins) were collected. An artificial line broadening of 30 Hz was applied prior to Fourier transformation. All the ^{13}C-MAS NMR spectra were referenced to the carbonyl resonance of solid tyrosine·(HCl) at 172.1 ppm. A small zero order phase correction was applied to correct line shape asymmetry to the dark and photo-CIDNP spectra of the RCs.

4.2.3 Theoretical models and methods

The coordinates for the initial model of the bacteriopheophytin molecule have been extracted from the 1M3X crystal structure of *R. sphaeroides* WT (Camara-Artigas *et al.*, 2002a). From this crystal structure, bacteriopheophytin *a* of the active

branch with residue id of 855 has been used. This model was partially optimized by relaxing carbons and nitrogens in the porphyrin ring, and all the hydrogen atoms, while fixing the positions of the peripheral carbon atoms. In this way x-ray crystallography and molecular modeling refinement artifacts were corrected by DFT, while preserving the supramolecular structure of the system due to the applied constraints. A DFT model of a fully relaxed BPhe *a* was obtained to mimic the free monomers in solution state. Both geometry optimizations have been carried out in vacuum within the DFT framework with the ADF program (Fonseca Guerra *et al.*, 1998; te Velde *et al.*, 2001; ADF2009.01, 2009) using the Becke's (Becke, 1988) and Lee-Young-Parr's (Lee *et al.*, 1988) gradient-corrected functional (BLYP) in conjunction with a TZP Slater-type basis set.

NMR chemical shifts have also been computed with ADF program. The calculated ^{13}C chemical shifts were referred to calculations performed on TMS and calibrated accordingly. The difference of chemical shifts between the constrained and fully relaxed geometry of the BPhe *a* has been obtained and compared with the experimental observations.

4.3 Results

The origin of the solid state photo-CIDNP effect is now well understood, which makes it applicable for in-depth biophysical investigations (Jeschke & Matysik, 2003; Daviso *et al.*, 2009a). The overview of the photo-CIDNP mechanisms in different RCs is presented in Chapter 2, Figure 2.2. We use different labeling patterns and perform photo-CIDNP on WT RCs under continuous illumination, where the enhancement is established by the combination of the three spin mixing (TSM) and differential decay (DD) mechanisms (Prakash *et al.*, 2005). In the electron-electron-nuclear TSM the symmetry of coherent spin evolution in the spin correlated radical pair is broken by the combined operation of nuclear Zeeman interaction, electron-electron coupling and pseudosecular *hf* coupling (Jeschke, 1997). In the DD mechanism, the symmetry of the coherent spin evolution in the correlated radical pair is broken by different lifetimes of singlet and triplet radical pairs (Polenova & McDermott,

1999). Understanding of these spin-chemical processes allowed to apply photo-CIDNP MAS NMR as an analytical tool for elucidating electronic structures of the special pair (Daviso *et al.*, 2009c). Here we build on these earlier studies and follow a self-consistent approach to assign the Φ_A response and apply photo-CIDNP magic-angle spinning (MAS) NMR to conclude on the characterization of the electronic and spatial structure of the donor-acceptor radical pair state $P^+\Phi_A^-$.

4.3.1 Signal intensity

Figure 4.2 shows ^{13}C MAS NMR spectra of RCs of *R. sphaeroides* WT containing uniformely ^{13}C labelled BChl and BPhe cofactors. The top trace (spectrum A) shows the data for the sample when it is measured in the dark. The signal is very weak and comprises a broad feature around 35 ppm from the aliphatic carbons in the protein. Upon illumination with continuous white light, however, strong emissive signals appear (spectrum B). All light induced signals are emissive and are negative relative to the absorptive spectrum in trace A. The light induced signals appear in spectral regions in which carbons of BChl and BPhe cofactors are resonating. This contrasts with data collected from RCs with ^{13}C at natural abundance (Prakash *et al.*, 2006), where only the response from the aromatic ^{13}C is

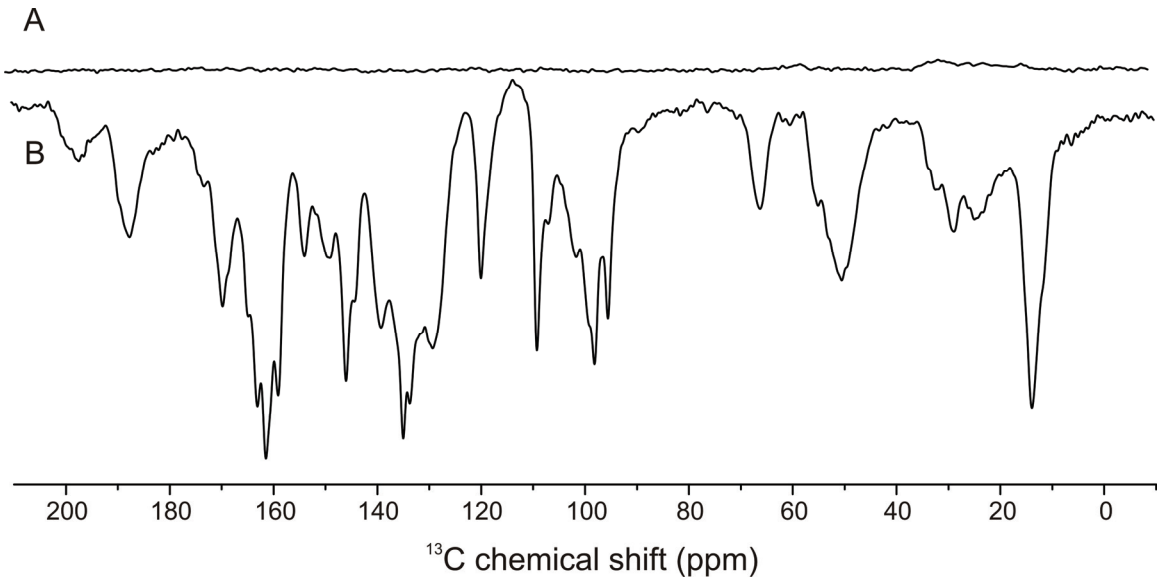

Figure 4.2 One-dimensional ^{13}C photo-CIDNP MAS NMR spectra of u-ALA labelled RCs of *R. sphaeroides* WT (A) in the dark and (B) under continuous illumination with white light. All the spectra have been collected at a magnetic field of 4.7 Tesla and a temperature of 223 K at a spinning frequency of 8 kHz.

enhanced. Obviously, the polarization is spread by spin diffusion within the frozen sample and allows also for enhancement of aliphatic carbons. Even though an increase in signal-to-noise of about one hundred is expected by incorporation of uniformly labelled cofactors, this is not experimentally observed. The overall signal intensity achieved here in samples with cofactors that are uniformly labelled in the macrocycle is significantly smaller than for samples with cofactors containing ^{13}C in natural abundance or samples with sparsely labelled cofactors (Schulten *et al.*, 2002; Prakash *et al.*, 2007; Daviso *et al.*, 2008b).

Although dense labeling opens new channels for spin diffusion and spin-spin relaxation, these effects can be ruled out as sink for intensity as shown by time-resolved experiments using laser excitation immediately before the NMR acquisition (data not shown). Hence, the addition of nuclear spins affects the build-up of nuclear polarization. In a future combined experimental and theoretical study, this phenomenon will be addressed further.

4.3.2 Peak assignments

By using different labeling patterns and by exploiting the additional selectivity offered by the photo-CIDNP mechanism it is possible to address the ground state NMR response with atomic selectivity for the ^{13}C carbons of the rings and the pheripheral side chains of the cofactors involved in the formation of the primary radical pair $P^{+}\Phi_{A}^{-}$. Isotopically labelled RCs prepared from 3-^{13}C-ALA, 4-^{13}C-ALA or 5-^{13}C-ALA substrate in the growth medium have been studied already and provided almost complete chemical shift assignments for signals originating from the donor BChls P_L and P_M, including the peripheral carbons. Here we make the next step, which is to resolve the weak response from the Φ_A from the strong background of the photo-CIDNP signals originating from the Special Pair, which has been partially assigned previously (Schulten *et al.*, 2002; Prakash *et al.*, 2005; Prakash *et al.*, 2006; Prakash *et al.*, 2007; Daviso *et al.*, 2009a).

In Figure 4.3A, the ^{13}C MAS NMR spectrum of u-ALA labelled RCs is shown. The data are aligned with spectra collected from RCs obtained by feeding the 3-^{13}C-ALA, 4-^{13}C-ALA or 5-^{13}C-ALA labelled precursors in the growth medium

for *R. sphaeroides* WT (Figure 4.3 B, C & D). From the spectra a peak list has been compiled consisting of 78 chemical shifts that are sequentially indexed (Table 4.1). Most of the signals from the Special Pair have been already assigned and these are indicated with the dotted lines in Figure 4.3. The peaks indicated by solid lines are attributed to bacteriopheophytin, and the corresponding shifts are given in parenthesis in the table 4.1 along with the index numbers, while table 4.2 presents a self-consistent assignment of the signals that is based on the comparison with solution data, 2D data for RCs reconstituted with plant Pheo *a* and chemical shift calculations.

In Figure 4.3A, in the region between 200 and 180 ppm, four signals are from the carbonyls of the Special Pair cofactors (Chapter 2). The peak at 197.0 ppm with index 1 is attributed to $C3^1$ of the Φ_A and the signal at 188.6 ppm (# 5) is ascribed to $C13^1$ of the Φ_A. The shifts are comparable with the chemical shifts observed for the $C3^1$ (199.2 ppm) and $C13^1$ (189.3 ppm) response from monomeric BPhe *a* in acetone solution and both signals align well with the downfield response from the 3-^{13}C-ALA labelled RCs in Figure 4.3B, where the carbonyl carbons are also labelled (Egorova-Zachernyuk *et al.*, 2008).

The region between 180 and 160 ppm shows two sets of signals that reproduce well across the collection of labelled samples. The 8 strongest signals (# 12 - 19) originate from the Special Pair (Prakash *et al.*, 2007; Daviso *et al.*, 2009a). In the downfield part of the region, 4 relatively weak peaks are discerned, (# 7 - 10) at 174.2, 172.9, 170.7 and 169.3 ppm. These signals match very well with the $C17^3$, C6, C19 and $C13^3$ of the BPhe *a* in solution and with the 2D correlation data collected from a sample reconstituted with uniformly labelled plant pheophytin *a* (Egorova-Zachernyuk *et al.*, 1997; Egorova-Zachernyuk *et al.*, 2008). In addition the peak at 168.2 ppm (# 11) is in line with a previous photo-CIDNP assignment for the C9 of the Φ_A (Daviso *et al.*, 2009a).

In the region between 160 and 140 ppm, most of the response is due to aromatic carbons of Special Pair cofactors P_L and P_M (Prakash *et al.*, 2007; Daviso *et al.*, 2009a). Only the signals with index 20, 24 and 29, are attributed to Φ_A. In the region between 140 and 119 ppm (# 30 - 41), all signals that originate from the

Table 4.1 Complete peak list of NMR ^{13}C chemical shifts with index numbers from u-ALA RCs spectrum (the signals attributed to the Φ_A are given in parenthesis).

index	^{13}C Chemical shift (ppm)	index	^{13}C Chemical shift (ppm)
1	(197.0)	40	126.9
2	195.6	41	119.5
3	193.5	42	108.7
4	189.4	43	(107.5)
5	(188.6)	44	106.6
6	187.5	45	104.1
7	(174.2)	46	103.0
8	(172.9)	47	102.0
9	(170.7)	48	101.2
10	(169.3)	49	100.4
11	(168.2)	50	(99.6)
12	166.5	51	98.3
13	165.9	52	(97.6)
14	164.4	53	(95.1)
15	162.6	54	(65.8)
16	161.0	55	(55.6)
17	160.1	56	54.7
18	158.5	57	52.7
19	157.2	58	(52.5)
20	(154.4)	59	51.7
21	153.6	60	50.9
22	151.5	61	50.0
23	149.8	62	49.1
24	(148.7)	63	48.3
25	148.5	64	47.4
26	145.6	65	46.1
27	144.5	66	(33.6)
28	143.5	67	32.1
29	(141.2)	68	(31.5)
30	138.7	69	29.9
31	137.2	70	29.5
32	136.8	71	28.4
33	136.2	72	(27.2)
34	134.3	73	(24.6)
35	132.8	74	22.6
36	130.8	75	(21.3)
37	129.7	76	19.1
38	128.8	77	(13.5)
39	127.4	78	(11.4)

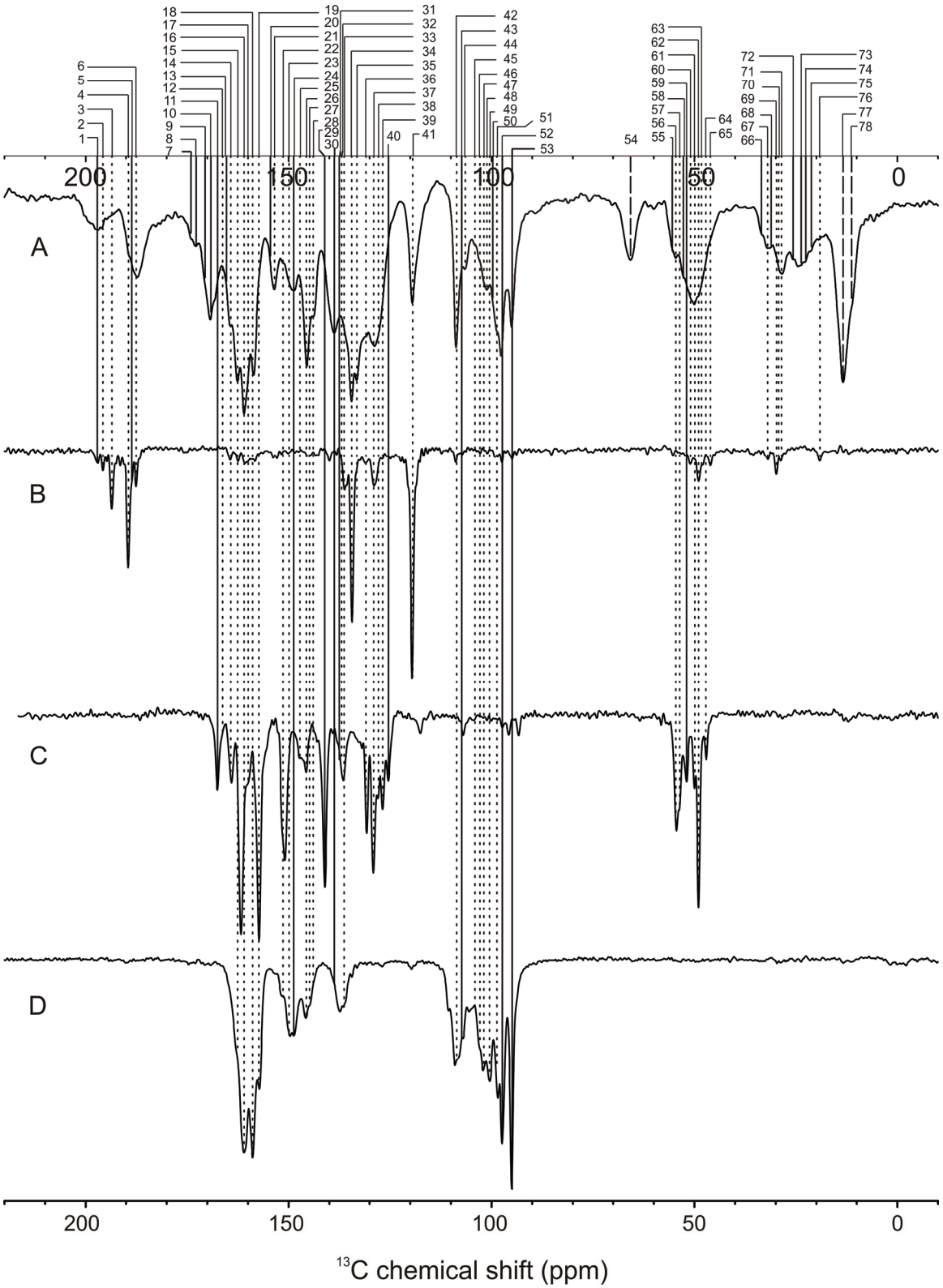

Figure 4.3 A set of one-dimensional ^{13}C photo-CIDNP MAS NMR spectra collected from (A) u-ALA, (B) 3-ALA, (C) 4-ALA, (D) 5-ALA labelled RCs of *R. sphaeroides* WT under continuous light in a magnetic field of 4.7 Tesla and at a temperature of 223 K. The spinning frequency was set to 8 kHz. The dotted lines indicate the responses from P_L and P_M using the assignments obtained in previous work, while the signals from the Φ_A are designated by solid lines. When signals from the P_L, P_M and the Φ_A coincide, their position is indicated with dashed lines.

Special Pair and bacteriopheophytin have been assigned before (Daviso *et al.*, 2009a). The relatively strong response in this region is in line withthe assignments to carbons of the aromatic ring, which is the source of buildup of nuclear spin polarization (Daviso *et al.*, 2009a).

For the region between 110 and 90 ppm four signals can be attributed to the Φ_A. Three of these signals (43, 52 & 53) have been identified earlier (Prakash *et al.*, 2007). The peak at 99.6 ppm (# 50) is ascribed to the C10 (Φ_A). The relatively intense response from the C5 at 97.6 ppm and the C20 at 95.1 ppm confirms that these Φ_A signals are from carbons in the aromatic ring.

In the aliphatic region of the spectrum, the signals at 55.6 (# 55) and 52.5 (# 58) ppm are attributed to the C8 and the C18 of the Φ_A, while the other signals were already assigned from photo-CIDNP MAS NMR data collected from 3-^{13}C-ALA and 4-^{13}C-ALA labelled RCs (Daviso *et al.*, 2009a). The distinct peak at 65.8 ppm (# 54) is assigned to carbon C13^2 from all the cofactors by analogy with data for the BChl and BPhe monomers in solution (Egorova-Zachernyuk *et al.*, 2008). In the region between 40 and 0 ppm, most of the signals, with indices between 66 and 78, are from the Special Pair and were rigorously assigned by 2D DARR experiments from 3-^{13}C-ALA labelled RCs (Chapter.3). The remaining peaks at 33.6, 31.5, 27.2, 24.6 and 21.3 ppm are tentatively assigned to the bacteriopheophytin by comparing with the solution data of BPhe (Egorova-Zachernyuk *et al.*, 2008). Two distinct signals at 13.5 and 11.4 ppm (# 77 & 78) indicated by dashed lines, represent the collective responses from the peripheral carbons C21 and 121 or 82 of all cofactors. The assignments for P_L and P_M are summarized in the tables provided in the appendix.

4.3.3 Electronic tuning of Φ_A in the protein matrix

During electron transfer, the bacteriopheophytin in the active branch forms a radical pair state with the Special Pair. In chapter 2, we learnt that the differences in chemical shifts of the BChl *a* in the Special Pair (P_L and P_M), are very significant, and that the variations in ^{13}C chemical shifts of macrocycles reflect the changes in shape of the macrocycles, the electronic properties of the protein surrounding and

Table 4.2 ^{13}C NMR chemical shifts assigned to BPhe *a* and its monomers in acetone, with respective theoretically calculated chemical shift differences between the monomer and protein-bound BPhe *a*

IUPAC	^{13}C Chemical shift (ppm)					
	Observed shifts of BPhe *a* in Acetone	Observed shifts of BPhe *a* by Photo-CIDNP MAS NMR	Experimental Δσ (solid-liquid)	Theoretically calculated shifts of fully relaxed BPhe *a*	Theoretically calculated shifts of constrained Bphe *a*	Theoretical Δσ (Const-relax)
1	139.7	141.2	1.5	140.7	140.7	0.0
2	138.5	138.7	0.2	149.2	145.4	-3.8
2^1	13.9	13.5	-0.4	17.2	17.0	-0.2
3^1	199.2	197.0	-2.2	201.9	201.4	-0.5
3^2	34.0	33.6	-0.4	35.2	37.8	2.6
4	138.1	137.2	-0.9	142.3	142.6	0.3
5	97.9	97.6	-0.3	100.5	100.4	-0.1
6	172.4	172.9	0.5	173.5	171.3	-2.2
7^1	23.7	24.6	0.9	25.7	26.5	0.8
8	55.4	55.6	0.2	66.0	65.5	-0.5
8^1	30.7	27.2	-3.5	39.6	45.5	5.9
8^2	11.5	11.4	-0.1	13.7	18.5	4.9
9	164.3	168.2	3.9	173.1	175.0	1.9
10	100.2	99.6	-0.6	101.7	100.2	-1.4
12^1	11.5	11.4	-0.1	12.1	13.1	1.0
13	129.2	126.9	-2.3	138.6	137.6	-1.0
13^1	189.3	188.6	-0.7	196.3	193.5	-2.8
13^2	65.5	65.8	0.3	76.3	75.1	-1.3
13^3	170.2	169.3	-0.9	179.4	178.5	-0.9
14	148.7	148.7	0.0	151.6	151.7	0.1
15	110.3	107.5	-2.8	119.3	117.8	-1.5
16	158.7	154.4	-4.3	171.1	170.6	-0.5
17	51.4	51.7	0.3	64.4	62.7	-1.7
17^1	31.3	31.5	0.2	35.3	33.3	-2.0
18	50.9	52.5	1.6	59.3	56.8	-2.5
18^1	22.9	21.3	-1.6	25.6	26.2	0.6
19	171.7	170.7	-1.0	174.4	172.1	-2.3
20	97.2	95.1	-2.1	102.4	101.4	-1.0

hydrogen bonding of *e.g.* the 3^1-acetyl and 13^1-keto carbonyl groups. Figure 4.4A and table 4.2 show the differences in the chemical shift ($\Delta\sigma$) for the Φ_A in the protein matrix relative to BPhe *a* monomer species in acetone. There are little changes in electron density in rings I and III, while for rings II and IV there are cumulative negative shifts. Significant $\Delta\sigma$'s for the $C8^1$, C9 and C16 atoms are around ~ 3.5 ppm and for the $C3^1$, C13, C15, and C20 the $\Delta\sigma$ ~ 2.0 ppm. The small changes in electron density in rings I and III indicate a planar ring conformation and a stable configuration with distinct pyrrole and pyridine nitrogen atoms in the bacteriopheophytin *a*, as opposed to the much softer and distorted bacteriochlorophyll ring system with the coordinated Mg^{2+} ion in the center that is subject to polymorphism, dynamics and electrostatic polarization (Chapter 2). Since the pheo is involved in the cascade of symmetry breaking events in the RC, and symmetry breaking is related to structural distortions in the ground state, the data indicate that the primary source of the symmetry breaking is in the deformation of P, while the extent of protein induced deformation of the BPhe *a* molecule appears much less (Pandit *et al.*, 2010; Wawrzyniak *et al.*, 2011). The deformation of the Φ_A has been analyzed with theoretical calculations, where the electronic structures of the bacteriopheophytin molecule in a completely relaxed state and in the protein matrix with constraints were computed. Figure 4.4B shows that the $\Delta\sigma$ from these calculations are similar and match the experimental observations. When a completely relaxed BPhe *a* from computer modeling is overlaid with BPhe *a* from the X-ray data for the bacterial RC (Figure in Appendix-B), the structural differences are small, within 0.2 Å. For the peripheral region the differences are larger, and produce chemical shift differences up to 10 ppm, in line with the experimental data (Table 4.2). In particular the conformation of the ethyl substituent on $C8^1$ and $C8^2$ appears affected.

Finally, an electrochemical investigation of the redox properties of bacteriopheophytin *a* in aprotic solvents was performed by cyclic voltammetry to determine the midpoint potential, which is -0.65 V with respect to the normal hydrogen electrode (Cotton & Van Duyne, 1979). This is very close to the experimental midpoint potential of -0.63 V determined for the BPhe *a* in both

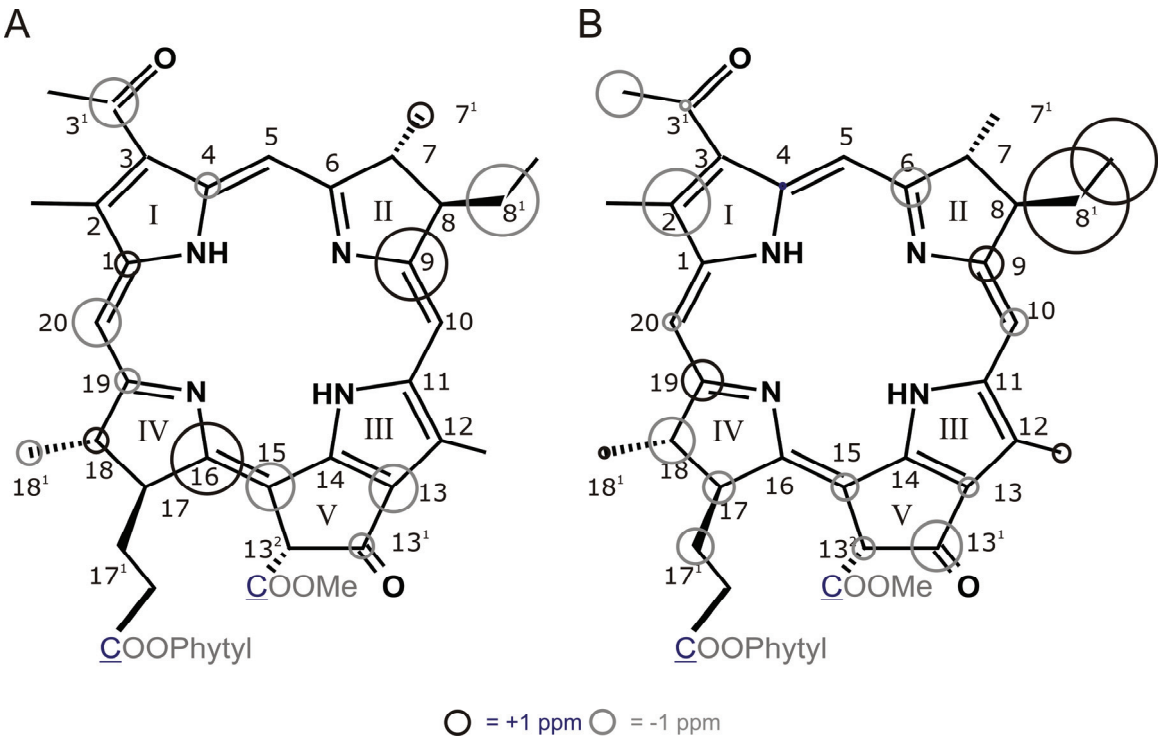

Figure 4.4 Relative electron densities of bacteriopheophytin (Φ_A) in the electronic ground state derived (A) experimentally from the chemical shift differences between BPhe *a* in solution in acetone and BPhe *a* cofactor in RC and (B) Theoretically calculated chemical shift differences between fully relaxed structure and constrained optimized structure of BPhe *a* from the x-ray structure from 1M3X (Camara-Artigas *et al.*, 2002b).

active and inactive branch in the protein (Woodbury & Parson, 1984; Noy *et al.*, 2006). This implies that the redox potential of the BPhe cofactor present in the protein matrix is only marginally affected by the surrounding environment.

This matches very well with our observation that the structure of the Φ_A is very similar to the structure of BPhe *a* in solution, with little evidence for packing effects from the protein matrix. We thus conclude that the BPhe of the active branch is not tuned in a special manner by its surroundings and represents an electron sink due to its redox potential that is different from P. A similar conclusion has been made for the subsequent cofactor namely the Quinone acceptor Q_A in RCs that they remain in the same orientation even upon illiumination light by ENDOR experiments (Flores *et al.*, 2010). Taking together, the cofactors in the active branch appear to be the same under normal conditions.

Chapter 5

Towards photo-CIDNP spin-torch experiments using protons

Abstract

In chapter 3, spin-torch experiments to transfer the strongly enhanced ^{13}C photo-CIDNP polarization to neighboring ^{13}C labelled atoms by the natural spin diffusion process have been reported. 2D DARR ^{13}C-^{13}C photo-CIDNP MAS NMR experiments have been performed and a polarization transfer up to a distance of 13.1 Å via relay transfer steps have been observed. Here, an alternative approach for spin-torch experiments is proposed. We aim for transferring the strong polarization of ^{13}C to directly bonded ^{1}H atoms and observe the ^{1}H NMR spectra. This experiment is challenging since the influence of homonuclear dipolar interactions from the proton pool is large. Several types of experiments have been performed to overcome this problem. For observing a ^{13}C-polarized proton spectrum, we recognized the importance of efficient phase cycling at the Lee-Goldburg condition. In addition, application of wPMLG techniques allows for improvement of proton resolution. This technique might allow for exploration of the proton contacts in the protein pocket. In particular, neighboring hydrogen bonds could be studied in great detail. We propose to implement the solid-state photo-CIDNP effect to ^{13}C-^{1}H heteronuclear correlation experiments to map the entire proton network in a single experiment.

5.1 Introduction

NMR is an insensitive technique. Since it is an invaluable tool to study structure and function of proteins close to their native states, as well as protein-protein interactions, great effort has been spent on increasing the signal-to-noise ratio. To this end, polarization transfer techniques have been developed by different groups both in solid- and liquid- state NMR. Cross-polarization (CP) is probably the most important signal enhancement technique in solid state NMR. It was introduced in 1962 by Hartmann and Hahn for the static condition (Hartmann & Hahn, 1962). Here the polarization is transferred from abundant spins (I = ^{1}H) to rare spins (S = ^{13}C, ^{15}N, ^{29}Si) and the signal is observed from the rare spin species. For Hartmann-Hahn matching, both abundant and rare spins are irradiated simultaneously at their Larmor frequencies, with matching according to

$$\gamma_I B_1(I) = \gamma_S B_1(S) \qquad (1)$$

In the picture of the doubly rotating frame, this condition is fulfilled if both spins are spin locked. Polarization transfer between I and S spins takes place, when the energy gaps in the rotating frame between the spin states of I and S spins are equal.

This polarization transfer followed by high power decoupling during signal detection resulted in the famous CP experiments introduced by Waugh and coworkers (Pines *et al.*, 1973). The combination of CP with magic angle spinning (MAS), explored by Schaefer's group experimentally and theoretically (Stejskal *et al.*, 1977), allowed for obtaining high resolution spectra of low abundant spins in polycrystalline samples.

The CP transfer can occur in both directions, from I → S as well as from S → I, depending on the relative magnitudes of the initial polarizations of the dipolar coupled spins. Inverse CP experiments from S → I are rare and unusual because of broad lines from the proton detection. Haw's was the first group to exploit this counterintuitive technique. Here, CP from the low-γ nuclei to protons allowed to identify the resonance of immobile protons closely associated with ^{31}P nuclei in

calcium phosphate samples (Crosby *et al.*, 1988). CP from deuterons to protons provides information on the rapid proton exchange in solids, especially in samples spin diluted by deuteration (Zheng *et al.*, 1993). Kinetics studies using CP in both directions, $^{1}H \rightarrow {}^{13}C$ and $^{13}C \rightarrow {}^{1}H$, enabled studying molecular motions of fullerene-70 solvated in toluene (Kolodziejski *et al.*, 1996). Collecting high resolution ^{1}H spectra is always challenging due to strong homonuclear dipolar interactions among protons, and requires both intermediate spinning frequency 12-15 kHz, along with multiple pulse decoupling schemes like LG, FSLG, PMLG etc. The homonuclear decoupling is even more difficult at very high MAS frequencies than at low and intermediate ones. Only in the last two years, it has been shown that homonuclear decoupling at 50-70 kHz is possible but still the resolution is not netter than at low frequencies (Leskes *et al.*, 2009). The details of multiple pulse decoupling approach have been discussed in the introduction chapter.

The solid-state photo-CIDNP effect was discovered by Zysmilich and McDermott in 1994 (Zysmilich & McDermott, 1994). They observed light-induced enhancement of NMR signals in frozen and quinone-blocked bacterial reaction

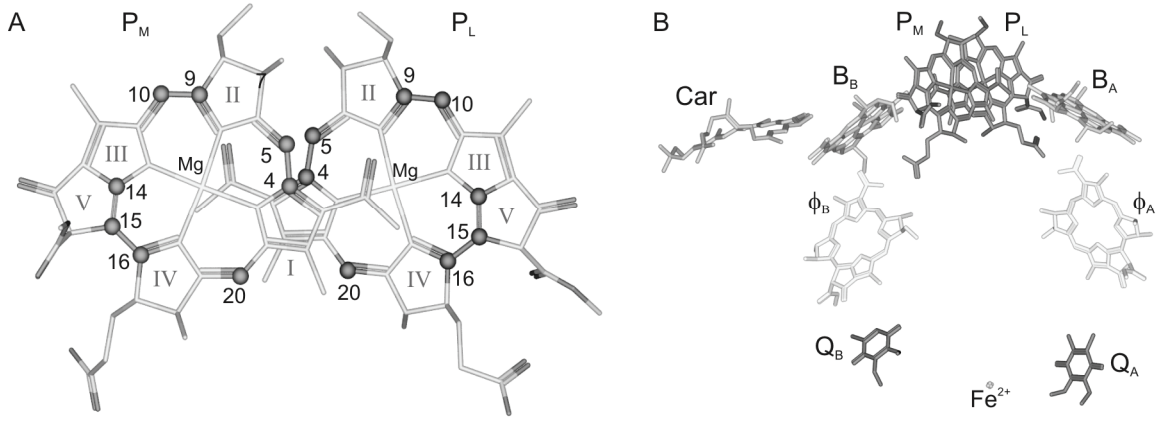

Figure 5.1 (A) Spatial arrangement of the two cofactors P_L (right, isotope labels in blue) and P_M (left, isotope labels in red) forming the Special Pair. The pyrrole rings are numbered with Roman numerals. Pyrrole rings I are overlapping. (B) The arrangement of cofactors in reaction centers (RCs) of *R. sphaeroides* wild type (WT). The primary electron donor, the special pair, is formed by the two bacteriochlorophyll *a* (BChl) molecules P_L and P_M. B_A and B_B are accessory BChl cofactors. Φ_A and Φ_B are bacteriopheophytin (BPhe) cofators. The acceptor side is formed by two ubiquinone-10 cofactors Q_A and Q_B and a non-heme iron. Side chains are omitted for sake of clarity. The apparent symmetry of the cofactor arrangement is broken by a carotenoid cofactor (Car). The light-induced electron transfer occurs selectively via branch A [PDB entry 1M3X, (Camara-Artigas *et al.*, 2002b) the figure has been made with Accelrys Discovery Studio].

centers (RCs) of *Rhodobacter (R.) sphaeroides* R26 by ^{15}N MAS NMR under continuous illumination with white light, which offered NMR access to the electron-nuclear processes during the charge separation (for reviews, (Jeschke & Matysik, 2003; Daviso *et al.*, 2008b)). By induction of a non-Boltzmann nuclear spin polarization upon photo-reaction in rigid samples, a signal enhancement of a factor of more than 10,000 has been observed by ^{13}C MAS NMR for RCs of the purple bacteria of *R. sphaeroides* wildtype (WT) (Prakash *et al.*, 2005; Prakash *et al.*, 2006). The structural properties of the RCs (Figure 5.1) and mechanisms of photo-CIDNP have been already described in detail in Chapter 2.

In this Chapter, we aim to transfer this strong enhancement of nuclear polarization from labelled carbon atoms to the nearby protons. Such spin-torch experiments might allow for better understanding of the proton environment in the pocket tuning the Special Pair. Since ^{1}H-^{1}H spin diffusion is very efficient, the enhanced ^{1}H polarization is rapidly transferred to other protons in the sample. In this outlook, I present an exploratory search for the best experimental conditions for detection of enhanced ^{1}H signals and look for the most suitable pulse scheme, allowing for efficient polarization transfer and fast ^{1}H detection under MAS conditions. The 5-ALA label pattern (Figure 5.2) is particularly suitable for these studies since the selectively labelled carbon positions C5, C10 and C20 carry directly bound protons. These protons might present the best targets for this initial study. This Chapter shows the present state of the development.

5.2 Materials and Methods

5.2.1 Sample preparation

Selective isotopic labelling in RCs of *R. sphaeroides* is achieved by feeding selectively labelled 5-$^{13}C_1$-δ-aminolevulinic acid (5-ALA), which is a precursor for the formation of BChl and BPhe, and leads to a ^{13}C enrichment of ~60%. The 5-ALA (Figure 5.2) has been purchased from Buchem B.V. (Apeldoorn, The Netherlands). The RCs were isolated as described earlier (Shochat *et al.*, 1994) and the quinones were removed by incubating the RCs at a concentration of 0.6 µM in

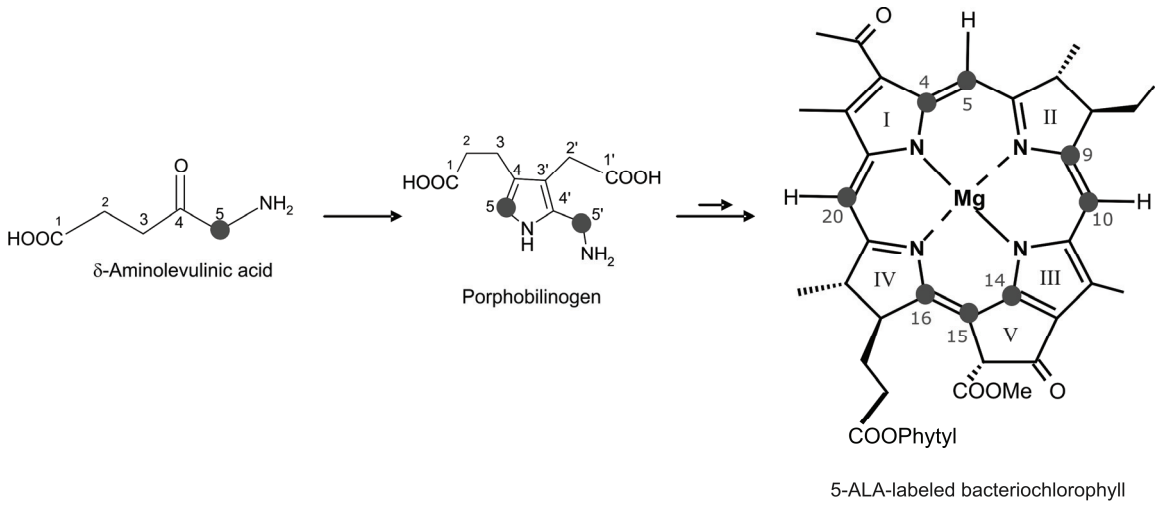

Figure 5.2 Biosynthetic pathway for the formation of selectively ^{13}C isotope labelled bacteriochlorophyll *a* (BChl *a*) by feeding bacteria with 5-^{13}C-δ-aminolevulinic acid (5-ALA).

4% LDAO, 10 mM o-phenanthroline, 10 mM Tris buffer, pH 8.0, containing 0.025% LDAO and 1 mM EDTA (Okamura *et al.*, 1975). Approximately 15 mg of RC protein complex embedded in LDAO micelles were used in the NMR experiment.

5.2.2 MAS NMR experiments

All NMR experiments were performed with an Avance DMX-400 (9.4 Tesla) NMR spectrometer equipped with a 4 mm MAS probe (Bruker BioSpin GmbH, Karlsruhe, Germany). The sample was loaded into a clear 4 mm sapphire rotor and inserted into the MAS probe. It was frozen slowly at a low spinning frequency of 600 Hz to ensure a homogeneous sample distribution against the rotor wall (Fischer *et al.*, 1992). All experiments were recorded with a MAS frequency of 8 kHz and at a set temperature of 223 K. The probe used for these experiments was a triple resonance probe with a special hole to insert the light fiber inside. The optimum length of the (π/2) proton pulse and carbon pulses, determined on uniformly ^{13}C labeled tyrosine, was ~3.1 µs and ~5.0 µs with a rf-field strengths of 80 kHz and 50 kHz, respectively. A recycle delay of 4 s was used for all experiments.

In several experiments, TPPM proton decoupling (Bennett *et al.*, 1995) with a pulse length of 5.5 µs and phase of 15^0 was used. For the spin lock experiments, the contact time used was 1 ms. The effective fields on proton and carbon used for

the Lee-Goldburg (LG-) CP experiments were 73 kHz and 65 kHz, respectively. The offset used for the LG-CP condition on the protons was 42.42 kHz. A proton pulse length of 1.1 µs for the wPMLG3 homonuclear decoupling was used. The phases of these pulses are 34.63, 103.90, 173.17, 353.17, 283.90 and 214.63 degrees. The magic flip angle used for the wPMLG experiment was around 1.3 µs. The acquisition window during wPMLG was 0.5 µs.

5.3 Results & discussion

5.3.1 Carbon polarization

To study whether the enhanced nuclear polarization of the carbons can be transferred to a nearby proton, a series of five experiments was performed. The first experiment (Figure 5.3A), the starting point for the further development of pulse schemes, was the standard Hahn echo scheme for the direct observation of the strong polarization on the carbon nuclei in a one-dimensional experiment. This pulse sequence is usually employed in one-dimensional photo-CIDNP ^{13}C MAS NMR experiments with continuous illumination. The obtained ^{13}C spectra are displayed in Figure 5.3A′. The spectrum measured in the dark is shown in black,

Table 5.9 : Chemical shifts of ^{13}C labels in the cofactors for 5-ALA-labelled RCs of *R. sphaeroides* WT

^{13}C position	BChl in solution[a] (ppm)	P_L[b] (ppm)	P_M[b] (ppm)	BPheo[b] (ppm)
4	150.0	136.3	144.5	137.2
5	99.9	97.3	105.4	97.6
9	158.5	160.8	158.8	162.8
10	102.4	100.4	98.3	101.9
14	160.8	157.2	-	148.7
15	109.7	110.6	106.9	107.9
16	152.0	145.7	149.5	151.6
20	96.3	108.8	103.1	94.9

while the spectrum observed with continuous illumination is shown in grey. The spectrum in the dark contains only noise. In the spectrum obtained with CI (shown in grey), strong light-induced signals occur in the range between 80 and 180 ppm. due to the strong enhancement of the solid-state photo-CIDNP effect. The total experimental time used for such a spectrum was 10 minutes under CI with a recycle of delay of 4 s. The observed light-induced signals have been assigned previously (Prakash *et al.*, 2007) and are summarized in Table 5.1.

5.3.2 Single-pulse proton experiments

Until now, the solid-state photo-CIDNP effect has been observed for ^{13}C and ^{15}N. Previous attempts to observe this effect directly on protons failed. In such

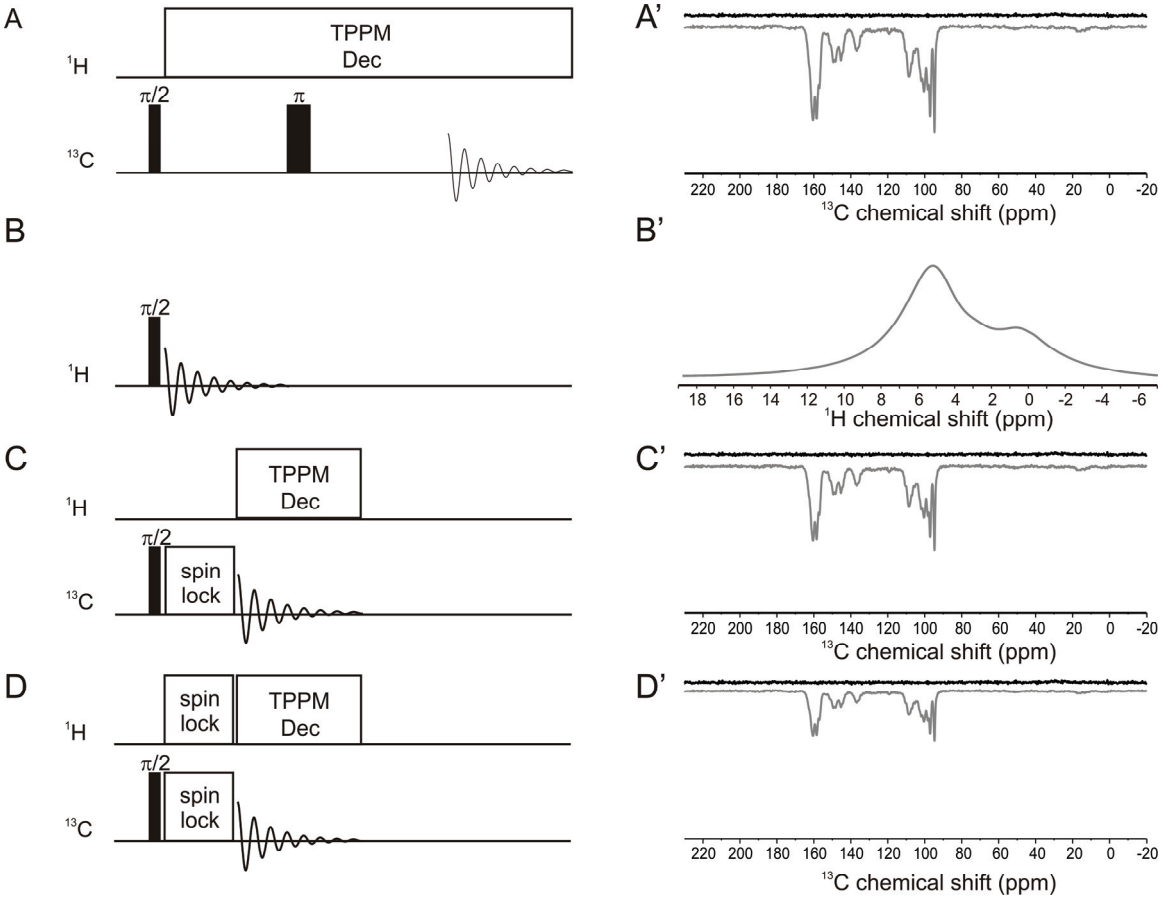

Figure 5.3 Pulse programs used for the experiments and their respective spectra are displayed adjacent to it (black spectra are obtained when the light is off and the grey colored spectra are obtained when the light was on). (A) Hahn echo experiment with carbon acquisition. (B) Single $\pi/2$ degree pulse on proton and acquisition on the same channel. (C) Spin lock pulse on carbon channel only after the $\pi/2$ pulse on carbon. (D) Spin lock pulse on both carbon and proton channel after the $\pi/2$ pulse just on carbon.

experiments a single $\pi/2$ pulse is used to excite the protons as shown in Figure 5.3B. The ^{1}H data obtained with this procedure are displayed in Figure 5.3B'. The spectra measured in the dark and with continuous illumination are almost identical. In both spectra, two broad peaks at around 0.5 and 5.0 ppm occur, having a FWHH of 2000 Hz. These signals are attributed to protons in the protein backbone and in the frozen water molecules of the buffer, and there is no evidence for direct solid-state photo-CIDNP of the protons.

To quantify the efficiency of polarization transfer from carbons to the protons, we first performed two spin lock experiments (Figure 5.3C & D). The first one consists of a $\pi/2$ pulse on the carbons, followed immediately by a spin lock pulse of 1 ms (Figure 5.3C) on the ^{13}C channel only. In the second experiment, spin lock pulses were applied in parallel on both the carbon and the proton channel (Figure 5.3D). In both experiments, the acquisition was performed on the ^{13}C channel. Comparing the two spectra obtained with continuous illumination (in grey), the ^{13}C photo-CIDNP signal intensity is reduced by ~30% when the spin lock field is applied to the ^{1}H channel (Figure 5.3C' & D'). This loss of intensity could imply that ~30% of photo-CIDNP polarization of carbons has been transferred to protons. Hence, this observation suggests that polarization transfer to the proton pool occurs and might be experimentally observable.

5.3.3 Inverse CP from carbons to protons

After observation of the loss of ^{13}C polarization, presumably to the proton pool in the CP experiment, the next aim is to observe the proton spectrum after the spin lock pulse on both channels. For optimal selectivity of the carbon to proton transfer during CP, the spin lock pulse on the protons was modified (Figure 5.4A) to satisfy the Lee-Goldburg (LG-) CP condition. At this condition the proton–proton interactions are largely suppressed by applying an off-resonance rf field resulting in an effective field in the rotating frame pointing along an axis tilted by the magic angle with respect to the direction of the external field (Lee & Goldburg, 1965). At the same time, transfer by the heteronuclear carbon–proton dipolar

interaction is allowed via a Hartmann–Hahn condition imposed on the effective rf fields experienced by the nuclei (Hartmann & Hahn, 1962). Additionally the phase cycling has been optimized to suppress the huge water peak coming from the buffer solution. It has been shown that under this condition the polarization can be transferred within a particular ^{1}H-^{13}C spin pair (van Rossum *et al.*, 2000).

The spectrum obtained with inverse LG-CP is displayed in Figure 5.4A'. The spectrum obtained with continuous illumination is shown in grey as a broad peak, while in the dark experiment, there were no signals observed in the spectrum displayed in black color. This broad peak occurs at 8.5 ppm, which is where the response from the protons at C5, C10 and C20 is expected, but with FWHH of 2800 Hz. For such a spectrum, 10 k scans and approximately 11 hrs were required. When the pattern of this spectra were compared to that of the spectra in Figure 5.3B, these data clearly prove that the photo-CIDNP polarization from ^{13}C has been transferred to ^{1}H and can be observed in a one-dimensional ^{1}H spectrum.

5.3.4 Inverse CP from carbon to proton with wPMLG

Caused by strong dipolar coupling, ^{1}H NMR in the solid-state is still a challenging task. To improve the proton resolution, various methods have been developed as, for example, MREV8, BR24, BLEW12, FSLG, PMLG, DUMBO, R-symmetry etc.

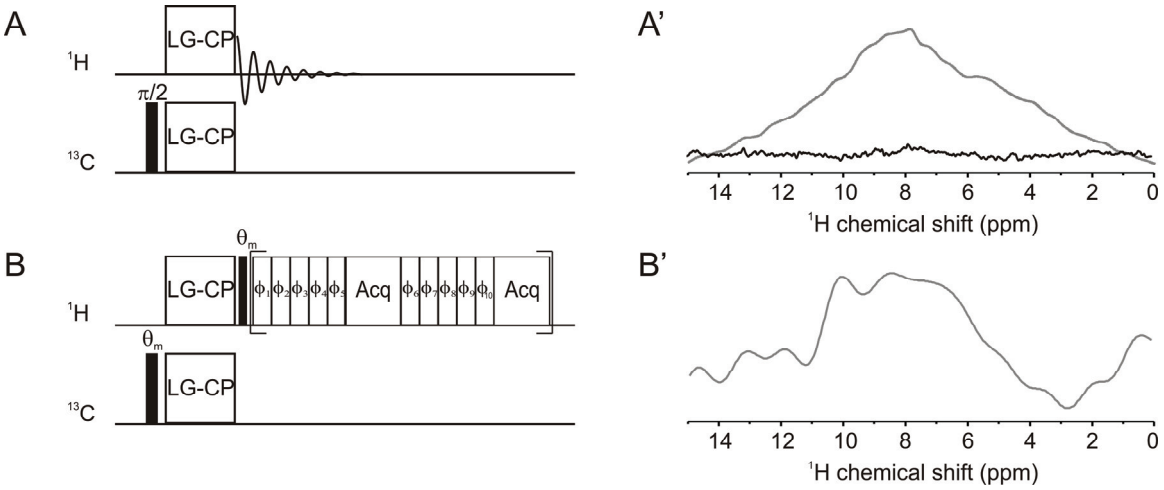

Figure 5.4 Pulse programs used for the experiments and their respective spectra are displayed adjacent to it (only the spectra with CI is displayed). (A) Polarization transfer from $^{13}C \rightarrow ^{1}H$ with LG-CP condition. (B) Polarization transfer from $^{13}C \rightarrow ^{1}H$ with LG-CP with wPMLG method. The corresponding spectra are displayed adjacent to the respective pulse program.

Recently, windowed phase-modulated Lee-Goldburg (wPMLG) homonuclear decoupling has been proposed by Vega's group (Leskes *et al.*, 2006). Here, acquisition is sandwiched by trains of pulses with specific phases reducing dipolar interactions (Figure 5.4B). Thus, by applying the LG-CP experiment followed by wPMLG detection, photo-CIDNP on the carbon atoms has been successfully transferred to attached protons (Figure 5.4B'). As the chemical shift suggests, the small broad light-induced peak at about 8.5 ppm with a FWHH of 2000 Hz originates from the protons directly bound to the carbons C5, C10 and C20.

For this experiment 3k scans were used, which corresponds to a measurement time of three hours. The reduction of time and line width, compared to the previous spectrum, is due to wPMLG detection. Since the signal is still rather broad (4-5 ppm), it is currently difficult to distinguish different hydrogen bonding networks around the Special Pair. Further improvement of the decoupling strategy will presumably yield better resolution.

5.4 Future experiments

The preliminary results presented here could be starting blocks for many new experiments in the future. For instance, two-dimensional ^{13}C-^{1}H experiments could be envisaged resolving the hydrogen bonding in the Special Pair of photosynthetic reaction centers. In addition, the solid-state photo-CIDNP effect can be used as a spin-torch to explore for example the protein vicinity of the Special Pair in detail. In particular, the conformational, electronic as well as protonic state of the amino acids surrounding the Special Pair can be studied.

5.4.1 2D photo-CIDNP ^{13}C-^{1}H correlation experiment

In the pilot experiments presented in Figure 5.4, the possibility for polarization transfer between the highly polarized ^{13}C and the thermally polarized ^{1}H has been demonstrated. Careful optimization of more advanced transfer experiments might provide more details on the proton network close to the carbonyl carbons of the cofactors. To obtain two-dimensional data, allowing for assignments, a pulse scheme is proposed in Figure 5.5. In this sequence, carbons are measured in the

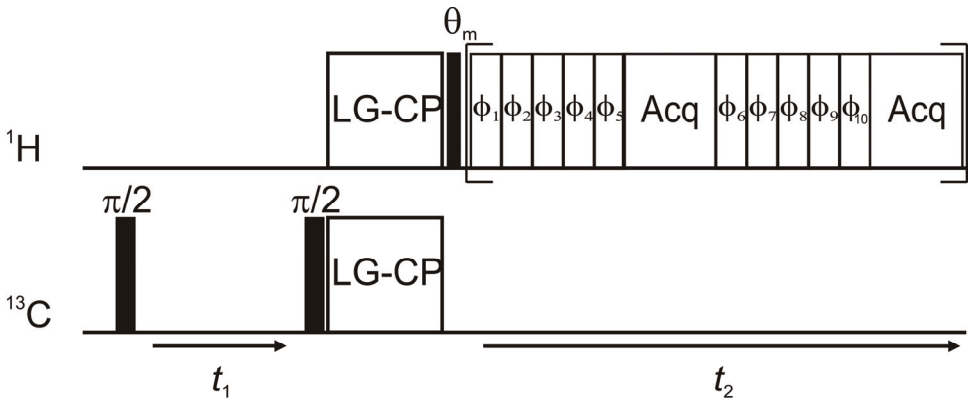

Figure 5.5 2D Pulse sequence proposed for 2D ^{13}C-^{1}H photo-CIDNP experiment.

indirect dimension, while the proton information is obtained during the direct acquisition. Hence, this scheme inverts the usual way of 2D ^{13}C-^{1}H experiments.

5.4.2 Labeled carotenoid in RCs

The presence of selectively ^{13}C labeled carotenoid (Car) would allow obtaining more insight into the conformation of the Car present in RCs. The distance between the Car and the special pair cofactor P_M is 10.1 Å (Figure 5.6). As we have seen in chapter 3, polarization transfer of 13.1 Å has been observed in 2D DARR experiments. Such a sample might be prepared by growing *R. sphaeroides* WT cells with a ^{13}C labeled precursor of the biosynthesis of the spheroidene such as pyruvate (Rohmer, 1999).

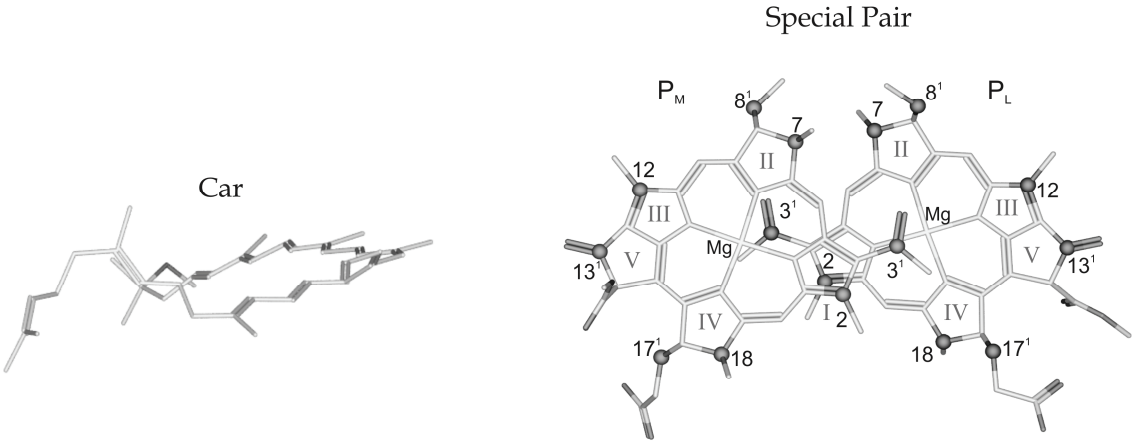

Figure 5.6 Visual display of Car and Special Pair in RC of *R. sphaeroides* WT cells.

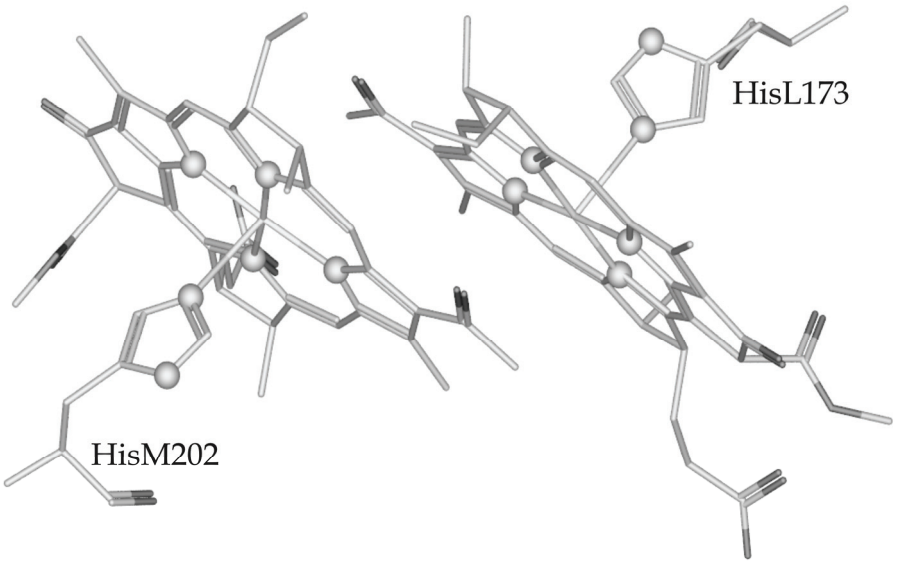

Figure 5.7 Presence of histidines HisL173 and HisM202 near the Special Pair.

5.4.3 ^{15}N labeled RCs with selectively Histidines

The presence of selectively ^{13}C labeled cofactors increases signal and selectivity of the photo-CINDP MAS NMR experiment. RCs also have been selectively isotope-labelled at histidines (Alia *et al.*, 2001). Polarization transfer experiments might be applied to study the axial histidines (HisL173 and HisM202) of the Special Pair, displayed in Figure 5.7. In particular, it would be of interest to determine their protonation characteristics and whether there is a change upon charge separation as indicated in chapters 2 and 3.

Appendix A

Figures of selectively labelled bacteriochlorophyll *a*

* for chapter 4

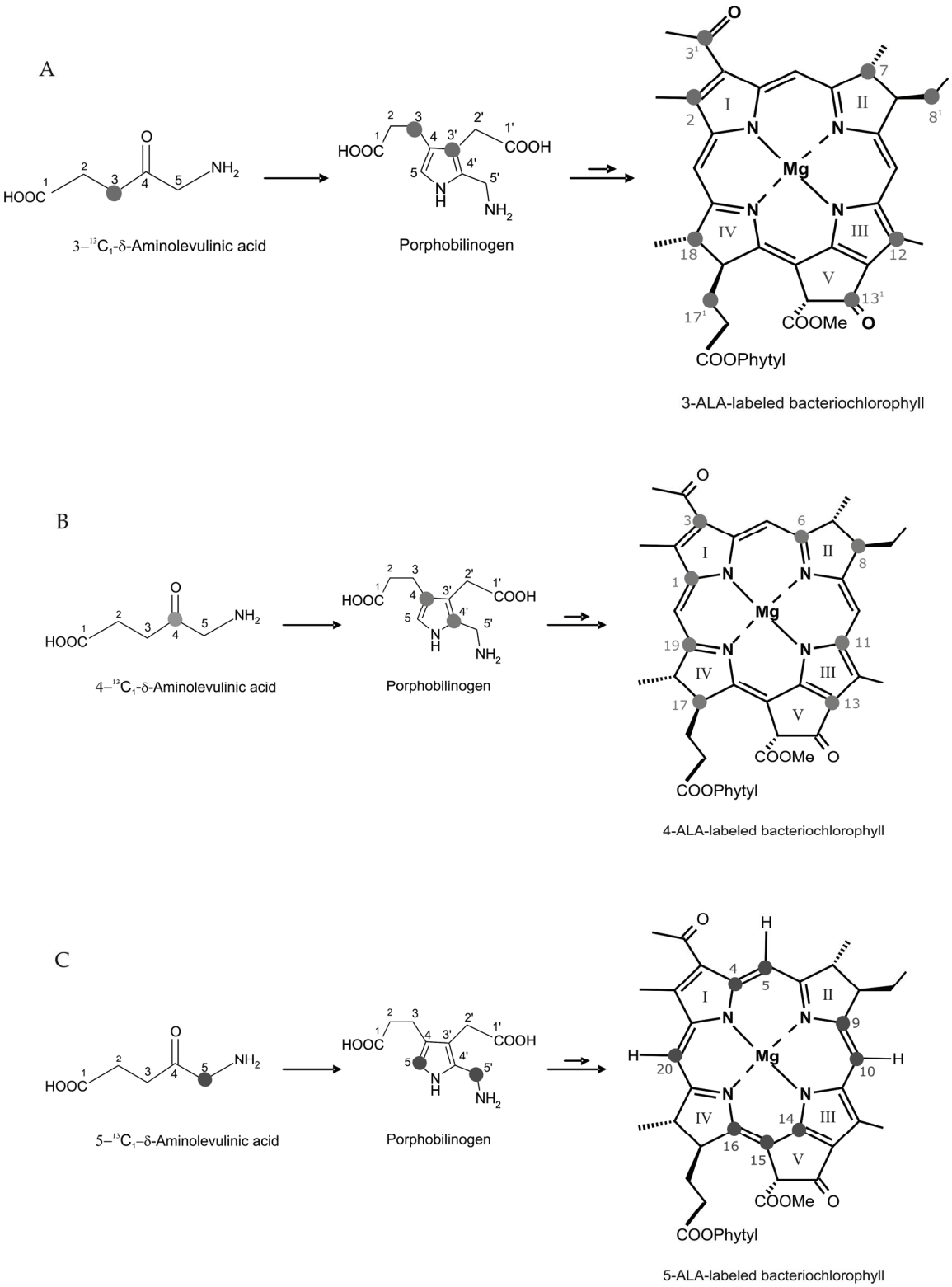

Appendix-A 1 Biosynthetic pathway for the formation of selectively ^{13}C isotope labelled bacteriochlorophyll *a* (BChl) by feeding the bacteria respectively with (A) 3-$^{13}C_1$-δ-aminolevulinic acid (3-ALA), (B) 4-$^{13}C_1$-δ-aminolevulinic acid (4-ALA) and (c) 5-$^{13}C_1$-δ-aminolevulinic acid (5-ALA).

Appendix B

Overlaid view of bacteriopheophytin

* for chapter 4

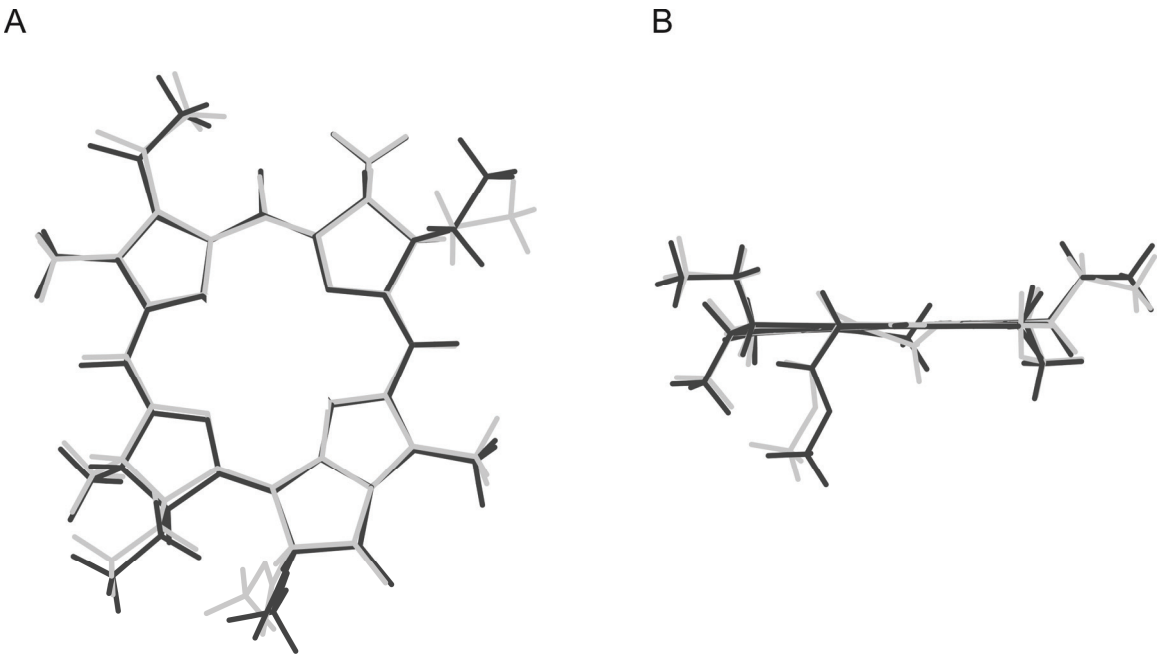

Appendix-B. 1 Overlaid view of bacteriopheophytin in two conformations. The molecule displayed in grey color is the bacteriopheophytin as in x-ray structure (Camara-Artigas et al., 2002b) and the molecule displayed in black is from the fully relaxed geometry by theoretical modelling. (A) view from the side and (B) view from the top.

References

(1) Abragam, A. (**1961**) *Principles of Nuclear Magnetism.* Oxford: Oxford University Press.

(2) ADF2009.01 (**2009**) SCM, Theoretical Chemistry, Vrije Universiteit, Amsterdam, The Netherlands, http://ww.scm.com.

(3) Alia, A., Matysik, J., Soede-Huijbregts, C., Baldus, M., Raap, J., Lugtenburg, J., Gast, P., van Gorkom, H. J., Hoff, A. J. and de Groot, H. J. M. (**2001**) Ultrahigh field MAS NMR dipolar correlation spectroscopy of the histidine residues in light-harvesting complex II from photosynthetic bacteria reveals partial internal charge transfer in the B850/His complex. *J. Am. Chem. Soc.*, 123, 4803-4809.

(4) Alia, A., Roy, E., Gast, P., van Gorkom, H. J., de Groot, H. J. M., Jeschke, G. and Matysik, J. (**2004**) Photochemically induced dynamic nuclear polarization in photosystem I of plants observed by ^{13}C magic-angle spinning NMR. *J. Am. Chem. Soc.*, 126, 12819-12826.

(5) Alia, A., Wawrzyniak, P. K., Janssen, G. J., Buda, F., Matysik, J. and de Groot, H. J. M. (**2009**) Differential charge polarization of axial histidines in bacterial reaction centers balances the asymmetry of the special pair. *J. Am. Chem. Soc.*, 131, 9626-9627.

(6) Allen, J. P., Feher, G., Yeates, T. O., Komiya, H. and Rees, D. C. (**1987**) Structure of the reaction center from *Rhodobacter sphaeroides* R-26 the protein subunits. *Proc. Natl. Acad. Sci. U. S. A.*, 84, 6162-6166.

(7) Andrew, E. R., Bradbury, A. and Eades, R. G. (**1958**) Nuclear magnetic resonance spectra from a crystal rotated at high speed. *Nature*, 182, 1659-1659.

(8) Andrew, E. R., Bradbury, A. and Eades, R. G. (**1959**) *Nature*, 162, 1659.

(9) Bahatyrova, S., Frese, R. N., Siebert, C. A., Olsen, J. D., van der Werf, K. O., van Grondelle, R., Niederman, R. A., Bullough, P. A., Otto, C. and Hunter, C. N. (**2004**) The native architecture of a photosynthetic membrane. *Nature*, 430, 1058-1062.

(10) Baldus, M. and Meier, B. H. (**1997**) Broadband polarization transfer under magic-angle spinning: Application to total through-space-correlation NMR spectroscopy. *J. Magn. Reson.*, 128, 172-193.

(11) Becke, A. D. (**1988**) Density-functional exchange-energy approximation with correct asymptotic-behavior. *Phys. Rev. A*, 38, 3098-3100.

(12) Bennett, A. E., Griffin, R. G., Ok, J. H. and Vega, S. (**1992**) Chemical shift correlation spectroscopy in rotating solids: Radio frequency-driven dipolar recoupling and longitudinal exchange. *J. Chem. Phys.*, 96, 8624-8627.

(13) Bennett, A. E., Rienstra, C. M., Auger, M., Lakshmi, K. V. and Griffin, R. G. (**1995**) Heteronuclear decoupling in rotating solids. *J. Chem. Phys.*, 103, 6951-6958.

(14) Bennett, A. E., Rienstra, C. M., Griffiths, J. M., Zhen, W., Lansbury, J. P. T. and Griffin, R. G. (**1998**) Homonuclear radio frequency-driven recoupling in rotating solids. *J. Chem. Phys.*, 108, 9463-9479.

(15) Bielecki, A., Kolbert, A. C. and Levitt, M. H. (**1989**) Frequency-switched pulse sequences: Homonuclear decoupling and dilute spin NMR in solids. *Chem. Phys. Lett.*, 155, 341-346.

(16) Blankenship, R. E., Babcock, G. T., Warden, J. T. and Sauer, K. (**1975**) Observation of a new EPR transient in chloroplasts that may reflect electron-donor to photosystem II at room-temperature. *FEBS Lett.*, 51, 287-293.

(17) Blankenship, R. E., Madigan, M. T. and Bauer, C. E., eds. (**1995**) *Anoxygenic Photosynthetic Bacteria.* Dordrecht: Kluwer Academic Publishers.

(18) Blankenship, R. E. (**2002**) *Molecular Mechanisms of Photosynthesis.* Oxford, London: Blackwell Science Ltd.

(19) Bloembergen, N. (**1949**) The interaction of nuclear spins in a crystalline lattice. *Physica*, 15, 386-426.

(20) Brinkmann, A. and Levitt, M. H. (**2001**) Symmetry principles in the nuclear magnetic resonance of spinning solids: Heteronuclear recoupling by generalized Hartmann--Hahn sequences. *J. Chem. Phys.*, 115, 357-384.

(21) Camara-Artigas, A., Magee, C., Goetsch, A. and Allen, J. P. (**2002a**) The structure of the heterodimer reaction center from Rhodobacter sphaeroides at 2.55 angstrom resolution. *Photosynth. Res.*, 74, 87-93.

(22) Camara-Artigas, A., Brune, D. and Allen, J. P. (**2002b**) Interactions between lipids and bacterial reaction centers determined by protein crystallography. *Proc. Natl. Acad. Sci. U. S. A.*, 99, 11055-11060.

(23) Caravatti, P., Deli, J., Bodenhausen, G. and Ernst, R. R. (**1982**) Direct evidence of microscopic homogeneity in disordered solids. *J. Am. Chem. Soc.*, 104, 5506-5507.

(24) Caravatti, P., Neuenschwander, P. and Ernst, R. R. (**1985**) Characterization of heterogeneous polymer blends by two-dimensional proton spin diffusion spectroscopy. *Macromolecules*, 18, 119-122.

(25) Carravetta, M., Edén, M., Zhao, X., Brinkmann, A. and Levitt, M. H. (**2000**) Symmetry principles for the design of radiofrequency pulse sequences in the nuclear magnetic resonance of rotating solids. *Chem. Phys. Lett.*, 321, 205-215.

(26) Castellani, F., van Rossum, B., Diehl, A., Schubert, M., Rehbein, K. and Oschkinat, H. (**2002**) Structure of a protein determined by solid-state magic-angle-spinning NMR spectroscopy. *Nature*, 420, 98-102.

(27) Chapter.2 This thesis.

(28) Chapter.3 This thesis.

(29) Cheung, T. T. P. (**1981**) Spin diffusion in NMR in solids. *Phys. Rev. B*, 23, 1404.

(30) Closs, G. L. and Closs, L. E. (**1969**) Induced dynamic nuclear spin polarization in reactions of photochemically and thermally generated triplet diphenylmethylene. *J. Am. Chem. Soc.*, 91, 4549.

(31) Cooper, D. E., Rands, M. B. and Woo, C. P. (**1975**) Sulfide reduction in fellmongery effluent by red sulfur bacteria. *J. Water Pollut. Con. F.*, 47, 2088-2100.

(32) Cotton, T. M. and Van Duyne, R. P. (**1979**) An electrochemical investigation of the redox properties of bacteriochlorophyll and bacteriopheophytin in aprotic solvents. *J. Am. Chem. Soc.*, 101, 7605-7612.

(33) Crocker, E., Patel, A. B., Eilers, M., Jayaraman, S., Getmanova, E., Reeves, P. J., Ziliox, M., Khorana, H. G., Sheves, M. and Smith, S. O. (**2004**) Dipolar assisted rotational resonance NMR of tryptophan and tyrosine in Rhodopsin. *J. Biomol. NMR*, 29, 11-20.

(34) Crofts, A. R., Meinhardt, S. W., Jones, K. R. and Snozzi, M. (**1983**) The role of the Quinone pool in the cyclic electron-transfer chain on *Rhodopseudomonas sphaeroides* a modified q-cycle mechanism. *Biochim. Biophys. ACTA*, 723, 202-218.

(35) Crosby, R. C., Reese, R. L. and Haw, J. F. (**1988**) Cross polarization magic angle spinning proton NMR-spectroscopy of solids. *J. Am. Chem. Soc.*, 110, 8550-8551.

(36) Daviso, E., Diller, A., Alia, A., Matysik, J. and Jeschke, G. (**2008a**) Photo-CIDNP MAS NMR beyond the T_1 limit by fast cycles of polarization extinction and polarization generation. *J. Magn. Reson.*, 190, 43-51.

(37) Daviso, E., Jeschke, G. and Matysik, J. (**2008b**) Photochemically induced dynamic nuclear polarization (Photo-CIDNP) magic-angle spinning NMR. In: T. Aartsma and J. Matysik, eds. *Biophysical techniques in photosynthesis II*. Dordrecht: Springer, 385-399.

(38) Daviso, E., Alia, A., Prakash, S., Diller, A., Gast, P., Lugtenburg, J., Matysik, J. and Jeschke, G. (**2009a**) Electron-nuclear spin dynamics in a bacterial photosynthetic reaction center. *J. Phys. Chem. C*, 113, 10269-10278.

(39) Daviso, E., Prakash, S., Alia, A., Gast, P., Jeschke, G. and Matysik, J. (**2009b**) Nanosecond-Flash ^{15}N Photo-CIDNP MAS NMR on Reaction Centers of Rhodobacter sphaeroides R-26. *Appl. Magn. Reson.*, 37, 49-63.

(40) Daviso, E., Prakash, S., Alia, A., Gast, P., Neugebauer, J., Jeschke, G. and Matysik, J. (**2009c**) The electronic structure of the primary electron donor of reaction centers of purple bacteria at atomic resolution as observed by photo-CIDNP ^{13}C NMR. *Proc. Natl. Acad. Sci. U. S. A.*, 106, 22281-22286.

(41) Daviso, E., Diller, A., Gast, P., Alia, A., Lugtenburg, J., Muller, M. G. and Matysik, J. (**2010**) Action Spectroscopy on Dense Samples of Photosynthetic Reaction Centers of Rhodobacter sphaeroides WT Based on Nanosecond Laser-Flash C-13 Photo-CIDNP MAS NMR. *Appl. Magn. Reson.*, 38, 105-116.

(42) de Boer, I., Bosman, L., Raap, J., Oschkinat, H. and de Groot, H. J. M. (**2002**) 2D ^{13}C-^{13}C MAS NMR correlation spectroscopy with mixing by true ^{1}H spin diffusion reveals long-range ntermolecular distance restraints in ultra high magnetic field. *J. Magn. Reson.*, 157, 286-291.

(43) De Paepe, G., Lewandowski, J. R., Loquet, A., Bockmann, A. and Griffin, R. G. (**2008**) Proton assisted recoupling and protein structure determination. *J. Chem. Phys.*, 129, 245101-245121.

(44) Deisenhofer, J., Epp, O., Miki, K., Huber, R. and Michel, H. (**1985**) Structure of the protein subunits in the photosynthetic reaction center of *Rhodopseudomonas viridis* at 3A resolution. *Nature*, 318, 618-624.

(45) Deisenhofer, J. and Norris, J. R. (**1993**) *The Photosynthetic Reaction Center*. San Diego: Academic.

(46) Deleeuv, D., Malley, M., Buttermann, G., Okamura, M. Y. and Feher, G. (**1982**) The stark-effect in reaction centers from *R. spheroides*. *Biophys. J.*, 37, A111.

(47) Diller, A., Alia, A., Roy, E., Gast, P., de Groot, H., van Gorkom, H., Jeschke, G. and Matysik, J. (**2007a**) The origin of the high redox force of photosystem II: A photo-CIDNP MAS NMR analysis. 91, PS246.

(48) Diller, A., Roy, E., Gast, P., van Gorkom, H. J., de Groot, H. J. M., Glaubitz, C., Jeschke, G., Matysik, J. and Alia, A. (**2007b**) ^{15}N photochemically induced dynamic nuclear polarization magic-angle spinning NMR analysis of the electron donor of photosystem II. *Proc. Natl. Acad. Sci. U. S. A.*, 104, 12767-12771.

(49) Diller, A., Alia, A., Gast, P., Jeschke, G. and Matysik, J. (**2008**) ^{13}C Photo-CIDNP MAS NMR on the LH1-RC Complex of *Rhodopseudomonas acidophila*. *Photosynthesis. Energy from the Sun*, 55-58.

(50) Douglass, D. C. and McBrierty, V. J. (**1978**) Cross Relaxation in Poly(vinylidene fluoride) from Transient Overhauser Measurements. *Macromolecules*, 11, 766.

(51) Duer, M. J. (**2004**) *Introduction to solid state NMR spectroscopy*. Oxford: Blackwell Publishing Ltd.

(52) Eden, M. and Levitt, M. H. (**1999**) Pulse sequence symmetries in the nuclear magnetic resonance of spinning solids: Application to heteronuclear decoupling. *J. Chem. Phys.*, 111, 1511-1519.

(53) Egorova-Zachernyuk, T., Rossum, B. v., Erkelens, C. and Groot, H. d. (**2008**) Characterisation of uniformly ^{13}C, ^{15}N labelled bacteriochlorophyll *a* and bacteriopheophytin *a* in solution and in solid state: complete assignment of the ^{13}C, ^{1}H and ^{15}N chemical shifts. *Magn. Reson. Chem.*, 46, 1074-1083.

(54) Egorova-Zachernyuk, T. A., van Rossum, B., Boender, G.-J., Franken, E., Ashurst, J., Raap, J., Gast, P., Hoff, A. J., Oschkinat, H. and de Groot, H. J. M. (**1997**) Characterization of pheophytin ground states in *Rhodobacter sphaeroides* R26 photosynthetic reaction centers from multispin pheophytin enrichment and 2-D ^{13}C MAS NMR dipolar correlation spectroscopy. *Biochemistry*, 36, 7513-7519.

(55) Ermler, U., Fritzsch, G., Buchanan, S. K. and Michel, H. (**1994**) Structure of the photosynthetic reaction-center from *Rhodobacter sphaeroides* at 2.65-Angstrom resolution cofactors and protein-cofactor interactions. *Structure*, 2, 925-936.

(56) Ernst, M. and Meier, B. H. (**1998**) Spin diffusion in solids. In: I. Ando and T. Asakura, eds. *Solid State NMR of Polymers*: Elsevier: Amsterdam.

(57) Etzkorn, M., Seidel, K., Li, L., Martell, S., Geyer, M., Engelhard, M. and Baldus, M. (**2010**) Complex formation and light activation in membrane-embedded sensory rhodopsin II as seen by solid-state NMR spectroscopy. *Structure*, 18, 293-300.

(58) Feher, G., Okamura, M. Y. and McElroy, J. D. (**1972**) Identification of an electron acceptor in reaction centers of *Rhodopseudomonas spheroides* by EPR spectroscopy. *BBA-Bioenergetics*, 267, 222-226.

(59) Fillingame, R. H. (**2000**) Getting to the bottom of the F_1 ATPase. *Nat. Struct. Biol.*, 7, 1002-1004.

(60) Fillingame, R. H., Jiang, W. and Dmitriev, O. Y. (**2000**) Coupling H^+ transport to rotary catalysis in F-type ATP synthases: Structure and organization of the transmembrane rotary motor. *J. Exp. Biol.*, 203, 9-17.

(61) Fischer, M. R., Degroot, H. J. M., Raap, J., Winkel, C., Hoff, A. J. and Lugtenburg, J. (**1992**) ^{13}C Magic angle spinning NMR-study of the light-induced and temperature-dependent changes in *Rhodobacter sphaeroides* R-26 reaction centers enriched in 4'-^{13}C tyrosine. *Biochemistry*, 31, 11038-11049.

(62) Flores, M., Savitsky, A., Paddock, M. L., Abresch, E. C., Dubinskii, A. A., Okamura, M. Y., Lubitz, W. and Moebius, K. (**2010**) Electron-nuclear and electron-electron double resonance spectroscopies show that the primary quinone acceptor Q(A) in reaction centers from photosynthetic bacteria *Rhodobacter sphaeroides* remains in the same orientation upon light-induced reduction. *J. Phys. Chem. B.*, 114, 16894-16901.

(63) Fonseca Guerra, C., Snijders, J. G., te Velde, G. and Baerends, E. J. (**1998**) Towards an order-N DFT method. *Theor. Chem. Acc.*, 99, 391-403-403.

(64) Förster, T. (**1948**) Zwischenmolekulare Energiewanderung und Fluoreszenz. *Ann. Phys.*, 437, 55-75.

(65) Franken, E. M., Shkuropatov, A. Y., Francke, C., Neerken, S., Gast, P., Shuvalov, V. A., Hoff, A. J. and Aartsma, T. J. (**1997a**) Reaction centers of *Rhodobacter sphaeroides* R-26 with selective replacement of bacteriopheophytin *a* by pheophytin *a*: II. Temperature dependence of the quantum yield of $P^+Q_A^-$ and ^3P formation. *BBA-Bioenergetics*, 1321, 1-9.

(66) Franken, E. M., Shkuropatov, A. Y., Francke, C., Neerken, S., Gast, P., Shuvalov, V. A., Hoff, A. J. and Aartsma, T. J. (**1997b**) Reaction centers of *Rhodobacter sphaeroides* R-26 with selective replacement of bacteriopheophytin by pheophytin *a* : I. Characterisation of steady-state absorbance and circular dichroism, and of the $P^+Q_A^-$ state. *BBA-Bioenergetics*, 1319, 242-250.

(67) Frese, R. N., Siebert, C. A., Niederman, R. A., Hunter, C. N., Otto, C. and van Grondelle, R. (**2004**) The long-range organization of a native photosynthetic membrane. *Proc. Natl. Acad. Sci. U. S. A.*, 101, 17994-17999.

(68) Friesner, R. and Won, Y. (**1989**) Spectroscopy and Electron-Transfer Dynamics of the Bacterial Photosynthetic Reaction Center. *Biochim. Biophys. Acta.*, 977, 99-122.

(69) Ganapathy, S., Oostergetel, G. T., Wawrzyniak, P. K., Reus, M., Gomez Maqueo Chew, A., Buda, F., Boekema, E. J., Bryant, D. A., Holzwarth, A. R. and de Groot, H. J. M. (**2009**) Alternating syn-anti bacteriochlorophylls form concentric helical nanotubes in chlorosomes. *Proc. Natl. Acad. Sci. U. S. A.*, 106, 8525-8530.

(70) Gardiennet, C., Loquet, A., Etzkorn, M., Heise, H., Baldus, M. and Bockmann, A. (**2008**) Structural constraints for the Crh protein from solid-state NMR experiments. *J. Biomol. NMR.*, 40, 239-250.

(71) Gennis, R. B., Barquera, B., Hacker, B., Vandoren, S. R., Arnaud, S., Crofts, A. R., Davidson, E., Gray, K. A. and Daldal, F. (**1993**) The bc(1) complexes of *Rhdobacter sphaeroides* and *Rhodobacter capsulatus*. *J. Bioenerg. Biomembr.*, 25, 195-209.

(72) Goldstein, R. A. and Boxer, S. G. (**1987**) Effects of nuclear-spin polarization on reaction dynamics in photosynthetic bacterial reaction centers. 51, 937-946.

(73) Gordon, S. L. and Wüthrich, K. (**1978**) Transient proton–proton Overhauser effects in horse ferrocytochrome c. *J. Am. Chem. Soc.*, 100, 7094–7096.

(74) Griffiths, J. M., Bennett, A. E., Engelhard, M., Siebert, F., Raap, J., Lugtenburg, J., Herzfeld, J. and Griffin, R. G. (**2000**) Structural investigation of the active site in bacteriorhodopsin: Geometric constraints on the roles of Asp-85 and Asp-212 in the proton-pumping mechanism from solid state NMR. *Biochemistry*, 39, 362-371.

(75) Grommek, A., Meier, B. H. and Ernst, M. (**2006**) Distance information from proton-driven spin diffusion under MAS. *Chem. Phys. Lett.*, 427, 404-409.

(76) Grondelle, R. and Novoderezhkin, V. (**2006**) Energy transfer in photosynthesis: experimental insights and quantitative models.

(77) Gullion, T. and Schaefer, J. (**1989**) Rotational-echo double-resonance NMR. *J. Magn. Reson.*, 81, 196-200.

(78) Hartmann, S. R. and Hahn, E. L. (**1962**) Nuclear Double Resonance in the Rotating Frame. *Phys. Rev.*, 128, 2042.

(79) Heinen, W., Wenzel, C. B., Rosenmoller, C. H., Mulder, F. M., Boender, G. J., Lugtenburg, J., de Groot, H. J. M., van Duin, M. and Klumperman, B. (**1998**) Solid-state NMR study of miscibility and phase separation in blends and semi-interpenetrating networks of ^{13}C-labeled poly(styrene-co-acrylonitrile) and poly(styrene-co-maleic anhydride). *Macromolecules*, 31, 7404-7412.

(80) Henrichs, P. M. and Linder, M. (**1984**) Carbon-13 spin diffusion in the determination of intermolecular structure in solids. *J. Magn. Reson.*, 58, 458-461.

(81) Hiller, M., Krabben, L., Vinothkumar, K. R., Castellani, F., van Rossum, B. J., Kuhlbrandt, W. and Oschkinat, H. (**2005**) Solid-state magic-angle spinning NMR of outer-membrane protein G from Escherichia coli. *Chembiochem*, 6, 1679-1684.

(82) Hing, A. W., Vega, S. and Schaefer, J. (**1992**) Transferred-echo double-resonance NMR. *J. Magn. Reson.*, 96, 205-209.

(83) Hoff, A. J., Rademaker, H., Vangrondelle, R. and Duysens, L. N. M. (**1977**) Magnetic-field dependence of yield of triplet-state in reaction centers of photosynthetic bacteria. *Biochim. Biophys. Acta*, 460, 547-554.

(84) Hoff, A. J. and Deisenhofer, J. (**1997**) Photophysics of photosynthesis. Structure and spectroscopy of reaction centers of purple bacteria. *Phys. Rep.*, 287, 2-247.

(85) Hohwy, M., Rienstra, C. M., Jaroniec, C. P. and Griffin, R. G. (**1999**) Fivefold symmetric homonuclear dipolar recoupling in rotating solids: Application to double quantum spectroscopy. *J. Chem. Phys.*, 110, 7983-7992.

(86) Holm, H. W. and Vennes, J. W. (**1970**) Occurrence of Purple Sulfur Bacteria in a Sewage Treatment Lagoon. *Appl. Environ. Microb.*, 19, 988-996.

(87) Holzwarth, A. R. and Muller, M. G. (**1996**) Energetics and kinetics of radical pairs in reaction centers from *Rhodobacter sphaeroides*. A femtosecond transient absorption study. *Biochemistry*, 35, 11820-11831.

(88) Hoshino, T., Kubo, A., Imashiro, F. and Terao, T. (**1998**) Proton two-dimensional multiple pulse NMR experiments on the nematic liquid crystal MBBA. *Mol. Phys.*, 93, 301-313.

(89) Hu, X. and Schulten, K. (**1998**) Model for the light-harvesting complex I (B875) of *Rhodobacter sphaeroides*. *Biophys. J.*, 75, 683-694.

(90) Hu, X. C., Damjanovic, A., Ritz, T. and Schulten, K. (**1998**) Architecture and mechanism of the light-harvesting apparatus of purple bacteria. *Proc. Natl. Acad. Sci. U. S. A.*, 95, 5935-5941.

(91) Huber, H., Meyer, M., Scheer, H., Zinth, W. and Wachtveitl, J. (**1998**) Photosynthesis Research. *SpringerLink*, 55, 153-162.

(92) Hughes, A. V., Rees, P., Heathcote, P. and Jones, M. R. (**2006**) Kinetic analysis of the thermal stability of the photosynthetic reaction center from *Rhodobacter sphaeroides*. *Biophys. J.*, 90, 4155-4166.

(93) Hull, W. E. and Sykes, B. D. (**1975**) Dipolar nuclear spin relaxation of ^{19}F in multispin systems. Application to ^{19}F labeled proteins. *J. Chem. Phys.*, 63, 867-880.

(94) Hunter, C. N., Daldal, F., Thurnauer, M. C. and Beatty, J. T., eds. (**2008**) *The Purple Phototrophic Bacteria.* Dordrecht: Springer.

(95) Igumenova, T. I., McDermott, A. E., Zilm, K. W., Martin, R. W., Paulson, E. K. and Wand, A. J. (**2004**) Assignments of carbon NMR resonances for microcrystalline ubiquitin. *J. Am. Chem. Soc.*, 126, 6720-6727.

(96) Janssen, G. J., Daviso, E., van Son, M., de Groot, H. J. M., Alia, A. and Matysik, J. (**2010**) Observation of the solid-state photo-CIDNP effect in entire cells of cyanobacteria Synechocystis. *Photosynth. Res.*, 104, 275-282.

(97) Jentzen, W., Ma, J.-G. and Shelnutt, J. A. (**1998**) Conservation of the conformation of the porphyrin macrocycle in hemoproteins. *Biophys. J.*, 74, 753-763.

(98) Jeschke, G. (**1997**) Electron-electron-nuclear three-spin mixing in spin-correlated radical pairs. *J. Chem. Phys.*, 106, 10072-10086.

(99) Jeschke, G. (**1998**) A new mechanism for chemically induced dynamic nuclear polarization in the solid state. *J. Am. Chem. Soc.*, 120, 4425-4429.

(100) Jeschke, G. and Matysik, J. (**2003**) A reassessment of the origin of photochemically induced dynamic nuclear polarization effects in solids. *Chem. Phys.*, 294, 239-255.

(101) Johnson, G. W., Lee, I. J. and Small, G. J. (**1991**) Excited state spectral line narrowing spectroscopies. In: H. Scheer, ed. *Chlorophylls*: CRC Pr I Llc.

(102) Jones, B. R. (**1956**) Studies of pigmented non-sulfur purple bacteria in relation to cannery waste lagoon odors. *Sewage Ind. Wastes*, 28, 883-893.

(103) Jones, M. R. (**2009**) The petite purple photosynthetic powerpack. *Biochem. Soc. T.*, 037, 400-407.

(104) Jordan, P. M. (**1991**) *In Bio Synthesis of tetrapyrroles.* Amsterdam: Elsevier.

(105) Jungas, C., Ranck, J. L., Rigaud, J. L., Joliot, P. and Vermeglio, A. (**1999**) Supramolecular organization of the photosynthetic apparatus of *Rhodobacter sphaeroides*. *Embo J.*, 18, 534-542.

(106) Junge, W., Lill, H. and Engelbrecht, S. (**1997**) ATP synthase: an electrochemical transducer with rotatory mechanics. *Trends Biochem. Sci*, 22, 420-423.

(107) Kalk, A. and Berendsen, H. J. C. (**1976**) Proton magnetic relaxation and spin diffusion in proteins. *J. Magn. Reson.*, 24, 343-366.

(108) Kaptein, R. and Oosterhoff, J. L. (**1969**) Chemically induced dynamic nuclear polarization II : (Relation with anomalous ESR spectra). *Chem. Phys. Lett.*, 4, 195.

(109) Kaptein, R. (**1971**) Simple rules for chemically induced dynamic nuclear polarization. *Chem. Commun.*, 14, 732-733.

(110) Karrasch, S., Bullough, P. A. and Ghosh, R. (**1995**) The 8.5-angstrom projection map of the light-harvesting complex from *Rhodospirillum rubrum* reveals a ring composed of 16 subunits. *EMBO J.*, 14, 631-638.

(111) Kolodziejski, W., Corma, A., Wozniak, K. and Klinowski, J. (**1996**) ^{13}C ---> ^{1}H Cross-polarization NMR in solids at natural ^{13}C abundance. *J. Phys. Chem.*, 100, 7345-7351.

(112) Kubo, A. and McDowell, C. A. (**1988**) Spectral spin diffusion in polycrystalline solids under magic-angle spinning. *J. Chem. Soc., Faraday Trans. 1*, 84, 3713 - 3730.

(113) Kumar, A., Ernst, R. R. and Wüthrich, K. (**1980**) A two-dimensional nuclear Overhauser enhancement (2D NOE) experiment for the elucidation of complete proton-proton cross-relaxation networks in biological macromolecules. *Biochem. Biophy. Res. Co.*, 95, 1-6.

(114) Kumar, A., Wagner, G., Ernst, R. R. and Wuethrich, K. (**1981**) Buildup rates of the nuclear Overhauser effect measured by two-dimensional proton magnetic resonance spectroscopy: implications for studies of protein conformation. *J. Am. Chem. Soc.*, 103, 3654-3658.

(115) Lee, C. T., Yang, W. T. and Parr, R. G. (**1988**) Development of the colle-salvetti correlation-energy formula into a functional of the electron-density. *Phys. Rev. B*, 37, 785-789.

(116) Lee, M. and Goldburg, W. I. (**1965**) Nuclear Magnetic Resonance line narrowing by a rotating rf field. *Phys. Rev.*, 140.

(117) Lee, Y. K., Kurur, N. D., Helmle, M., Johannessen, O. G., Nielsen, N. C. and Levitt, M. H. (**1995**) Efficient dipolar recoupling in the NMR of rotating solids - a sevenfold symmetrical radiofrequency pulse sequence. *Chem. Phys. Lett.*, 242, 304-309.

(118) Lendzian, F., Huber, M., Isaacson, R. A., Endeward, B., Plato, M., Bonigk, B., Mobius, K., Lubitz, W. and Feher, G. (**1993**) The electronic-structure of the primary donor cation-radical in *Rhodobacter sphaeroides* R-26 - endor and triple-resonance studies in single-crystals of reaction centers. *Biochim. Biophys. Acta.*, 1183, 139-160.

(119) Leskes, M., Madhu, P. K. and Vega, S. (**2006**) Proton line narrowing in solid-state nuclear magnetic resonance: New insights from windowed phase-modulated Lee-Goldburg sequence. *J. Chem. Phys.*, 125, 124506-124518.

(120) Leskes, M., Madhu, P. K. and Vega, S. (**2009**) Why does PMLG proton decoupling work at 65 kHz MAS? *J. Magn. Reson.*, 199, 208-213.

(121) Levitt, M. H., Oas, T. G. and Griffin, R. G. (**1988**) Rotary resonance recoupling in heteronuclear spin pair systems. *Isr.J.Chem*, 28, 271-282.

(122) Levitt, M. H., Kolbert, A. C., Bielecki, A. and Ruben, D. J. (**1993**) High-resolution 1H NMR in solids with frequency-switched multiple-pulse sequences. *Solid State Nucl. Mag.*, 2, 151-163.

(123) Levitt, M. H. (**2002**) Symmetry-based pulse sequences in magic-angle spinning solid-state NMR. In: D. M. Grant and R. K. Harris, eds. *Encyclopedia of Nuclear Magnetic Resonance; Advances in NMR*. Chichester, UK: John Wiley & Sons Ltd., 165–196.

(124) Linder, M., Henrichs, P. M., Hewitt, J. M. and Massa, D. J. (**1985**) Use of carbon--carbon nuclear spin diffusion for the study of the miscibility of polymer blends. *J. Chem. Phys.*, 82, 1585-1598.

(125) Lockhart, D. J. and Boxer, S. G. (**1987**) Magnitude and direction of the change in dipole moment associated with excitation of the primary electron donor in *Rhodopseudomonas sphaeroides* reaction centers. *Biochemistry*, 26, 664-668.

(126) Lockhart, D. J. and Boxer, S. G. (**1988**) Stark effect spectroscopy of *Rhodobacter sphaeroides* and *Rhodopseudomonas viridis* reaction centers. *Proc. Natl. Acad. Sci. U. S. A.*, 85, 107-111.

(127) Loquet, A., Bardiaux, B., Gardiennet, C., Blanchet, C., Baldus, M., Nilges, M., Malliavin, T. and Bockmann, A. (**2008**) 3D structure determination of the Crh protein from highly ambiguous solid-state NMR restraints. *J. Am. Chem. Soc.*, 130, 3579-3589.

(128) Lowe, I. J. (**1959**) Free induction decays of rotating solids. *Phys. Rev. Lett.*, 2, 285.

(129) Lubitz, W., Abresch, E. C., Debus, R. J., Isaacson, R. A., Okamura, M. Y. and Feher, G. (**1985**) Electron nuclear double resonance of semiquinones in reaction centers of Rhodopseudomonas sphaeroides. *BBA-Bioenergetics*, 808, 464-469.

(130) Lubitz, W. and Feher, G. (**1999**) The primary and secondary accepters in bacterial photosynthesis III. Characterization of the quinone radicals $Q_{A}^{-\cdot}$ and $Q_{B}^{-\cdot}$ by EPR and ENDOR. *Appl. Magn. Reson.*, 17, 1-48.

(131) Lyle, P. A., Kolaczkowski, S. V. and Small, G. J. (**1993**) Photochemical hole-burned spectra of protonated and deuterated reaction centers of *Rhodobacter sphaeroides*. *J. Phys. Chem*, 97, 6924-6933.

(132) Madigan, M. T. (**1984**) A novel photosynthetic purple bacterium isolated from a yellowstone hot spring. *Science*, 225, 313-315.

(133) Marcus, R. A. (**1956a**) On the theory of oxidation-reduction reactions involving electron transfer *J. Chem. Phys.*, 24, 966-978.

(134) Marcus, R. A. (**1956b**) Electrostatic free energy and other properties of states having nonequilibrium polarization *J. Chem. Phys.*, 24, 979-989.

(135) Marcus, R. A. (**1965**) On the theory of electron-transfer reactions. VI. Unified treatment for homogeneous and electrode reactions. *J. Chem. Phys.*, 43, 679-701.

(136) Marcus, R. A. and Sutin, N. (**1985**) Electron transfers in chemistry and biology. *Biochim. Biophys. Acta - Reviews on Bioenergetics*, 811, 265-322.

(137) Martin, J. L., Breton, J., Hoff, A. J., Migus, A. and Antonetti, A. (**1986**) Femtosecond spectroscopy of electron-transfer in the reaction center of the photosynthetic bacterium *Rhodopseudomonas-sphaeroides* R-26 - direct electron-transfer from the dimeric bacteriochlorophyll primary donor to the bacteriopheophytin acceptor with a time constant 2.8 +/- 0.2 psec. *Proc. Natl. Acad. Sci. U. S. A.*, 83, 957-961.

(138) Matysik, J., Alia, Gast, P., van Gorkom, H. J., Hoff, A. J. and de Groot, H. J. M. (**2000a**) Photochemically induced nuclear spin polarization in reaction centers of photosystem II observed by ^{13}C-solid-state NMR reveals a strongly asymmetric electronic structure of the P680.+ primary donor chlorophyll. *Proc. Natl. Acad. Sci. U. S. A.*, 97, 9865-9870.

(139) Matysik, J., Alia, Holland, J., Egorova-Zachernyuk, T., Gast, P. and de Groot, H. J. M. (**2000b**) Sample illumination and photo-CIDNP in a magic-angle spinning NMR probe. *Indian J. Biochem. Biophys.*, 37, 418-423.

(140) Matysik, J., Schulten, E., Alia, Gast, P., Raap, J., Lugtenburg, J., Hoff, A. J. and de Groot, H. J. M. (**2001**) Photo-CIDNP ^{13}C magic angle spinning NMR on bacterial reaction centres: Exploring the electronic structure of the special pair and its surroundings. *Biol. Chem.*, 382, 1271-1276.

(141) Matysik, J., Diller, A., Roy, E. and Alia, A. (**2009**) The solid-state photo-CIDNP effect. *Photosynth. Res.*, 102, 427-435.

(142) McBrierty, V. J. (**1979**) Heterogeneity in polymers as studied by nuclear magnetic resonance. *Faraday Discuss. Chem. Soc.*, 68, 78-86.

(143) McDermott, A., Zysmilich, M. G. and Polenova, T. (**1998**) Solid state NMR studies of photoinduced polarization in photosynthetic reaction centers: mechanism and simulations. *Solid State Nucl. Mag.*, 11, 21-47.

(144) McDermott, G., Prince, S. M., Freer, A. A., Hawthornthwaitelawless, A. M., Papiz, M. Z., Cogdell, R. J. and Isaacs, N. W. (**1995**) Crystal-structure of an integral membrane light-harvesting complex from photosynthetic bacteria. *Nature*, 374, 517-521.

(145) Mehring, M. and Waugh, J. S. (**1972**) Magic-angle NMR experiments in solids. *Phys. Rev. B*, 5, 3459.

(146) Moore, L. J., Zhou, H. and Boxer, S. G. (**1999**) Excited-state electronic asymmetry of the special pair in photosynthetic reaction center mutants: Absorption and Stark spectroscopy. *Biochemistry*, 38, 11949-11960.

(147) Mulder, F. M., Heinen, W., van Duin, M., Lugtenburg, J. and de Groot, H. J. M. (**2000**) Cross-linking induced phase separation in SAN/SMA semi-interpenetrating polymer networks observed by solid state NMR and site specific isotope enrichment. *Macromolecules*, 33, 5544-5548.

(148) Nielsen, N. C., Creuzet, F., Griffin, R. G. and Levitt, M. H. (**1992**) Enhanced double-quantum nuclear magnetic resonance in spinning solids at rotational resonance. 96, 5668.

(149) Novoderezhkin, V. I., Yakovlev, A. G., van Grondelle, R. and Shuvalov, V. A. (**2004**) Coherent nuclear and electronic dynamics in primary charge separation in photosynthetic reaction centers: A redfield theory approach. 108, 7445-7457.

(150) Noy, D., Moser, C. C. and Dutton, P. L. (**2006**) Design and engineering of photosynthetic light-harvesting and electron transfer using length, time, and energy scales. *BBA - Bioenergetics*, 1757, 90-105.

(151) Oas, T. G., Griffin, R. G. and Levitt, M. H. (**1988**) Rotary resonance recoupling of dipolar interactions in solid-state nuclear magnetic resonance spectroscopy. *J. Chem. Phys.*, 89, 692-695.

(152) Okamura, M. Y., Steiner, L. A. and Feher, G. (**1974**) Characterization of reaction centers from photosynthetic bacteria. I. Subunit structure of the protein mediating the primary photochemistry in *Rhodopseudomonas spheroides* R-26. *Biochemistry*, 13, 1394-1403.

(153) Okamura, M. Y., Isaacson, R. A. and Feher, G. (**1975**) Primary acceptor in bacterial photosynthesis - obligatory role of ubiquinone in photoactive reaction centers of *Rhodopseudomonas-spheroides*. *Proc. Natl. Acad. Sci. U. S. A.*, 72, 3491-3495.

(154) Palaniappan, V., Martin, P. C., Chynwat, V., Frank, H. A. and Bocian, D. F. (**1993**) Comprehensive resonance Raman study of photosynthetic reaction centers from Rhodobacter sphaeroides. Implications for pigment structure and pigment-protein interactions. *J. Am. Chem. Soc.*, 115, 12035-12049.

(155) Pandit, A., Buda, F., van Gammeren, A. J., Ganapathy, S. and de Groot, H. J. M. (**2010**) Selective chemical shift assignment of bacteriochlorophyll *a* in uniformly [^{13}C, ^{15}N]-labeled light-harvesting 1 complexes by solid-state NMR in ultrahigh magnetic field. *J. Phys. Chem. B.*, 114, 6207-6215.

(156) Pines, A., Gibby, M. G. and Waugh, J. S. (**1973**) Proton-enhanced NMR of dilute spins in solids. *J. Chem. Phys.*, 59, 569-590.

(157) Polenova, T. and McDermott, A. E. (**1999**) A coherent mixing mechanism explains the photoinduced nuclear polarization in photosynthetic reaction centers. *J. Phys. Chem. B*, 103, 535-548.

(158) Potter, J., Fyfe, P., Frolov, D., Wakeham, M., van Grondelle, R., Robert, B. and JONES, M. (**2005**) Strong effects of an individual water molecule on the rate of light-driven charge separation in the *Rhodobacter sphaeroides* reaction center. *J. Biol. Chem.*, 280, 27155-27164.

(159) Prakash, S., Alia, Gast, P., de Groot, H. J. M., Jeschke, G. and Matysik, J. (**2005**) Magnetic field dependence of photo-CIDNP MAS NMR on photosynthetic reaction centers of *Rhodobacter sphaeroides* WT. *J. Am. Chem. Soc.*, 127, 14290-14298.

(160) Prakash, S., Alia, Gast, P., de Groot, H. J. M., Matysik, J. and Jeschke, G. (**2006**) Photo-CIDNP MAS NMR in intact cells of *Rhodobacter sphaeroides* R-26: Molecular and atomic resolution at nanomolar concentration. *J. Am. Chem. Soc.*, 128, 12794-12799.

(161) Prakash, S., Alia, A., Gast, P., de Groot, H. J. M., Jeschke, G. and Matysik, J. (**2007**) ^{13}C chemical shift map of the active cofactors in photosynthetic reaction centers of *Rhodobacter sphaeroides* revealed by photo-CIDNP MAS NMR. *Biochemistry*, 46, 8953-8960.

(162) Purchase, R. and Völker, S. (**2009**) Spectral hole burning: examples from photosynthesis. *Photosynth. Res.*, 101, 245-266-266.

(163) Qian, P., Hunter, C. N. and Bullough, P. A. (**2005**) The 8.5 angstrom projection structure of the core RC-LH1-PufX dimer of *Rhodobacter sphaeroides*. *J. Mol. Biol.*, 349, 948-960.

(164) Reddy, N. R. S., Lyle, P. A. and Small, G. J. (**1992**) Applications of spectral hole burning spectroscopies to antenna and reaction center complexes. *Photosynth. Res.*, 31, 167-194.

(165) Reddy, N. R. S., Kolaczkowski, S. V. and Small, G. J. (**1993**) A Photoinduced Persistent Structural Transformation of the Special Pair of a Bacterial Reaction Center. *Science*, 260, 68-71.

(166) Rohmer, M. (**1999**) The discovery of a mevalonate-independent pathway for isoprenoid biosynthesis in bacteria, algae and higher plants. *Nat. Prod. Rep.*, 16, 565-574.

(167) Roy, E., Alia, Gast, P., van Gorkom, H., de Groot, H. J. M., Jeschke, G. and Matysik, J. (**2007**) Photochemically induced dynamic nuclear polarization in the reaction center of the green sulphur bacterium *Chlorobium tepidum* observed by ^{13}C MAS NMR. *BBA-Bioenergetics.*, 1767, 610-615.

(168) Roy, E., Rohmer, T., Gast, P., Jeschke, G., Alia, A. and Matysik, J. (**2008**) Characterization of the primary radical pair in reaction centers of *Heliobacillus mobilis* by ^{13}C Photo-CIDNP MAS NMR. *Biochemistry*, 47, 4629-4635.

(169) Sarles, L. R. and Cotts, R. M. (**1958**) Double nuclear magnetic resonance and the dipole interaction in solids. *Phys. Rev.*, 111, 853.

(170) Scheuring, S., Sturgis, J. N., Prima, V., Bernadac, A., Levy, D. and Rigaud, J. L. (**2004**) Watching the photosynthetic apparatus in native membranes. *Proc. Natl. Acad. Sci. U. S. A.*, 101, 11293-11297.

(171) Scheuring, S. and Sturgis, J. N. (**2005**) Chromatic adaptation of photosynthetic membranes. *Science*, 309, 484-487.

(172) Scheuring, S., Levy, D. and Rigaud, J. L. (**2005**) Watching the components of photosynthetic bacterial membranes and their in situ organisation by atomic force microscopy. *BBA-Biomembranes*, 1712, 109-127.

(173) Schmidt-Rohr, K. and Spiess, H. W. (**1994**) *Multidimensional solid state NMR and polymers.* London, United Kingdom: Academic Press Ltd.

(174) Schmidt, S., Arlt, T., Hamm, P., Huber, H., Nägele, T., Wachtveitl, J., Meyer, M., Scheer, H. and Zinth, W. (**1994**) Energetics of the primary electron transfer reaction revealed by ultrafast spectroscopy on modified bacterial reaction centers. *Chem. Phys. Lett.*, 223, 116-120.

(175) Scholz, I., Huber, M., Manolikas, T., Meier, B. H. and Ernst, M. (**2008**) MIRROR recoupling and its application to spin diffusion under fast magic-angle spinning. *Chem. Phys. Lett.*, 460, 278-283.

(176) Schulten, E. A. M., Matysik, J., Alia, Kiihne, S., Raap, J., Lugtenburg, J., Gast, P., Hoff, A. J. and de Groot, H. J. M. (**2002**) ^{13}C MAS NMR and photo-CIDNP reveal a pronounced asymmetry in the electronic ground state of the special pair of *Rhodobacter sphaeroides* reaction centers. *Biochemistry*, 41, 8708-8717.

(177) Shelnutt, J. A., Song, X. Z., Ma, J. G., Jia, S. L., Jentzen, W. and Medforth, C. J. (**1998**) Nonplanar porphyrins and their significance in proteins. *Chem. Soc. Rev.*, 27, 31-41.

(178) Shkuropatov, A. Y. and Shuvalov, V. A. (**1993**) Electron transfer in pheophytin a-modified reaction centers from *Rhodobacter sphaeroides* R-26. *FEBS Lett.*, 322, 168-172.

(179) Shochat, S., Arlt, T., Francke, C., Gast, P., Vannoort, P. I., Otte, S. C. M., Schelvis, H. P. M., Schmidt, S., Vijgenboom, E., Vrieze, J., Zinth, W. and Hoff, A. J. (**1994**) Spectroscopic characterization of reaction centers of the (M)Y210W mutant of the photosynthetic bacterium *Rhodobacter sphaeroides*. *Photosynth. Res.*, 40, 55-66.

(180) Shuvalov, V. and Yakovlev, A. (**2003**) Coupling of nuclear wavepacket motion and charge separation in bacterial reaction centers. 540, 26-34.

(181) Siebert, C. A., Qian, P., Fotiadis, D., Engel, A., Hunter, C. N. and Bullough, P. A. (**2004**) Molecular architecture of photosynthetic membranes in *Rhodobacter sphaeroides*: the role of PufX. *Embo J.*, 23, 690-700.

(182) Siefert, E., Irgens, R. L. and Pfennig, N. (**1978**) Phototrophic purple and green bacteria in a sewage treatment plant. *Appl. Environ. Microbiol.*, 35, 38-44.

(183) Stejskal, E. O., Schaefer, J. and Waugh, J. S. (**1977**) Magic-angle spinning and polarization transfer in proton-enhanced NMR. *J. Magn. Reson.*, 28, 105-112.

(184) Stejskal, E. O., Schaefer, J. and McKay, R. A. (**1984**) Analysis of double cross-polarization rates in solid proteins. *J. Magn. Reson.*, 57, 471-485.

(185) Suter, D. and Ernst, R. R. (**1982**) Spectral spin diffusion in the presence of an extraneous dipolar reservoir. *Phys. Rev. B*, 25, 6038.

(186) Szeverenyi, N. M., Sullivan, M. J. and Maciel, G. E. (**1982**) Observation of spin exchange by two-dimensional fourier-transform C13 cross polarization-magic-angle spinning. *J. Magn. Reson.*, 47, 462-475.

(187) Takegoshi, K., Nakamura, S. and Terao, T. (**2001**) ^{13}C-^{1}H dipolar-assisted rotational resonance in magic angle spinning NMR. *Chem. Phys. Lett.*, 344, 631-637.

(188) Takegoshi, K. and Terao, T. (**2002**) ^{13}C nuclear Overhauser polarization nuclear magnetic resonance in rotating solids: Replacement of cross polarization in uniformly ^{13}C labeled molecules with methyl groups. *J. Chem. Phys.*, 117, 1700-1707.

(189) Takegoshi, K., Nakamura, S. and Terao, T. (**2003**) ^{13}C-^{1}H dipolar-driven ^{13}C-^{13}C recoupling without ^{13}C rf irradiation in nuclear magnetic resonance of rotating solids. *J. Chem. Phys.*, 118, 2325-2341.

(190) Takegoshi, K. (**2008**) Homonuclear shift-correlation experiment in solids. In: G. A. Webb, ed. *Modern Magnetic Resonance*: Springer.

(191) te Velde, G., Bickelhaupt, F. M., Baerends, E. J., Fonseca Guerra, C., van Gisbergen, S. J. A., Snijders, J. G. and Ziegler, T. (**2001**) Chemistry with ADF. *J. Comput. Chem.*, 22, 931-967.

(192) Tycko, R. and Dabbagh, G. (**1990**) Measurement of nuclear magnetic dipole--dipole couplings in magic angle spinning NMR. *Chem. Phys. Lett.*, 173, 461-465.

(193) Valesco, F. J. and Crofts, A. R. (**1991**) Complexes or super complexes - inhibitor titrations show that electron-transfer in chromatophores from *Rhodobacter sphaeroides* involves a dimeric unbiquinol: cytochrome *c* oxidoreductase, and is delocalized. *Biochem. Soc. Trans.*, 19, 588-593.

(194) van Gammeren, A. J., Buda, F., Hulsbergen, F. B., Kiihne, S., Hollander, J. G., Egorova-Zachernyuk, T. A., Fraser, N. J., Cogdell, R. J. and de Groot, H. J. M. (**2005**) Selective

chemical shift assignment of B800 and B850 bacteriochlorophylls in uniformly [13C,15N]-labeled light-harvesting complexes by solid-state NMR spectroscopy at ultra-high magnetic field. *J. Am. Chem. Soc.*, 127, 3213-3219.

(195) van Niel, C. B. (**1944**) The culture, general physiology, morphology, and classification of the non-sulfur purple and brown bacteria. *Microbiol. Mol. Biol. Rev.*, 8, 1-118.

(196) van Rossum, B. J., de Groot, C. P., Ladizhansky, V., Vega, S. and de Groot, H. J. M. (**2000**) A method for measuring heteronuclear (^{1}H-^{13}C) distances in high speed MAS NMR. *J. Am. Chem. Soc.*, 122, 3465-3472.

(197) Vinogradov, E., Madhu, P. K. and Vega, S. (**2002**) Proton spectroscopy in solid state nuclear magnetic resonance with windowed phase modulated Lee-Goldburg decoupling sequences. *Chem. Phys. Lett.*, 354, 193-202.

(198) Vinogradov, E., Madhu, P. K. and Vega, S. (**2005**) Strategies for High-Resolution Proton Spectroscopy in Solid-State NMR. In: J. Klinowski, ed. *New Techniques in Solid-State NMR*. Germany: Springer.

(199) Wawrzyniak, P. K., Beerepoot, M., de Groot, H. J. M. and Buda, F. (**2011**) Acetyl group orientation modulates the electronic ground-state asymmetry of the special pair in purple bacterial reaction centers. *Phys. Chem. Chem. Phys.*, 13, 10270-10279.

(200) Wawrzyniak, P. K. (**2011**) Ab initio modeling of primary processes in photosynthesis : protein induced activation of bacteriochlorophylls for efficient light harvesting and charge separation *SSNMR*: Leiden University, 150.

(201) Woodbury, N. W. T. and Parson, W. W. (**1984**) Nanosecond fluorescence from isolated photosynthetic reaction centers of *Rhodopseudomonas sphaeroides*. *BBA - Bioenergetics*, 767, 345-361.

(202) Xia, D., Yu, C. A., Kim, H., Xian, J. Z., Kachurin, A. M., Zhang, L., Yu, L. and Deisenhofer, J. (**1997**) Crystal structure of the cytochrome bc_1 complex from bovine heart mitochondria. *Science*, 277, 60-66.

(203) Yakovlev, A., Vasilieva, L., Khmelnitskaya, T., Shkuropatova, V., Shkuropatov, A. and Shuvalov, V. (**2010a**) Primary electron transfer in reaction centers of YM210L and YM210L/HL168L mutants of *Rhodobacter sphaeroides*. *Biochemistry (Moscow)*, 75, 832-840.

(204) Yakovlev, A. G., Shkuropatov, A. Y. and Shuvalov, V. A. (**2002**) Nuclear Wave Packet Motion between P* and P+BA- Potential Surfaces with a Subsequent Electron Transfer to HA in Bacterial Reaction Centers at 90 K. Electron Transfer Pathway. *Biochemistry*, 41, 14019-14027.

(205) Yakovlev, A. G., Vasilieva, L. G., Khmelnitskaya, T. I., Shkuropatova, V. A., Shkuropatov, A. Y. and Shuvalov, V. A. (**2010b**) Primary electron transfer in reaction centers of YM210L and YM210L/HL168L mutants of Rhodobacter sphaeroides. 75, 832-840.

(206) Yamasaki, H., Takano, Y. and Nakamura, H. (**2008**) Theoretical Investigation of the Electronic Asymmetry of the Special Pair Cation Radical in the Photosynthetic Type-II Reaction Center. *J. Phys. Chem. B*, 112, 13923-13933.

(207) Yeates, T. O., Komiya, H., Rees, D. C., Allen, J. P. and Feher, G. (**1987**) Structure of the reaction center from *Rhodobacter sphaeroides* R-26 membrane-protein interactions. *Proc. Natl. Acad. Sci. U. S. A.*, 84, 6438-6442.

(208) Yeates, T. O., Komiya, H., Chirino, A., Rees, D. C., Allen, J. P. and Feher, G. (**1988**) Structure of the reaction center from Rhodobacter-sphaeroides r-26 and 2.4.1-protein-cofactor (bacteriochlorophyll, bacteriopheophytin, and carotenoid) interactions .4. *Proc. Natl. Acad. Sci. U. S. A.*, 85, 7993-7997.

(209) Zheng, L., Fishbein, K. W., Griffin, R. G. and Herzfeld, J. (**1993**) Two-dimensional solid-state proton NMR and proton exchange. *J. Am. Chem. Soc.*, 115, 6254-6261.

(210) Zysmilich, M. G. and McDermott, A. (**1994**) Photochemically induced dynamic nuclear-polarization in the solid-state ^{15}N spectra of reaction centers from photosynthetic bacteria *Rhodobacter sphaeroides* R-26. *J. Am. Chem. Soc.*, 116, 8362-8363.

Summaries

Summary in English

Photosynthesis is the physico-chemical process by which plants, algae and photosynthetic bacteria use light energy to drive the synthesis of organic compounds. Light-induced electron transfer in photosynthetic reaction centers (RCs) is highly efficient, having a quantum yield close to unity. In RCs of *Rhodobacter* (*R.) sphaeroides* wild type *(*WT), the primary electron donor is a bacteriochlorophyll *a* (BChl) dimer, called the Special Pair P, comprising two dimer halves P_L and P_M. Two additional BChl cofactors called accessory BChls (B_A and B_B), two bacteriopheophytins (Φ_A and Φ_B), two quinones and a non-heme iron are organized into two pseudo-symmetric branches named A and B. After the photo excitation the electron is transferred only via the active "A" branch. On the other hand, in structurally similar RCs, as that of photosystem I, the electron transfer occurs equally over both branches. Neither the reason for the high efficiency nor that of the directionality of the electron transfer has been elucidated so far. To solve these questions, the solid-state photo-chemically induced nuclear polarization (photo-CIDNP) effect with its dramatic enhancement of local NMR signals provides an analytical tool especially suited for studying electron transfer in photosynthetic RCs. In fact, photo-CIDNP MAS NMR has been applied to explore electronic structures of the electron donors and acceptors in RCs.

In this Thesis, the first goal was to reach a complete picture of the electronic ground state of the donor of the RC of *R. sphaeroides* WT. **Chapter 2** reports 2D photo-CIDNP DARR experiments by nanosecond laser flash excitation on ^{13}C labelled bacterial RCs at selected positions in the Special Pair. Combined with previous results, a complete chemical shift assignment of the Special Pair is obtained. The shielding pattern of the ^{13}C nuclei confirms that there is excess electron density towards pyrrole ring III of P_L compared with pyrrole ring III of P_M, and the pattern of ^{13}C shifts for the ring carbons is well in line with the $P_L^{\delta-}P_M^{\varepsilon-}$ charge transfer character, with $\delta > \varepsilon$. Hence symmetry breaking of the electronic

structure with excess negative charge on the P_L is detected in the ground state. The results suggest that asymmetric distribution of electron density mediates the asymmetric electron transfer following excitation.

Functional properties may also depend on dynamic aspects. Therefore, in **Chapter 3**, we probe the dynamics of the Special Pair by a new strategy that is based on photo-CIDNP MAS NMR experiments. Spin-torch based experiments are introduced, where the polarization transfer of enhanced photo-CIDNP signals between ^{13}C-^{13}C of different isotope labels is observed by spin diffusion process, This experiment, thus allows probing the local mobility in the Special Pair. Polarization transfer among the ^{13}C labelled carbon atoms of the Special Pair in 3-ALA bacterial RCs is studied by 2D photo-CIDNP DARR experiments with continuous illumination. From a series of experiments with different mixing times, dynamic asymmetry in the Special Pair is observed. It appears that the break of the pseudo-C_2 symmetry is related to the entire supermolecule rather than to the individual P_L and P_M molecules. The dynamic picture is compared with polymorphism in terms of Shelnutt's NSD (normal-coordinate structural decomposition) analysis, suggesting that collective modes are localized towards the P_M bacteriochlorophyll. The arising picture is also in line with Redfield's theory approach. Possible implications of the localized dynamics for symmetry breaking and charge transfer are discussed.

In **Chapter 4**, the study of the electronic ground state is extended from the Special Pair to the primary electron acceptor. To this end, bacterial RCs containing u-$^{13}C_4$-δ-aminolevulinic acid (u-ALA) labelled BChl and BPhe are studied under continuous illumination. By comparison with the literature, a full assignment for the bacteriopheophytin (Φ_A) has been obtained. It appears that the electronic structure of Φ_A is very similar to that of a BPhe *a* in solution, with little evidence for packing effects induced by the protein matrix. It is concluded that the Φ_A of the active branch is not tuned in a special manner by its environment.

To explore the protein pocket which might tune the Special Pair, alternative spin-torch experiments are proposed in **Chapter 5**. In this concept, the strong polarization of the donor carbons is transferred to the pocket, which can be

studied at atomic resolution. To this end, the possibility to use ^{13}C photo-CIDNP for ^{13}C-^{1}H transfer is explored. In this Chapter, results on polarization transfer between the highly polarized ^{13}C and the thermally polarized ^{1}H are discussed. An outlook is presented for the application of such spin-torch experiments to study the aromatic environment of the Special Pair.

Summary in Dutch *(Samenvatting)*

Fotosynthese is het fysisch-chemische proces waarmee planten, algen en fotosynthetische bacteriën licht energie gebruiken voor de synthese van organische bestanddelen. Door licht veroorzaakte elektron overdracht in fotosynthetische reactie centra (RC) is zeer efficiënt, met een kwantum efficiëntie van bijna 100%. In RCs van *Rhodobacter (R). sphaeroides* WT, de primaire elektron donor is een bacteriochlorophyll (BChl) dimeer, het zogenaamde Special Pair P, bestaande uit P_L en P_M. In het RC zijn verder twee extra BChl cofactoren accessory BChls (B_A en B_B) genaamd, twee bacteriopheophytines (Φ_A en Φ_B), twee quinonen en een non-heem-ijzer zijn onderverdeeld in twee pseudo-symmetrische takken A en B. Het elektron wordt alleen overgedragen via de actieve "A" tak. Maar in structureel gelijksoortige RC, zoals in het reactie centrum van fotosysteem I, vindt elektronen overdracht in gelijke mate plaats via beide takken. Het geheim van de hoge kwantum efficiëntie in de richting van de elektronen overdracht is tot op heden ontrafeld. Om deze vraagstukken op te lossen is het photo-CIDNP effect (photo-chemically induced nuclear polarization), met zijn zeer grote versterking van lokale NMR signalen, een uitzonderlijk prakisch analytisch gereedschap dat speciaal geschikt is om elektronen overdracht in fotosynthetische reactie centra te bestuderen. Zo is photo-CIDNP toegepast om de elektronische structuur van de elektron donor in kaart te brengen.

Het eerste doel van dit proefschrift was om een compleet beeld van de elektronische grondtoestand van de donor van het RC van *R. sphaeroides* WT te verkrijgen. **Hoofdstuk 2** doet verslag van 2D photo-CIDNP DARR experimenten met nanosecond laser flash excitatie van bacteriële RC, die op specifieke plaatsen

in het Special Pair zijn verrijkt met ^{13}C isotopen. Samen met eerder behaalde resultaten is een complete chemical shift bepaling van het Special Pair verkregen. Het 'shielding' patroon van de ^{13}C kernen bevestigt dat er een lichte overmaat van elektronen dichtheid is op pyrrool ring III van P_L in vergelijking met pyrrool ring III van P_M, verder is het patroon van de ^{13}C shifts voor de ring koolstoffen in goede overeenkomst met het verwachte karakter van de $P_L^{\delta-}P_M^{\varepsilon-}$ ladingsoverdracht waarbij geldt dat $\delta > \varepsilon$. Er is dus een breking van de symmetrie in de elektronische grondtoestand met een overmaat van negatieve lading op P_L gedetecteerd. De asymmetrische distributie van elektronen dichtheid draagt mogelijkerwijs bij aan de asymmetrie van de elektronen overdracht die na excitatie uitsluitend langs de actieve tak plaatsvindt.

Functionele eigenschappen kunnen ook afhangen van dynamische aspecten. Daarom is in **Hoofdstuk 3** de dynamiek van de Special Pair onderzocht met behulp van een nieuwe strategie die is gebaseerd op photo-CIDNP MAS NMR experimenten. Spin-torch gebaseerde experimenten, waar de polarisatie overdracht tussen verschillende ^{13}C isotopen door spin diffusie mee kan worden geobserveerd, worden in dit hoofdstuk geïntroduceerd. Deze experimenten maken het mogelijk om de locale mobiliteit in het Special Pair te meten. Polarisatie overdracht tussen de met ^{13}C isotopen verrijkte atomen van het Special Pair in 3-ALA bacteriële RC is onderzocht met behulp van 2D photo-CIDNP DARR experimenten onder constante belichting. Met behulp van de gepresenteerde serie van experimenten met verschillende 'mixing times' is de dynamische asymmetrie van het Special Pair in kaart gebracht. Het lijkt erop dat de breking van de pseudo-C_2 symmetrie meer is gerelateerd aan het totale supermolecuul dan aan de individuele moleculen P_L en P_M. Het dynamische plaatje is vergeleken met polymorfisme in termen van Shelnutt's NSD analyse die mogelijke variabiliteit in de kristallijne toestanden aangeeft, in de richting van de P_M bacteriochlorophyll. Het resultaat is tevens in lijn met de 'Redfield's theory' benadering. Mogelijke implicaties van de lokale dynamiek van de symmetrie breking en de ladingsoverdracht worden besproken.

In **Hoofdstuk 4** wordt naast de elektronische grondtoestand van het Special Pair ook die van de primaire elektronen acceptor onderzocht. Hiervoor zijn bacteriële RC met u-$^{13}C_4$-δ-aminolevulinic acid (u-ALA) verrijkte BChl en BPhe bestudeerd onder constante belichting. Door vergelijking met al bekende waarden uit de literatuur is een complete toekenning van de signalen van bacteriële pheophytine (Φ_A) gerealiseerd. Het lijkt erop dat de elektronische structuur van Φ_A in sterke mate overeenkomt met die van een BPhe *a* molecuul in oplossing, en er is weinig bewijs gevonden voor packing effecten van de eiwit matrix. Daarom is geconcludeerd dat de Φ_A van de actieve tak niet op een speciale manier is afgestemd door zijn directe omgeving.

Om het eiwit pocket, dat mogelijkerwijs de Special Pair afstemt, te bestuderen, zijn alternatieve spin-torch experimenten voorgesteld (**Hoofdstuk 5**). In dit concept wordt de sterke polarisatie overdracht van de donor koolstoffen aan de pocket tot op atomair nivo bekeken. Hiervoor is de mogelijkheid om ^{13}C photo-CIDNP te gebruiken voor ^{13}C-^{1}H overdracht onderzocht. In dit hoofdstuk worden de resultaten van polarisatie overdracht tussen sterk gepolariseerde ^{13}C atomen en thermisch gepolariseerde ^{1}H besproken. Een vooruitblik van de mogelijke toepassing van dergelijke spin-torch experimenten om in de toekomst de omgeving van het aromatische systeem van het Special Pair te onderzoeken wordt hier gepresenteerd.

Summary in Tamil (*ஆய்வு சுருக்கம்*)

தாவரங்கள், பாசிகள் மற்றும் ஒளிச்சேர்க்கை செய்யும் பாக்டீரியாக்கள், ஒளிச்சேக்ர்கை என்ற இயற்-வேதிய செய்முறையை கொண்டு ஒளி ஆற்றலை உபயோகித்து, கரிமச் சேர்மங்களை உற்பத்தி செய்து கொள்கின்றன. இந்த ஒளிச்சேர்க்கை வினைமைய நிலையங்களில் நிகழும், ஒளியால் தூண்டப்பட்ட எலக்ட்ரான் பரிமாற்றம், மிகவும் சிறப்பாக நடைபெறுகின்ற ஒரு வேதிவினையாகும். மேலும், இந்த வேதிவினையின் குவாண்டம் செயல்திறனின் மதிப்பு இலக்கம் ஒன்றை நெருங்குகிறது. ஆர். ஸ்பொராய்ட்ஸ் WT என்ற நுண்ணுயிரியின் ஒளிச்சேர்க்கை வினைமையத்தில், எலக்ட்ரான் பரிமாற்றத்திற்கு, இணைகாரணியின் இரண்டு சமச்சீர் கிளைகளில், ஒன்று தான் தேர்வு செய்யப்படுகிறது. மற்றொரு பக்கம், அதே அமைப்புடைய போட்டோசிஸ்டம் I-ல் உள்ள ஒளிச்க்சேர்கை வினைமையத்தில், எலக்ட்ரான் பரிமாற்றம், இணைகாரணியின் இரண்டு கிளைகளிலும் நடைபெறுகின்றது. இத்தகைய எலக்ட்ரான் பரிமாற்றத்தின் செயல்திறன் மற்றும் திசை, இன்னும்

அறியப்படாத ஒன்றாகும். இதை கண்டறிய, ஒளிச்சேர்க்கை வினைமையத்திலிருந்து, திண்மநிலை போட்டோ-சி.ஐ.டி.என்.பி என்கின்ற பரிசோதனையின் மூலம் கிடைக்கும், மிகைப்படுத்தப்பட்ட என்.எம்.ஆர் உள்சைகை ஒரு பகுக்கின்ற கருவியாக விழங்குகின்றது. எனவே, இந்த ஆய்வில் போட்டோ-சி.ஐ.டி.என்.பி என்.எம்.ஆர் உத்தி மூலம் எலக்ட்ரான் வழங்கியின் இலத்திரனமைப்பு ஆய்வு செய்யப்பட்டுள்ளது. இந்த ஆய்வுக்கட்டுரை ஐந்து அத்தியாயங்களாக பிரிக்கப்பட்டுள்ளன.

அத்தியாயம் ஒன்று: இந்த ஆய்வு பற்றிய நோக்கம் மற்றும் அதை சார்ந்த பல விபரங்கள் முன்னுரையாக வழங்கப்பட்டுள்ளது.

அத்தியாயம் இரண்டு: இந்த பரிசோதனைக்கு தேர்வு செய்யப்பட்ட சிறப்பு இடங்களில் கதிரியக்க ^{13}C கரிமத்தால் அடையாளம் செய்யப்பட்ட, சிறப்பு இணை கொண்ட ஒளிச்சேர்க்கை வினைமையமானது, நானோ விநாடி ஊடொளி ஒளித்தெரிப்பு கொண்டு, கிளர்வு செய்யப்பட்டது. இந்த பரிசோதனையின் மூலம் சிறப்பு இணையின் முழுமையான வேதி நகர்வின் ஒதுக்கல் பெறப்பட்டது. மேலும், P_M பிரோல் வளையம் III -ஐ விட, P_L பிரோல் வளையம் III-னை நோக்கி, கூடுதல் எலக்ட்ரான் அடர்த்தி இருப்பதால், கதிரியக்க ^{13}C அணுக்கருவின் வேதி நகர்வு அமைப்பு , $P_L^{\delta-}P_M^{\varepsilon-}$ $\delta > \varepsilon$ ன் மின்னுட்ட பரிமாற்ற தன்மைக்கு சமநிலையில் இருக்கின்றது. இதனால் தாழ்நிலை P_L -ல் உள்ள கூடுதல் குறை மின்னுட்டம் அதனின் சமச்சீர் எலக்ட்ரான் அமைப்பை முறிவுசெய்கின்றது. இந்த கண்டறியப்பட்ட சமச்சீரற்ற எலக்ட்ரான் அடர்த்தி பரவல், கிளர்வுற்ற நிலையில் நடைபெறும் சமச்சீரற்ற எலக்ட்ரான் பரிமாற்றத்திற்கு செயல்தூக்கியாக செயல்படலாம்.

அத்தியாயம் மூன்று: ஒரு புதிய உத்தியான, போட்டோ-சி.ஐ.டி.என்.பி மாஸ் என்.எம்.ஆர் பரிசோதனை கொண்டு, சிறப்பு இணையின் இயக்க பண்பு ஆராயப்பட்டுள்ளன. மேலும், இந்த பரிசோதனையின் மூலம் சிறப்பு இணையின் உள் நகர்திறனை ஆய்வு செய்ய முடிகின்றது. தொடர்ச்சியான ஒளியூட்டம் கொண்ட 2D போட்டோ-சி.ஐ.டி.என்.பி DARR பரிசோதனை கொண்டு, 3-ALA பாக்டீரிய வினை மையத்தில் உள்ள, சிறப்பு இணையில், அடையாளமிடப்பட்ட கதிரியக்க ^{13}C கரிம அணுக்கருக்களுக்குள் நடைபெறும் ஒருமுனையாக்கல் பறிமாற்றம் ஆய்வு செய்யப்பட்டுள்ளன. மேற்கண்ட பரிசோதனைகளில் பெறப்பட்ட இயக்கவியல் அமைப்பு பற்றி, Shelnutt's NSD பகுப்பாய்வு கொண்டு விளக்கம் அளிக்கப்பட்டுள்ளது. சமச்சீர் முறிவு மற்றும் மின்னூட்ட பரிமாற்றத்திற்கு தொடர்புடைய, குறிப்பிட்ட இடத்தில் ஏற்ப்படும் இயக்க நிலை பண்பால், ஏற்படக்கூடிய விளைவுகள் பற்றி கருத்துக்கள் தெரிவிக்கப்பட்டுள்ளன.

அத்தியாயம் நான்கு: முதலில், சிறப்பு இணையின் தாழ்நிலை பற்றிய தகவல்கள், முதன்மை எலக்ட்ரான் ஏற்பிக்கு விரிவு செய்யப்பட்டுள்ளன. U-ALA BChl மற்றும் BPhe பாக்டீரியாவின் வினைமையங்கள், தொடர்ச்சியான ஒளியூட்டம் மூலம் பரிசோதனை செய்யப்பட்டுள்ளன. இதன்மூலம், Φ_A-ன் முழுமையான வேதி நகர்வின் ஒதுக்கல் பெறப்பட்டுள்ளன. இதனால் BPhe - யின் உந்தப்பட்ட கிளை, தனது சுற்றத்தால் இசைப்புறவில்லை என்பது உறுதி செய்யப்பட்டுள்ளன.

அத்தியாயம் ஐந்து: சிறப்பு இணையை இசைப்புற வைக்கக்கூடிய புரத வினை மையத்தை, வேறுபட்ட ஸ்பின்-டார்ச் பரிசோதனை கொண்டு ஆய்வு செய்யும் முறைகள், முன்மொழியப்பட்டுள்ளது. மேலும், கதிரியக்க ^{13}C கொண்ட போட்டோ-சி.ஐ.டி.என்.பி பரிசோதனை மூலம், ^{13}C-^{1}H அணுக்களின் இடையில் இயலக்கூடிய பரிமாற்றம் விளக்கமாக கொடுக்கப்பட்டுள்ளது. இறுதியாக, ஸ்பின்-டார்ச் பரிசோதனையின் எதிர்கால பயன்பாடாக, சிறப்பு இணையின் அரோமேடிக் கரிம அணுக்களின் சுற்றத்தை, ஆய்வு செய்யக்கூடிய உத்திகள் விளக்கப்பட்டுள்ளன.

Publications

"Dynamic asymmetry in the Special Pair of *Rhodobacter sphaeroides* observed by photochemically induced dynamic nuclear polarization ^{13}C NMR"

(Chapter-2, *Manuscript to be submitted*)

"**Two-dimensional nanosecond laser-flash photo-CIDNP MAS NMR experiments provide direct access to the electronic structure of the donor in bacterial reaction centers**"

(Chapter-3, *Manuscript to be submitted*)

"Characterization of bacteriopheophytin a in the active branch of the reaction center of *Rhodobacter sphaeroides* by ^{13}C photo-CIDNP MAS NMR"

(Chapter-4, *Manuscript to be submitted*)

"Proton NMR using photo-CIDNP on *Rhodobacter sphaeroides*"

(Chapter-5, *Manuscript to be submitted*)

"On the configuration of spheroidene in the photosynthetic reaction center of *Rhodobacter sphaeroides*: a comparison of wild type and reconstituted R26"

Guinevere Mathies, Marc C. van Hemert, Peter Gast, Karthick Babu Sai Sankar Gupta, Harry A. Frank, Johan Lugtenburg, Edgar J. J. Groenen

J. Phys. Chem. A 115, 34, 9552–9556 (2011)

"Phytochrome as molecular machine: Revealing chromophore action during the Pfr-to-Pr photoconversion by magic-angle spinning NMR spectroscopy"

Thierry Rohmer, Christina Lang, Christian Bongard, Karthick Babu Sai Sankar Gupta, Jon Hughes, Wolfgang Gärtner, Jörg Matysik

J. Am. Chem. Soc. 132, 4431-4437 (2010)

"^{15}N photo-CIDNP MAS NMR on RCs of *Rhodobacter sphaeroides* (WT) and R26"

Eugenio Daviso, Karthick Babu Sai Sankar Gupta, Shipra Prakash, A. Alia, Peter Gast, Gunnar Jeschke, Jörg Matysik

In: Energy from the sun (J. Allen, E. Gantt, J. Golbeck, B. Osmond, eds.) Springer Dordrecht, pp. 63-66 (2008)

Science Career article:

"Towards spin-torch experiments and artificial reaction centers "

Karthick Babu Sai Sankar Gupta

Rev. Env. Sci. Biotech. Vol. 8, Number 4, 313-316 (2009)

Curriculum vitae

The author of this thesis, Karthick Babu Sai Sankar Gupta was born on 9th August 1979 in Bangalore, India. During his childhood, he had been travelling and did schooling in different places namely, Chennai, Madurai, Pondicherry and finally finished school education in Tiruppur. He was ranked first among the graduating class of year 1996 (12th standard) from Nanjappa Boys Higher Secondary School, Tiruppur. He was awarded a study scholarship in Sri Sathya Sai Institute of Higher Learning in Whitefield, Bangalore to support his studies of B.Sc (Chemistry) (Hons) from 1996 to 1999. He proceeded further to pursue master's course in chemistry with his scholarship. During this study, he completed grades with distinction from Sri Sathya Sai Institute of Higher Learning, Puttaparthi in 2001. Part of his master's project was "Phytochemical Investigation of *Croton bonplandianum*" under the supervision of Dr. Nageshwar Rao. During his academic endeavors, he actively participated in social-work events and took additional responsibilities in voluntary activities in the "Grama Seva" (Village service) project. After his master's, he worked as a project assistant under the supervision of Prof. K .V. Ramanathan and Prof. N. Suryaprakash in NMR Research Centre at the Indian Institute of Science, Bangalore, India from 2001 till 2003. In 2004, he worked as a research assistant in Laboratoire de Résonance Magnétique Biomoléculaire at EPFL, Switzerland under the supervision of Prof. G. Bodenhausen. There he studied internal motions in free and bound Major Urinary Protein by ^{15}N CPMG relaxation dispersion rates and further worked on the thermodynamic theory of cross polarization with adamantane and polarization transfer from abundant nuclei to insensitive nuclei using rotary resonance and other techniques in SSNMR.

In 2006, he started his doctoral studies at Leiden University in the Solid-State NMR group of Prof. Dr. H. J. M de Groot under the supervision of Dr. J. Matysik. The project was entitled "Transfer of photo-CIDNP polarization to surrounding atoms in solids". During his research, he received several travel grants and got the opportunity to attend the following summer schools (1) *European School on Solid State NMR*, Advanced level course, Biological Solids, Germany (May 29th - June 2nd, 2006); (2) *EMBO Workshop on Multidimensional NMR in Structural Biology*, Il Ciocco- Lucca, Italy (27th Aug – 1st Sep, 2006); (3) *HRSMC's Summer School on Photochemistry 2008: Fundamentals and Applications*, Maastricht, The Netherlands (31st May – 4th June, 2008); (4) *Summer School NMRCM*, St.Petersburg, Russia (3rd – 5th July, 2008). In 2008, he received a short-term grant from EMBO for "Spin-torch experiments with ^{13}C photo-CIDNP MAS NMR for exploring biological structures". This gave him the opportunity to visit and work with Prof G. Jeschke and Prof. M. Ernst in Laboratorium für Physikalische Chemie at ETH, Switzerland. The results from his doctoral research work have been presented both orally and as posters at various conferences. From March 2011, he has been working as "interim hoofd van de NMR afdeling" at the Leids Instituut voor Chemisch Onderzoek, The Netherlands.

ஆசிரியர் குறிப்பு

இந்த ஆய்வறிக்கையின் ஆசிரியர், கார்த்திக் பாபு சாய் சங்கர் குப்தா, 9 ஆகஸ்ட் 1979ல், இந்திய நாட்டில் உள்ள பெங்களூரில் பிறந்தார். தனது பள்ளிப்படிப்பை, சென்னை, மதுரை, பாண்டிச்சேரி ஆகிய இடங்களில் மேற்கொண்டார். இறுதியாக 1996 ஆம் ஆண்டு, திருப்பூரில் உள்ள நஞ்சப்பர் நகராட்சி ஆண்கள் மேல்நிலைப்பள்ளியில், தனது பள்ளிப்படிப்பை முடித்தார். மேல்நிலை படிப்பின் இறுதி ஆண்டில், பள்ளியின் முதல் மாணவனாக தேர்ச்சி பெற்றார். 1996 முதல் 2001 வரை ஸ்ரீ சத்யா சாய் உயர் கல்வி கழகத்தில், கல்வி உதவித்தொகை பெற்று, வேதியலை சிறப்புப் பாடமாகக்கொண்டு, இளங்கலை மற்றும் முதுகலை படிப்பபில் மேற்கொண்டு, தனிச்சிறப்பு பட்டங்களை பெற்றார். முதுகலை பட்டத்திற்கு தேவையான ஆய்வு திட்டத்தை "பைடோ கெமிகல் இன்வஷ்டிகேஷன் ஆப் இக்ரோடான் போன்பிலன்டியானம்" என்னும் தலைப்பில், பேராசிரியர் நாகேஷ்வர் ராவ் அவர்களின் கீழ் மேற்கொண்டார். மேலும் தனது பட்டப்படிப்பின் போது "கிராம சேவை" என்ற தன்னார்வுத்திட்டதில் சமூகப்பணி நிகழ்ச்சிகளில் சேவை செய்தார். முதுகலை படிப்பிர்க்குப்பிறகு, 2003 ஆம் ஆண்டு வரை, இந்திய அறிவியல் கழகத்தில் உள்ள அணுக்கரு காந்த ஒத்ததிர்வு (என்.எம்.ஆர்) ஆய்வுமையத்தில் பேராசிரியர்கள் கே.வி. ராமநாதன் மற்றும் என். சூர்யபிரகாஷ் ஆகிய இருவரின் கீழ் ஆய்வுத்திட்ட உதவியாளராக பணிபுரிந்தார். பின்னர் 2004-ஆம் ஆண்டில், சுவிட்சர்லாந்து நாட்டில் உள்ள இ.பி.எப்.ல் ஆய்வுக்கழகத்தில், பேராசிரியர் ஜி. போடன் ஹவுசென்-இன் கீழ் ஆய்வு உதவியாளராக பணிபுரிந்தார். இங்கு, ஒரு முக்கிய சிறுநீர் புரத மூலக்கூறின் உள் இயக்கத்தை, கதிரியக்க ^{15}N சி.பி.எம்.ஜி தளர்வு பரவல் வேகத்தை கொண்டு ஆய்வு செய்தார். மேலும் அடமண்டேன் என்கின்ற கரிமச்சேர்மத்தின் குறுக்கு ஒருமுனையாக்கலின் வெப்ப இயக்கவியல் கோட்பாட்டையும், மிகுதியான அணுக்கருவிலிருந்து மற்ற கதிர் உணர்வட்ற அணுகருவிர்க்கு ரோட்டரி ஒத்ததிர்வு மூலம் முனையாக்கல் பரிமாற்றத்தையும், மற்றும் மற்ற திண்மநிலை என்.எம்.ஆர் உத்திகளையும் கற்றறிந்தார்.

2006-ஆம் ஆண்டு லைடன் பல்கலைகழகத்தில், பேராசிரியர் முனைவர் ஹ.ஜே.எம். க்ரூத் அவர்களின் திண்மநிலை என்.எம்.ஆர் குழுமத்தில், முனைவர் ஜே. மட்டிசிக் அவர்களின் மேற்பார்வையில் தனது முனைவர் பட்டத்திற்கான ஆய்வை துவங்கினார். இவரது ஆய்வின் தலைப்பு ‘’டிரான்ஸ்வர் ஆப் போட்டோ - சி.ஐ.டி.என்.பி போலரய்சேசன் டு சரவுன்டிங் ஆட்டம்ஸ் இன் சாலிட்ஸ்”. தனது ஆராய்ச்சியின் போது பல பயண மாணியங்களை பெற்றார். பின்குறிப்பிட்ட பல சர்வதேச கோடை கால பள்ளிகளில் கலந்து கொண்டார். (1) *ஜரோப்பியன் ஸ்கூல் ஆன் சாலிட் ஸ்டேட் என்.எம்.ஆர், அட்வான்ஸ்டு லெவல் கோர்ஸ், பயலாஜிகல் சாலிட்ஸ்*, ஜெர்மனி (மே 29 - ஜூன் 2, 2006); (2) *எம்போ வொர்க்சாப் ஆன் மல்டிடய்மென்ஷனல் என்.எம்.ஆர் இன் ஸ்டிரக்சுரல் பயாலஜி*, சிஒகோ - லூகா. இத்தாலி (27 ஆகஸ்ட் - 1 செப்டம்பர், 2006); (3) *எச்.ஆர்.எம்.சி'ஸ் சம்மர் ஸ்கூல் ஆன் போடோ கெமிஸ்ட்ரி*: பண்டமெண்டல்ஸ் அண்டு அப்ளிகேஷண்ஸ், மாஸ்திரிக்த், நெதர்லாண்டு (31 மே - 4 ஜூன் 2008); (4) *சம்மர் ஸ்கூல் என்.எம்.ஆர்.சி.எம். எஸ்டி.* பீட்டர்ஸ்பர்க், ரஷ்யா (3 - 5 ஜூலை, 2008). 2008 ஆம் ஆண்டு, எம்போ நிறுவனத்திடமிருந்து குறுகிய கால ஆய்வுக்கல்வி உதவித்தொகையை *“இஸ்பின்-டார்ச் எக்ஸ்பிரிமென்ட் வித் ^{13}C போடோ-சி.ஐ.டி.என்.பி மாஸ் என்.எம்.ஆர் பார் எக்ஸ்பிளோரிங் பயலாஜிகல் ஸ்டிரக்சர்ஸ்”* என்கின்ற ஆய்விற்கு பெற்றார். இந்த மாணியத்தின் மூலம் மேற்கூறிய குறிகிய கால ஆய்வை சுவிட்சர்லாந்து நாட்டில் உள்ள இ.டி.ஹச் ஆய்வு மையத்தில் பேராசிரியர்கள் கு. எஷ்ஹ்கி மற்றும் ம. எர்ன்ஸ்ட் ஆகியோரின் கீழ் மேற்கொண்டார். இவர் தனது முனைவர் பட்ட ஆய்வின் முடிவுகளை பல அறிவியல் ஆராய்ச்சி மாநாடுகளில் பங்குபெற்று உரைகள் மற்றும் அச்சு மூலம் அறிமுகப்படுத்தினார். மார்ச் 2011 முதல் லைடன் பல்கலைகழகத்தின், எல்.ஐ.சி ஆய்வுமையத்தில், என்.எம்.ஆர் துறையின் இடைக்கால தலைமை ஆய்வுப் பொருப்பாளராக பணிபுரிந்துவருகிறார்.

Acknowledgements

This is the page I have waited to write at the end, so that I could mention all the people who had helped and guided me to this point. From the bottom of my heart, I acknowledge all the people who had supported me in one way or the other. This has been a long fun-filled adventurous journey in quest for science and life.

I enjoyed scientific discussions and collaborations with Prof. Shimon Vega, Prof. Gunnar Jeschke and Prof. Matthias Ernst for which I am always indebt. Dr. Peter Gast was there for any discussions regarding the isolation of RCs and reconstitution of carotenoid samples. Working with Dré de Wit and Wouter van der Meer in the Biophysics group was a nice experience. Dr. Alia's guidance provided especially during the labelled sample preparations is appreciated. Dr. Francesco Buda's explanations of theoretical simulations and his insight on the mechanisms were useful. The concepts discussed with Bela helped me to look at the photo-CIDNP theory more deeply. Setting up laser experiments along with Eugenio was a good learning experience. Discussions with all the above mentioned people and SSNMR group members had helped me to gain insight and knowledge about the photosynthetic process. I am very grateful to Kees Erkelens for his constant support and encouragement to try the new NMR experiments with confidence. "If any experiment doesn't give good results in one hour, try another experiment or change the sample" are his words, which have stayed in my mind forever. The useful tips and notes pasted on the walls of the NMR room by Fons Lefeber and his patience for correcting my Dutch pronunciations were invaluable.

Life in the SSNMR group and in Holland was a great experience, especially within an international atmosphere. The time I spent with Anjali, Chen, Esha, Firat, Fu, Geerten, Jose-Luis, Kiran, Khuram, Prashant, Saeed, Sameera, Shipra, Smitha, Thomas & Wim was unforgettable. Assisting student practicals with William and Virginie was fun. Rob's guitar tips and Reinier's tips on "running" were always encouraging. I also want to thank Geertje for translating my thesis summary. The sports activities with Anna, Niels, Swapna and Johan were nice and

enjoyable. Discussions with Ben and Bela about any topic in science were always exciting. Sharing the LCP-2 office with Piotr, Thierry and the other intern students was very enjoyable. The break time discussions on history, culture and abstract ideas were exhilarating. Swapna and Johan were always there to appreciate my culinary creations, running circuits and cycling trips.

Liesbeth was always very kind and supportive in the administrative activities and her tips about life in Leiden were useful. Esther's help in dealing with IND and other townhall related issues were always spontaneous. Raphael's timely solution for any mechanical problem is very much appreciated. All the support for the tools, accessories and many other things from Trudie, Arjan, Arnold, Mark and Paul are very much acknowledged.

Life outside the lab was also very pleasant, especially with my apartment mates Alfi, Ma Tao, Hung Bo and Chang. The badminton sessions with Ding were always fun and challenging. Thanks to Raja, Krishna, Ravi, Prasad, Uma, Sudeshna, Sushmit and Nusrat for all the memorable get-togethers. Support from Shiva anna's family makes me feel as a member in their family. Special thanks to Amol and Monica for their interesting conversations over science and philosophy. I also would like to thank Anand, Sathish, Raghupathy, Subi and Vishwa for their constant support in all my ventures. Mani's commitment for the Tamil translation and all other friends who helped at various instances are highly valued. I am very lucky to have Malou as "Taal maatje". Her support in learning language and decoding the Dutch expressions were very useful.

The warmth and affection from my mom and dad has always nourished me in many ways. Their constant support, encouragement and wishes helped me to achieve this goal. The interesting stories from my sister and brother-in-law about Arvind and Sakthi's activities were always refreshing and relaxing. I want to thank all my relatives for their support given to my family while I was away from home. I would like to thank my in-law's family for their special support. This endeavor is incomplete without acknowledging my beloved wife, Naveena who could understand me very well and make me smile always. I am very lucky and happy that I can spend rest of my life with her.